

# Modeling and Analysis of Small-Scale Hydraulic Systems

A THESIS  
SUBMITTED TO THE FACULTY OF THE GRADUATE SCHOOL  
OF THE UNIVERSITY OF MINNESOTA  
BY

Jicheng Xia

IN PARTIAL FULFILLMENT OF THE REQUIREMENTS  
FOR THE DEGREE OF  
Doctor of Philosophy

Advisor: Professor William Durfee

May, 2015

© Jicheng Xia 2015  
ALL RIGHTS RESERVED

# Acknowledgements

I would like to sincerely express my gratitude to my advisor, Professor William Durfee, for his everlasting guidance, support, and inspiration, without which this research work would have not been possible. I would also like to thank the rest of my doctoral committee: Prof. Kim Stelson, Prof. Thomas Chase and Prof. Peter Seiler, for their time, commitment, and support.

This research was supported by the Center for Compact and Efficient Fluid Power, a National Science Foundation Engineering Research Center, funded under cooperative agreement number EEC-0540834. I am grateful for this five year long financial support.

I would also like to thank the rest of my research colleagues: Brett Neubauer, Andy Ries, Kathy Houle, Jonathan Nath, Dr. Haink Tu, Dr. Lei Tian, Ellen Weburg, Dr. Yifan (David) Li, Dr. Alex Shorter and Prof. Elizabeth Hsiao-Wecksler for their continuous support and insightful inputs on respective parts of this work. I wish the best of luck to each of them in their endeavors in the future.

Lastly, I would like to thank my family, especially my wife Wanshu He. Her continuous encouragement throughout my PhD study was crucial for me to finish this work.

## Abstract

**OBJECTIVE** To determine the scaling law and design guidelines of small-scale hydraulic systems whose output power is in the range of 10 to 100 Watts.

**METHODS** Fundamental fluid mechanics equations were employed to model the friction and leakage losses in the hydraulic components including cylinders, hoses, and pumps. Basic structural design equations were deployed to predict their weight. Customized test stands were built to validate the efficiency models, and catalog data of off-the-shelf components was compiled to validate the weight models. The electro-mechanical components including electric motors, gear heads and batteries were modeled using their catalog data.

**RESULTS** The efficiency and the weight of both hydraulic and electro-mechanical components were modeled in analytical forms. These models were validated against either experimental data or existing catalog data.

**CONCLUSION** The analytical models suggested the following design guidelines: first, high operating pressure is needed for hydraulic actuation systems to weigh lighter than equivalent electro-mechanical systems; second, critical dimension thresholds exist for hydraulic and electro-mechanical components, which should not be exceeded to achieve reasonable system efficiency; third, component efficiency plays a more important role than component weight to gain higher system power density; lastly, for applications where the actuator system weight matters the most, high pressure small-scale hydraulic systems are preferred over electro-mechanical systems, but for applications where the overall system weight matters the most, electro-mechanical systems work better.

# Contents

|                                                                  |             |
|------------------------------------------------------------------|-------------|
| <b>Acknowledgements</b>                                          | <b>i</b>    |
| <b>Abstract</b>                                                  | <b>ii</b>   |
| <b>List of Tables</b>                                            | <b>vii</b>  |
| <b>List of Figures</b>                                           | <b>viii</b> |
| <b>1 Introduction</b>                                            | <b>1</b>    |
| 1.1 Background . . . . .                                         | 1           |
| 1.2 Literature Review . . . . .                                  | 3           |
| 1.2.1 Efficiency . . . . .                                       | 4           |
| 1.2.2 Power Density . . . . .                                    | 7           |
| 1.2.3 Small Scale Hydraulic Components . . . . .                 | 9           |
| <b>2 Power Density Analysis of Small Scale Hydraulic Systems</b> | <b>16</b>   |
| 2.1 Introduction . . . . .                                       | 16          |
| 2.2 Benchmark System . . . . .                                   | 19          |
| 2.3 Hydraulic System Analysis . . . . .                          | 20          |
| 2.3.1 Hydraulic Cylinder . . . . .                               | 20          |
| 2.3.2 Hydraulic Conduit . . . . .                                | 28          |
| 2.3.3 Hydraulic System Weight . . . . .                          | 32          |

|          |                                                                                                |           |
|----------|------------------------------------------------------------------------------------------------|-----------|
| 2.4      | Electromechanical System Analysis . . . . .                                                    | 33        |
| 2.4.1    | DC Electric Motor . . . . .                                                                    | 33        |
| 2.4.2    | Ball Screw . . . . .                                                                           | 34        |
| 2.4.3    | Wire . . . . .                                                                                 | 36        |
| 2.4.4    | Electromechanical System Weight . . . . .                                                      | 37        |
| 2.5      | Method to Compare Hydraulic and Electromechanical Systems . . . . .                            | 38        |
| 2.6      | Results . . . . .                                                                              | 38        |
| 2.7      | Design Example . . . . .                                                                       | 41        |
| 2.8      | Discussion . . . . .                                                                           | 44        |
| <b>3</b> | <b>Modeling of Tiny Hydraulic Cylinders</b>                                                    | <b>47</b> |
| 3.1      | Introduction . . . . .                                                                         | 48        |
| 3.2      | Cylinder Efficiency Modeling . . . . .                                                         | 48        |
| 3.2.1    | Clearance Seal Model . . . . .                                                                 | 49        |
| 3.2.2    | Rubber O-ring Seal Model . . . . .                                                             | 50        |
| 3.2.3    | Cylinder efficiency model . . . . .                                                            | 54        |
| 3.3      | Simulation Results . . . . .                                                                   | 56        |
| 3.4      | Conclusion . . . . .                                                                           | 56        |
| <b>4</b> | <b>Experimentally Validated Efficiency Models of O-ring Seals for Tiny Hydraulic Cylinders</b> | <b>60</b> |
| 4.1      | Introduction . . . . .                                                                         | 60        |
| 4.2      | Cylinder Efficiency Model . . . . .                                                            | 61        |
| 4.2.1    | Leakage . . . . .                                                                              | 61        |
| 4.2.2    | Friction . . . . .                                                                             | 61        |
| 4.2.3    | Force Efficiency . . . . .                                                                     | 62        |
| 4.3      | Methods . . . . .                                                                              | 63        |
| 4.3.1    | Test Apparatus . . . . .                                                                       | 63        |
| 4.3.2    | Test Protocol . . . . .                                                                        | 65        |

|          |                                                        |           |
|----------|--------------------------------------------------------|-----------|
| 4.4      | Results . . . . .                                      | 66        |
| 4.5      | Discussion . . . . .                                   | 68        |
| 4.5.1    | Seal Leakage . . . . .                                 | 68        |
| 4.6      | Conclusion . . . . .                                   | 70        |
| <b>5</b> | <b>Efficiency Models for Small Hydraulic Pumps</b>     | <b>72</b> |
| 5.1      | Introduction . . . . .                                 | 72        |
| 5.2      | Vane Pump Model . . . . .                              | 73        |
| 5.2.1    | Geometry . . . . .                                     | 73        |
| 5.2.2    | Mechanical Efficiency . . . . .                        | 74        |
| 5.2.3    | Volumetric Efficiency . . . . .                        | 76        |
| 5.2.4    | Overall Efficiency . . . . .                           | 77        |
| 5.2.5    | Model Validation . . . . .                             | 79        |
| 5.3      | Piston Pump Model . . . . .                            | 80        |
| 5.3.1    | Geometry . . . . .                                     | 80        |
| 5.3.2    | Basic Equations . . . . .                              | 82        |
| 5.3.3    | Mechanical Efficiency . . . . .                        | 84        |
| 5.3.4    | Volumetric Efficiency . . . . .                        | 85        |
| 5.3.5    | Overall Efficiency . . . . .                           | 86        |
| 5.3.6    | Model Validation . . . . .                             | 88        |
| 5.4      | Design Case Study . . . . .                            | 89        |
| 5.5      | Discussion . . . . .                                   | 91        |
| <b>6</b> | <b>Design Example: a Hydraulic Ankle Foot Orthosis</b> | <b>93</b> |
| 6.1      | Introduction . . . . .                                 | 93        |
| 6.2      | AFO Configuration Selection . . . . .                  | 95        |
| 6.3      | HFAO Packaging and Integration . . . . .               | 98        |
| 6.4      | HAFO Component Design . . . . .                        | 101       |
| 6.4.1    | HAFO Governing Equations . . . . .                     | 101       |

|          |                                                                       |            |
|----------|-----------------------------------------------------------------------|------------|
| 6.4.2    | HAFO Component Selection . . . . .                                    | 107        |
| 6.5      | Conclusion . . . . .                                                  | 112        |
| <b>7</b> | <b>Dynamic Analysis of HAFO Hydraulic Circuits, Fluids, and Hoses</b> | <b>114</b> |
| 7.1      | HAFO System Hydraulic Circuit Design . . . . .                        | 114        |
| 7.1.1    | Circuit 1: a Simplified EHA Circuit . . . . .                         | 116        |
| 7.1.2    | Circuit 2: Directional Solenoid Valves . . . . .                      | 119        |
| 7.1.3    | Circuit 3: Solenoid Valves and Pilot Check Valves . . . . .           | 121        |
| 7.1.4    | Circuit 4: Pilot-Operated Check Valves . . . . .                      | 123        |
| 7.2      | Hose Effects . . . . .                                                | 125        |
| 7.3      | Fluid Effects . . . . .                                               | 128        |
| 7.4      | Cable Slackness . . . . .                                             | 130        |
| <b>8</b> | <b>Design Guidelines for Small Scale Hydraulic Systems</b>            | <b>133</b> |
| 8.1      | Run at High Pressure . . . . .                                        | 133        |
| 8.2      | Small but not too Small . . . . .                                     | 134        |
| 8.3      | Efficiency Influences Weight . . . . .                                | 135        |
| 8.4      | Design Process Chart . . . . .                                        | 135        |
| <b>9</b> | <b>Conclusions</b>                                                    | <b>138</b> |
| 9.1      | Limitations . . . . .                                                 | 138        |
| 9.2      | Contributions . . . . .                                               | 140        |
|          | <b>References</b>                                                     | <b>141</b> |



# List of Tables

|     |                                                                                       |    |
|-----|---------------------------------------------------------------------------------------|----|
| 1.1 | Specific energy and energy volume density comparison [1] . . . . .                    | 9  |
| 1.2 | Pump comparison [2] . . . . .                                                         | 11 |
| 2.1 | Hydraulic cylinder parameters . . . . .                                               | 22 |
| 2.2 | Symbols used in (2.10) and (2.11) . . . . .                                           | 25 |
| 2.3 | AFO systems weight comparison . . . . .                                               | 44 |
| 3.1 | Parameters to be used in the modelling process . . . . .                              | 49 |
| 5.1 | Vane pump symbols. . . . .                                                            | 75 |
| 5.2 | Piston pump symbols. . . . .                                                          | 81 |
| 5.3 | Pump nominal design parameters. Symbols are defined in Tables 5.1 and<br>5.2. . . . . | 89 |
| 5.4 | Power supply weight (gms) for vane and piston pump configurations. . .                | 91 |

# List of Figures

|     |                                                                                                                                                                                                                                                                |    |
|-----|----------------------------------------------------------------------------------------------------------------------------------------------------------------------------------------------------------------------------------------------------------------|----|
| 1.1 | Power transmission process in a hydraulic power system . . . . .                                                                                                                                                                                               | 1  |
| 1.2 | Tapered clearance seal structure . . . . .                                                                                                                                                                                                                     | 6  |
| 1.3 | Fluid power system components block diagram . . . . .                                                                                                                                                                                                          | 9  |
| 2.1 | Architecture for powered actuation system. Top row is generic, middle row is electromechanical, bottom row is hydraulic. . . . .                                                                                                                               | 19 |
| 2.2 | Ideal hydraulic cylinder used for analysis. . . . .                                                                                                                                                                                                            | 21 |
| 2.3 | Wall loading scenario used to calculate wall thickness. . . . .                                                                                                                                                                                                | 21 |
| 2.4 | Cylinder efficiency as a function of bore size. The plot was generated assuming 500 psi operating pressure and 0.1 m/s rod speed. . . . .                                                                                                                      | 25 |
| 2.5 | Experimentally determined cylinder force efficiency as a function of pressure for two rod speeds. The lines are the predicted efficiency curves from the O-ring model for the extremes of the coefficient of friction. . . . .                                 | 27 |
| 2.6 | Experimentally determined cylinder force efficiency as a function of cylinder bore and two rod speeds. Overlaid are the equivalent results from the O-ring model. . . . .                                                                                      | 27 |
| 2.7 | Comparison between the actual weight and the weight predicted from the theoretical analysis for 187 commercial cylinders. The solid line indicates an exact match between actual and predicted. The inset expands the data for light weight cylinders. . . . . | 29 |

|      |                                                                                                                                                                                                                                                                                                                                              |    |
|------|----------------------------------------------------------------------------------------------------------------------------------------------------------------------------------------------------------------------------------------------------------------------------------------------------------------------------------------------|----|
| 2.8  | Hydraulic conduit efficiency at several pressures and levels of output power, showing that the efficiency of the conduit is high unless the pressure is low. Conduit length: 1 m, conduit inner diameter: 5 mm. . . . .                                                                                                                      | 31 |
| 2.9  | Method for calculating the weight of a hydraulic system. . . . .                                                                                                                                                                                                                                                                             | 32 |
| 2.10 | Motor weight vs. output power. . . . .                                                                                                                                                                                                                                                                                                       | 33 |
| 2.11 | Motor efficiency vs. output power. . . . .                                                                                                                                                                                                                                                                                                   | 34 |
| 2.12 | Ball screw weight vs. rated dynamic load at .01 m (top) and .04 m (bottom) stroke. . . . .                                                                                                                                                                                                                                                   | 35 |
| 2.13 | Method for calculating the weight of an electromechanical system. . . .                                                                                                                                                                                                                                                                      | 37 |
| 2.14 | Hydraulic and electromechanical system weight at several output velocities. Output power: 10 W, stroke: 0.05 m, transmission line length: 0.1 m. The 100 psi, 100 mm/s data point is missing because there is no low pressure, high speed hydraulic system that can match the efficiency of the equivalent electromechanical system. . . . . | 39 |
| 2.15 | Hydraulic and electromechanical system weight at several output velocities. Output power: 100 W, stroke: 0.05 m, transmission line length: 0.1 m. . . . .                                                                                                                                                                                    | 39 |
| 2.16 | Hydraulic and electromechanical system weight at several stroke lengths. Output power: 10 W, velocity: 0.01 m/s, transmission line length: 0.1 m.                                                                                                                                                                                            | 40 |
| 2.17 | Hydraulic and electromechanical system weight at several stroke lengths. Output power: 100 W, velocity: 0.01 m/s, transmission line length: 0.1 m.                                                                                                                                                                                           | 40 |
| 2.18 | Hydraulic and electromechanical system weight at several transmission line lengths. Output power: 10 W, stroke: 0.05 m, velocity: 0.01 m/s. .                                                                                                                                                                                                | 40 |
| 2.19 | Hydraulic and electromechanical system weight at several transmission line lengths. Output power: 100 W, stroke: 0.05 m, velocity: 0.01 m/s. .                                                                                                                                                                                               | 41 |
| 2.20 | Hydraulic and electromechanical system weight at several output powers. Stroke: 0.05 m, velocity: 0.01 m/s, transmission line length: 0.1 m. . . .                                                                                                                                                                                           | 41 |

|      |                                                                                                                                                                                                                      |    |
|------|----------------------------------------------------------------------------------------------------------------------------------------------------------------------------------------------------------------------|----|
| 2.21 | Operating pressure required for the hydraulic system to be the same weight as the equivalent electromechanical system at several output powers. Stroke: 0.05 m, velocity: 0.01 m/s, transmission line length: 0.1 m. | 42 |
| 2.22 | Ankle torque (solid) and velocity (dashed) for one step when walking at normal speed. The vertical dot-dash line marks the peak power point. Data from [3].                                                          | 42 |
| 2.23 | Conceptual design for a hydraulic AFO.                                                                                                                                                                               | 43 |
| 3.1  | Four cylinder configurations with different sealing strategies.                                                                                                                                                      | 49 |
| 3.2  | Parameters illustration for a clearance seal.                                                                                                                                                                        | 50 |
| 3.3  | Pressure-induced (1st row) and velocity-induced (2nd row) gap flow velocity distribution.                                                                                                                            | 51 |
| 3.4  | An O-ring seal before and after installation.                                                                                                                                                                        | 51 |
| 3.5  | Illustration of O-ring contact width and maximum contact pressure.                                                                                                                                                   | 53 |
| 3.6  | Cylinder overall efficiency vs. bore size ( $\delta = 20 \mu\text{m}$ ).                                                                                                                                             | 57 |
| 3.7  | Cylinder overall efficiency vs. bore size ( $\delta = 10 \mu\text{m}$ ).                                                                                                                                             | 57 |
| 3.8  | Cylinder force efficiency vs. bore size ( $\delta = 10 \mu\text{m}$ ).                                                                                                                                               | 58 |
| 3.9  | Volumetric efficiency vs. bore size ( $\delta = 10 \mu\text{m}$ ).                                                                                                                                                   | 58 |
| 4.1  | Pistons with O-ring seals and matching cylinder blocks.                                                                                                                                                              | 63 |
| 4.2  | Cylinder efficiency test stand.                                                                                                                                                                                      | 64 |
| 4.3  | Pressure recorded during a typical characterization trial where the load was descending.                                                                                                                             | 65 |
| 4.4  | Piston position during a slow (1 mm/s) load descent.                                                                                                                                                                 | 66 |
| 4.5  | Cylinder force efficiency with pressure, 4 mm bore.                                                                                                                                                                  | 67 |
| 4.6  | Cylinder force efficiency with pressure, 6 mm bore.                                                                                                                                                                  | 67 |
| 4.7  | Cylinder force efficiency with pressure, 9 mm bore.                                                                                                                                                                  | 67 |
| 4.8  | Cylinder force efficiency with bore size.                                                                                                                                                                            | 68 |
| 4.9  | Piston position during O-ring leak test.                                                                                                                                                                             | 68 |

|      |                                                                                                                                                                                                                                                                                            |     |
|------|--------------------------------------------------------------------------------------------------------------------------------------------------------------------------------------------------------------------------------------------------------------------------------------------|-----|
| 4.10 | Typical Stribeck curve showing how friction depends on speed. Three friction regions are identified: boundary, mixed and fluid, or hydrodynamic. The pistons had lower friction (more efficient) at higher speeds, which indicates moving down the curve in the mixed friction region. . . | 70  |
| 5.1  | Layout of a hydraulic balanced vane pump. . . . .                                                                                                                                                                                                                                          | 74  |
| 5.2  | Illustration of the slip flow differential. . . . .                                                                                                                                                                                                                                        | 76  |
| 5.3  | Efficiency as a function of displacement for a vane pump. . . . .                                                                                                                                                                                                                          | 78  |
| 5.4  | Sensitivity of the hydraulic balanced vane pump efficiency model. . . . .                                                                                                                                                                                                                  | 79  |
| 5.5  | Validation of the efficiency model for the vane pump. . . . .                                                                                                                                                                                                                              | 80  |
| 5.6  | Key geometrical dimensions associated with the piston pump efficiency modeling. . . . .                                                                                                                                                                                                    | 81  |
| 5.7  | Key valve plate dimensions for a axial piston pump. . . . .                                                                                                                                                                                                                                | 83  |
| 5.8  | Efficiency as a function of displacement for a piston pump. . . . .                                                                                                                                                                                                                        | 86  |
| 5.9  | Sensitivity of the hydraulic axial piston pump efficiency model, slipper gap = 6 $\mu\text{m}$ . . . . .                                                                                                                                                                                   | 87  |
| 5.10 | Sensitivity of the hydraulic axial piston pump efficiency model, slipper gap = 8 $\mu\text{m}$ . . . . .                                                                                                                                                                                   | 87  |
| 5.11 | Piston pump efficiency model verification. . . . .                                                                                                                                                                                                                                         | 88  |
| 5.12 | Piston pump weight vs output power. . . . .                                                                                                                                                                                                                                                | 90  |
| 5.13 | Energy density model of LiPo battery. . . . .                                                                                                                                                                                                                                              | 91  |
| 6.1  | Both rotary and linear actuators can power an AFO. . . . .                                                                                                                                                                                                                                 | 95  |
| 6.2  | AFO configuration candidates. . . . .                                                                                                                                                                                                                                                      | 96  |
| 6.3  | Power density comparison of AFO candidates. The weight of the hydraulic motors is large since 68 cc/rev displacement is needed to achieve the desired ankle torque. The piston motor weight was estimated based on the vane motor weight. . . . .                                          | 97  |
| 6.4  | HAFO packaging options. . . . .                                                                                                                                                                                                                                                            | 99  |
| 6.5  | HAFO system rendering. . . . .                                                                                                                                                                                                                                                             | 100 |

|      |                                                                                                                                                       |     |
|------|-------------------------------------------------------------------------------------------------------------------------------------------------------|-----|
| 6.6  | Conceptual rendering of an integrated HAFO actuation system. . . . .                                                                                  | 100 |
| 6.7  | The extreme operating condition during level ground walking – the extreme torque in blue dot and the corresponding velocity in green dot [3]. . . . . | 101 |
| 6.8  | Gear head efficiency as a function of its gear ratio. . . . .                                                                                         | 105 |
| 6.9  | Electric motor efficiency as a function of its output power. . . . .                                                                                  | 106 |
| 6.10 | Energy density model of LiPo batteries. . . . .                                                                                                       | 107 |
| 6.11 | Pump operating conditions to be analyzed. . . . .                                                                                                     | 107 |
| 6.12 | HAFO design candidates. . . . .                                                                                                                       | 109 |
| 6.13 | Weight model of axial piston pumps. . . . .                                                                                                           | 110 |
| 6.14 | Electric DC motor torque density - Maxon Motor data only. . . . .                                                                                     | 111 |
| 6.15 | The average output torque of human ankle joint while walking [3]. . . . .                                                                             | 112 |
| 6.16 | HAFO system final design choice. . . . .                                                                                                              | 113 |
| 7.1  | The hydraulic portion of the HAFO system. . . . .                                                                                                     | 115 |
| 7.2  | SimHydraulics model for the HAFO system. Full page image shown in Appendix 9.2. . . . .                                                               | 117 |
| 7.3  | HAFO hydraulic circuit candidate - a simplified EHA circuit. . . . .                                                                                  | 118 |
| 7.4  | HAFO position tracking result - a simplified EHA circuit. . . . .                                                                                     | 118 |
| 7.5  | HAFO force balancing profile - a simplified EHA circuit. . . . .                                                                                      | 119 |
| 7.6  | HAFO hydraulic circuit candidate - directional solenoid valves. . . . .                                                                               | 120 |
| 7.7  | HAFO position tracking result - directional solenoid valves. . . . .                                                                                  | 120 |
| 7.8  | HAFO force balancing profile - directional solenoid valves. . . . .                                                                                   | 121 |
| 7.9  | HAFO hydraulic circuit candidate - directional solenoid valves and pilot-operated check valves. . . . .                                               | 122 |
| 7.10 | HAFO position tracking result - directional solenoid valves and pilot-operated check valves. . . . .                                                  | 122 |
| 7.11 | HAFO hydraulic circuit candidate - pilot-operated check valves. . . . .                                                                               | 123 |

|      |                                                                                                                                         |     |
|------|-----------------------------------------------------------------------------------------------------------------------------------------|-----|
| 7.12 | PF and DF cylinder chamber pressure profile during a gait cycle - pilot-operated check valves. . . . .                                  | 124 |
| 7.13 | Position tracking result - pilot check valves. The gray oval highlights the glitch during the position tracking. . . . .                | 125 |
| 7.14 | Glitch height as a function of hose dimensions. . . . .                                                                                 | 126 |
| 7.15 | Maximum pump as a function of hose dimensions . . . . .                                                                                 | 126 |
| 7.16 | Index $\zeta$ as a function of hose dimensions. . . . .                                                                                 | 127 |
| 7.17 | Position tracking results with 1 m long and 2 mm wide hoses. . . . .                                                                    | 127 |
| 7.18 | Hose pressure drop as a function of hose dimensions. Inlet pressure = 2000 psi. Inlet flow rate = 2000 rpm $\times$ 0.4 cc/rev. . . . . | 128 |
| 7.19 | Glitch height as a function of fluid properties. . . . .                                                                                | 129 |
| 7.20 | Maximum pump speed as a function of fluid properties. . . . .                                                                           | 129 |
| 7.21 | Index $\zeta$ as a function of fluid properties. . . . .                                                                                | 130 |
| 7.22 | Index $\zeta$ as a function of hydraulic fluids in SimHydraulics library . . . . .                                                      | 131 |
| 7.23 | Position tracking result with DOT 3 brake fluid. . . . .                                                                                | 131 |
| 7.24 | Position tracking result with 50W oil. . . . .                                                                                          | 132 |
| 7.25 | The cable displacements during HAFO operation. . . . .                                                                                  | 132 |
| 8.1  | Design process chart for small-scale hydraulic systems. . . . .                                                                         | 137 |
| 9.1  | SimHydraulics model for the HAFO system. . . . .                                                                                        | 154 |
| 9.2  | SimScape script for the customized cable rod. . . . .                                                                                   | 155 |

# Chapter 1

## Introduction

### 1.1 Background

A minimal hydraulic power system contains six parts: an energy source, a prime mover, a pump, a valve, conduit and an actuator, as shown in Figure 1.1. The energy source, which can be a battery or liquid fuel, provides energy to the prime mover, being an electric motor or an internal combustion engine; the prime mover generates torque to spin the shaft of the pump by converting chemical energy to mechanical power; the pump produces fluid flow and pressure by converting mechanical power to hydraulic power; the valve regulates the fluid flow and pressure; the conduit routs the regulated hydraulic power to the actuator; and the actuator generates mechanical force and speed by converting hydraulic power to mechanical power.

A small-scale hydraulic power system is one that generates power between 10 and 100 watts, while a large-scale system generates power greater than 100 watts. Large-scale hydraulic systems are well-known for their high power-to-weight ratios compared

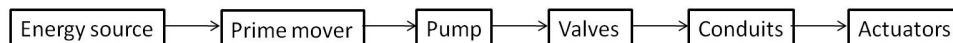


Figure 1.1: Power transmission process in a hydraulic power system



to electro-mechanical systems. To maintain this advantage in small-scale hydraulic systems, new design guidelines are required because properties such as area-to-volume ratio and flow rate requirements change in small-scale hydraulic systems.

The challenge of miniaturizing hydraulic components and systems is not only to satisfy the size and weight requirement, but to achieve reasonable efficiency within a given space. As the components become small, the conventions of efficiency that apply at large scale no longer hold. Force-to-weight still applies at small scales because it still holds that  $\text{Force} = \text{Pressure} \times \text{Area}$ . Efficiency, however, is different because friction and leakage losses depend on circumference while actuation force and speed depend on area. When the components get small, the circumference to area ratio increases, which indicates that their efficiency drops at small-scale.

The efficiency not only determines the amount of output power that can be extracted for a given input power, but also determines the operation time of the system. Moreover, efficient actuators will downsize the pump, which will in turn downsize the power source. Small and efficient components will lead to a portable small-scale hydraulic system with longer operation time. Therefore, new design guidelines that maximizes the power density of small-scale hydraulic components and systems need to be identified. Ultimately, practical applications will benefit from these new design guidelines.

The goal of this thesis was to identify the design guidelines for small-scale hydraulic components and systems. To achieve this goal, the efficiency and weight models for the key components were developed and validated.

Basic analysis such as ring sealing friction formula and cantilever beam failure theory were used to model the efficiency of small-scale hydraulic components. The weight of small-scale hydraulic components was formulated using basic machine design theories such as thin-walled cylinder formula and shaft sizing formula. To validate the efficiency and weight models, experimental data from prototype testings and catalog data for small and large-scale hydraulic components were used.

Small-scale electromechanical systems was used as a comparison baseline for small-scale hydraulic systems. Small-scale electromechanical components are commercially available, so their catalog data was compiled to model their efficiency and weight.

## 1.2 Literature Review

Reviews of large-scale hydraulic technology can be found in [4] and [5, 6]. This section reviews research in the small-scale hydraulic field and identifies open questions and challenges.

Examples of small-scale mobile systems include prosthetic hands [7], orthoses [8], small robots and powered hand tools. All of these systems demand light weight, small size and high efficiency to ease human operation and to reduce energy consumption. To achieve these goals, one has to understand the differences between small-scale and large-scale hydraulic systems. Small-scale hydraulic systems are not simply smaller versions of large-scale hydraulic systems. Though large-scale and small-scale hydraulic systems are both governed by continuum equations, their design principles are different. For example, take a hydraulic cylinder. The cylinder sealing friction force is proportional to the bore size while the cylinder actuation force is proportional to the bore size squared so the ratio between the sealing friction force and the actuation force is anti-proportional to the bore size, as summarized in (1.1) - (1.3).

$$f_{\text{cyl}} \propto B \tag{1.1}$$

$$F_{\text{cyl}} \propto B^2 \tag{1.2}$$

$$\frac{f_{\text{cyl}}}{F_{\text{cyl}}} \propto \frac{1}{B} \tag{1.3}$$

where  $f_{\text{cyl}}$  is the cylinder friction force,  $B$  is the cylinder bore size, and  $F_{\text{cyl}}$  is the cylinder actuation force. To prevent the friction force from dominating, as the bore size scales down alternative design methods for cylinder sealing are required.

### 1.2.1 Efficiency

One challenge in miniaturizing hydraulic systems is to maintain reasonable efficiency. Hydraulic system efficiency is determined by power losses, which originate from sealing friction and leakage. Effects such as vibration and noise also cause power losses, but their effects are small, and will not be considered here.

Physical variables in a hydraulic system can be divided into two categories: across and through [9]. Across variables include rotary torque, linear force and fluid pressure, while through variables include angular speed, linear speed and volumetric flow rate. Power losses in a hydraulic power system can thus be separated into two parts: force transmission losses and speed transmission losses. For example, force transmission losses happen when converting the rotary torque of the electric motor to the hydraulic pressure in the hydraulic pump, and when converting the hydraulic pressure to the linear rod force at the cylinder. These losses can be further understood by reviewing the definitions of force efficiency, volumetric efficiency and overall efficiency, which are illustrated for a hydraulic cylinder in (1.4) - (1.6) [10]

$$\eta_f = \frac{F}{P \cdot A} = \frac{P \cdot A - F_{\text{frict}}}{P \cdot A} \quad (1.4)$$

$$\eta_q = \frac{V \cdot A}{Q} = \frac{V \cdot A}{V \cdot A + Q_{\text{leak}}} \quad (1.5)$$

$$\eta_o = \frac{F \cdot V}{P \cdot Q} \quad (1.6)$$

where  $\eta_f$  is the cylinder force efficiency,  $F$  is the output rod force,  $P$  is the input chamber pressure,  $A$  is the piston area,  $F_{\text{frict}}$  is the sealing friction force,  $\eta_q$  is the cylinder volumetric efficiency,  $V$  is the output rod velocity,  $Q$  is the input fluid flow rate,  $Q_{\text{leak}}$  is the leakage across the seals, and  $\eta_o$  is the cylinder overall efficiency. From (1.4) - (1.6), one can see that

$$\eta_o = \eta_f \cdot \eta_q \quad (1.7)$$

which indicates that the overall efficiency can be separated into force efficiency and volumetric efficiency. The force efficiency is determined by sealing friction and the volumetric efficiency is determined by the leakage across the seals. Since there is a tradeoff between sealing friction and leakage, there is also a tradeoff between force efficiency and volumetric efficiency [10], [11].

### **Friction Losses**

There are two types of friction that causes power losses along the force transmission path: the viscous friction between the wall and the fluid, and the sealing friction between the seal and the wall. The viscous friction in an annular gap can be theoretically quantified [11], while the sealing friction for polymer seals is still a subject of research [12], [13], [14]. Analytical solutions are not available for sealing friction of polymer seals due to its complex mechanism [15], [16]. Empirical sealing friction models are given in [17] and [18], which have coefficients that must be identified experimentally. Recently, numerical simulations have been used to model the sealing friction of polymer seals. An example is the work of Salant and co-workers [19], [20]. Practically, empirical formulas are preferred due to their simplicity [16], [21]. However, these empirical formulas were derived by fitting experimental data instead of using first principles, so they must be validated before being applied to seals of new dimensions.

To increase the efficiency of a small-scale hydraulic system, clearance gaps have been proposed to replace polymer seals [22], [23], [24]. Clearance seals improve force efficiency by trading off the volumetric efficiency. An example of using clearance seals is Airpot cylinder product line [25]. Tapered clearance seals, shown in Figure 1.2, are sometimes used in servo systems where high control precision is required [26], [27]. Liquid seals such as ferrofluid seals are able to improve force efficiency while maintaining reasonable volumetric efficiency [24], [28]. Fluids at 1.6 MPa (230 psi) were successfully sealed with little leakage. In case of using clearance seal, precision manufacturing is necessary as practically 20 micron is the minimum clearance that can be machined [15].

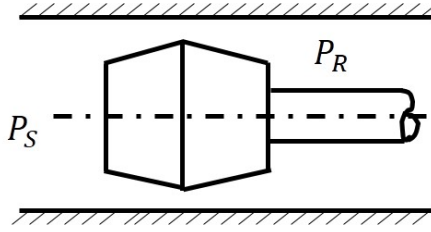


Figure 1.2: Tapered clearance seal structure

### Leakage Losses

Power losses along the speed transmission path are due to leakage through clearance gaps or rubber seals. Analytical solutions for leakage through clearance gaps are available [2, 10, 11]

$$Q_{\text{leak}} = \frac{\pi \cdot B \cdot \delta^3 \cdot \Delta P}{12 \cdot \mu \cdot l} \quad (1.8)$$

where  $Q_{\text{leak}}$  is the leakage across the gap,  $B$  is the bore size,  $\delta$  is the gap size,  $\mu$  is the fluid dynamic viscosity,  $\Delta P$  is the pressure drop across the piston and  $l$  is the gap width.

Solution for leakage through rubber seals is still a subject of research. Reviews of progresses made and problems existing in sealing technology can be found in [29] and [30]. Previous research assumed full hydrodynamic lubrication condition and perfectly smooth seal surface [31], [32], [33], which were shown incomplete assumptions by Salant [19], [20]. As pointed out in [15] and [16] hydrodynamic lubrication condition only occurs in certain conditions, e.g. high viscosity fluid running at high speeds. It was found that mixed lubrication is the most common lubrication condition in hydraulic systems. In mixed lubrication condition, the load is partly supported by the solid contact of asperities and partly by hydrodynamic oil film [34]. It was also found that sealing surface roughness plays an important role in determining seal performance. Empirical formulas for leakage through polymer seals are available [35, 36, 37, 38], which also must be validated before being applied to seals of new dimensions.

## Compressibility

Compressibility is another factor that decreases hydraulic power system volumetric efficiency. Bulk modulus can be used to characterize the compressibility effect for hydraulic systems. Bulk modulus is defined as

$$\beta = -\frac{\Delta P}{\Delta V/V} \quad (1.9)$$

where  $\beta$  is the bulk modulus,  $\Delta P$  is the change in pressure applied to hydraulic oil volume,  $\Delta V$  is the hydraulic oil volume change and  $V$  is the original hydraulic oil volume. Typical hydrocarbon oil has a bulk modulus of 1860 MPa when devoid of entrained air [39]. Fluid containers and undissolved gas may significantly reduce the system bulk modulus, so effective bulk modulus is used in hydraulic power systems, as defined in (1.10).

$$\frac{1}{\beta_e} = \frac{1}{\beta_l} + \frac{1}{\beta_c} + \frac{V_g}{V_t} \cdot \frac{1}{\beta_g} \quad (1.10)$$

where the subscripts  $l$ ,  $c$  and  $g$  refer to the liquid, container and gas.  $V_t$  is the initial total volume of the container  $V_t = V_l + V_g$ .

The effective bulk modulus will be less than any of the values  $\beta_l$ ,  $\beta_c$  or  $\frac{V_t}{V_g} \cdot \beta_g$ .

### 1.2.2 Power Density

Besides efficiency, mass is another major concern for portable applications. Efficiency and mass are related by power density, which is defined as

$$\psi = \frac{P_{\text{out}}}{m} = \frac{P_{\text{in}} \cdot \eta}{m} \quad (1.11)$$

where  $\psi$  is the power density,  $P_{\text{in}}$  is the input power,  $\eta$  is the system efficiency and  $m$  is the mass.  $\psi$  is an important index since it tells how much power can be generated per

unit mass. Portability is usually required for small-scale hydraulic power systems, so  $\psi$  should be maximized.

For the same input power, efficiency must increase or mass must decrease to increase output power density. To increase efficiency, power losses have to be decreased. This can be done by decreasing friction and leakage. Other methods of increasing system efficiency include load sensing [10], energy harvesting [40], designing more efficient controllers and building more efficient pumps, valves, conduits and actuators. While these methods have been successful in large-scale systems, their effectiveness needs to be proven in small-scale systems.

To decrease mass, one has to look at the relationship between system operating conditions and the system mass. Take a hydraulic cylinder. Suppose the cylinder is in extension mode, then the rod force and the cylinder operating pressure is related by

$$F = \frac{\pi}{4} \cdot P \cdot B^2 \quad (1.12)$$

where  $F$  is the rod force,  $P$  is the operating pressure and  $B$  is the bore size.  $B$  becomes smaller in small-scale systems, which means  $P$  must go up to get the same rod force. Higher operating pressure requires thicker containing wall, so a systematic analysis must be conducted to determine the net effect on mass caused by increasing the operating pressure.

A common way of reducing cylinder mass is replacing its structural material with a lighter one. Steel is a common material for hydraulic cylinders, while copper is sometimes used as an alternative [41]. Aluminum is lighter than steel, but its yield strength is lower. Lower yield strength implies thicker wall to sustain the same operating pressure, so whether replacing steel with aluminum gives lighter mass requires calculation. Another material is plastic. Plastic is lighter than steel, but its heat transfer is worse, which can cause heat accumulation. Other materials of interest are glass and composite.

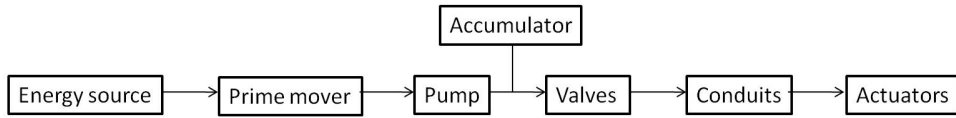


Figure 1.3: Fluid power system components block diagram

Table 1.1: Specific energy and energy volume density comparison [1]

| Source                  | EM (MJ/kg) | EV (MJ/L) |
|-------------------------|------------|-----------|
| Battery, NiCd           | 0.1        | 1.1       |
| Battery, NiMH           | 0.4        | 1.6       |
| 4350 psi compressed air | 0.5        | 0.2       |
| Battery, Li-ion         | 0.7        | 3.6       |
| Hydrogen peroxide       | 2.7        | 3.8       |
| Battery, Li-air         | 3.6        | N./A      |
| Methanol                | 19.7       | 15.6      |
| Ethanol                 | 30.0       | 24.0      |
| Vegetable oil           | 42.2       | 33.0      |
| Diesel fuel             | 46.2       | 37.3      |
| Gasoline                | 46.4       | 34.2      |

Choice of material is also affected by corrosion, temperature condition and machinability. Methods of selecting materials are provided in [42].

### 1.2.3 Small Scale Hydraulic Components

#### Energy Source

The most common energy source for hydraulic power systems are battery and hydrocarbon fuel. The specific energy **EM** (MJ/kg) and energy volume density **EV** (MJ/L) of various batteries and fuels are listed in Table 1.1. It can be seen that the specific energy of the fuel is much higher than that of the battery, so fuel driven devices such as internal combustion engines are potentially better candidates for small-scale hydraulic systems.



## **Prime Mover**

Though liquid fuel has higher specific energy density than batteries, it is hard for small-scale internal combustion engines to achieve the same efficiency as small-scale electric motors. Many problems exist when building such devices. In internal combustion engines the generated power is proportional to volume, while the heat dissipation is proportional to the surface area. As the size of the internal combustion engine decreases, heat losses become detrimental since the surface area to volume ratio increases. Quenching due to thermal losses may occur in small-scale engines such as hot gas engines [43] or HCCI engines [22], [44], [45].

Clearance seal is commonly used in tiny engines to avoid the detrimental effect brought by polymer seals. Tiny engines are commonly designed to operate at high speed to alleviate leakage through clearance seals, but high speed can bring several problems such as high viscous friction force, and incomplete chemical reaction [22]. Therefore, system level analysis are needed to identify the optimal operating speed.

## **Pumps**

A hydraulic pump is a device used to move hydraulic oil. There are three main types of positive displacement hydraulic pumps: gear pumps, vane pumps and piston pumps. A comparison among these three types of pumps is given in Table 1.2. The comparison is based on large-scale pumps, but the tradeoff maintains for small-scale pumps. Pump efficiency is primarily governed by the lubricating conditions. When thin fluid film forms in between moving parts, the friction losses are governed by viscous friction. When direct body-to-body contact forms between moving parts, Coulomb friction will dominate. Leakage losses occur in both scenarios, but are anti-proportional to the friction losses.

In gear pumps the friction losses are high since the gap between the gear and the sealing wall can not be hydro-statically balanced, which leads to the lowest efficiency.

Table 1.2: Pump comparison [2]

| <b>Type</b> | <b>Efficiency</b> | <b>Construction</b> | <b>Cost</b> | <b>Size</b> | Mass   |
|-------------|-------------------|---------------------|-------------|-------------|--------|
| GEAR        | Low               | Easy                | Low         | Medium      | Medium |
| VANE        | Medium            | Medium              | Medium      | Small       | Small  |
| PISTON      | High              | Difficult           | High        | Large       | Large  |

In vane pumps, the gap between the vane tip and the cam ring can only be partially hydro-statically balanced since the vanes need to contact the cam ring to achieve fluid sealing, thus giving a medium pump efficiency. In piston pumps, the gaps between the slipper and swash plate, and between the cylinder wall and the valve plate can be hydro-statically balanced. In addition, the gap between the piston and the cylinder wall can be made very small due to the cylindrical shape of the piston. These facts make the piston pump the most efficient among all three types of pumps. As to the size, the vane pump only has one moving part, the rotor-vane assembly, which means it has the most favorable displacement-volume ratio since the least volume is allotted to functions unproductive in the delivery process.

To formulate the power density of each pump, the pump efficiency must be modeled. Current pump efficiency models are empirical. These efficiency models included coefficients that must be identified experimentally. Efficiency models of this kind can be found in [2], [10], [11], [46], [47], [48]. In 2005, researchers derived analytical efficiency models for vane pumps [49] and axial swash plate piston pumps [50, 51]. These analytical models do not have coefficients that must be identified experimentally so that they can be used to identify optimal operating conditions for both existing and non-existing pumps. However these models are incomplete. For example, the vane pump efficiency model only considered the friction between the vanes and the cam ring [49]. Both the leakage and the friction between the rotor and the side plates are missing in the model. A complete pump efficiency model is needed to develop design guidelines for small-scale hydraulic pumps, and such a model is presented in Chapter 5 of this thesis.

To increase the power density of a small-scale hydraulic power system, the power

density of the hydraulic pump should be increased. Possible ways include increasing the pump efficiency or decreasing the pump weight. Though hydraulic pumps have higher power density than electric motors, prime movers are needed to drive the pump shaft, which offsets the power density advantage. Piezoelectric pump [52], SMA pump [53] and air turbine [54] are alternative candidates for small-scale hydraulic power system.

### Valves

For mobile applications such as prosthetic hands, orthoses, small robots and powered hand tools, the load requirements vary with time, which demands varying fluid flow from the pump. Variable fluid flow is typically accomplished by varying the swash plate angle [55] of an axial piston pump. These techniques require moving a significant mass, which leads to a low control bandwidth, as well as bulky and expensive control equipment. Flow can also be varied using metering valve control, which usually consists of diverting excess flow across a pressure relief valve. This involves little moving mass, so a high bandwidth can be achieved. However, the diverted flow is bled off at a high pressure, which results in a large amount of wasted energy. Four-way spool valves are the common control valve for hydraulic circuitry, but their efficiency can be as low as 12% [10].

To improve the efficiency of a hydraulic valve, one has to look at the governing equation for a valve, which is the orifice equation (1.13) [9].

$$Q = C_d \cdot A \cdot \sqrt{\frac{2 \cdot \Delta P}{\rho}} \quad (1.13)$$

The orifice equation involves flow coefficient  $C_d$ , which is usually assumed to be a constant value 0.62, independent of Reynolds number. However, for very small orifice openings,  $C_d$  varies significantly and can result in substantial error if assumed constant. The turbulent flow assumption may become invalid when the orifice is very small, as happens in a barely open poppet valve.  $C_d$  is a function of Reynolds number and the

orifice geometries that have to be determined experimentally [11]. Wu et al. proposed a closed-form empirical formula for  $C_d$  that can be used in dynamic simulations [56].

Alternative way of regulating a hydraulic power system is to use an electric motor to control the speed of the pump and to control the motor with a high efficiency PWM motor driver. Since the inertia of the moving part of a small-scale motor is small, a high control bandwidth is theoretically achievable. This being said, the inertia of the pump rotor attached to the electric motor shaft can be significant. So reducing the weight of the pump rotor is important to achieve high control bandwidth.

Eliminating the hydraulic control valves can decrease the weight and size of the system, and ease the components integration process, which is essential for a portable device. Shifting all the controls to the electric motor will also simplify the design of the hydraulic system.

### **Accumulators**

Hydraulic accumulators are used for temporarily storing pressurized oil [9]. The oil enters a chamber and acts against a piston or a bladder to raise a weight, compress a spring or a gas. Heat generated in accumulator during air compression and expansion decreases efficiency. Many methods have been proposed to keep the air compression and expansion process as isothermal as possible. An example is to put elastomeric foam in the accumulator [57]. Small-scale hydraulic power systems can be approximately isothermal due to bigger area-to-volume ratio, which is advantageous for accumulator design purpose. Accumulators have lower energy density than batteries[1], but their power density is excellent, and can be used for bursts of power. One potential application would be the toe-off burst for an ankle exoskeleton.

### **Conduits**

Conduits are the pipe or channel for conveying hydraulic oil. Hydraulic pipes can cause problems such as producing larger system stiffness compared to electrical wires [58],

increasing system weight [59] and introducing time delay during pressure buildup. Integrating system components into a single manifold can eliminate hydraulic pipes, which leads to weight and size reduction. Given the limited space in small-scale hydraulic systems, drilling holes in a manifold gives more flexibility than using pipes to route the fluid. 3D metal printing is another way to realize complex manifold design. Components integration also decreases the number of leaking points and eases maintaining procedure. An example of components integration is the small electro-hydraulic actuator (EHA) from Parker Oildyne [60]. Though components integration has many benefits, one cannot completely eliminate hydraulic pipes when the actuator is far from the power supply.

A major drawback of small diameter hydraulic pipes is the pressure drop along the pipe. The pressure drop is proportional to the pipe length and is anti-proportional to the pipe diameter [61]. To decrease the power losses along a pipe, short, large diameter pipe should be used. On the other hand, large diameter pipes don't work for small-scale applications, so system level analysis is needed to trade off weight against efficiency.

## **Cylinders**

Major challenges in miniaturizing cylinders are to achieve a reasonable efficiency and designing appropriate rod structure.

Cylinder efficiency drops as bore size scales down. This is mainly caused by polymer seal friction. One way to increase cylinder efficiency is to find alternative sealing methods. Clearance seal is an option, but it cannot be used to seal hydraulic cylinder rod because it will cause leakage into surrounding environment. Ferrofluid seal is a promising option for sealing rod, though it is still a subject of research [24, 28, 62]. 230 psi pressure fluid can be kept in without leakage by using ferrofluid seal. Single ferrofluid seal becomes problematic when pressure is higher than 230 psi. Multistage ferrofluid seals have to be used to achieve higher sealing pressure [63].

Cylinder rod design becomes challenging when tiny bore cylinder is operating at

high pressure, because the rod can buckle. Two methods can be used to prevent rod buckling: first, find a stronger rod structure; second, make the cylinder always operate in retraction mode. When a cylinder retracts the rod is in tension. The rod structures are way stronger in tension than in compression because in compression they can buckle way before the material hits its yield limit. One possibility for the second method is to use wire-type rod [64].

### **Controllers**

Basic controllers such as PI controllers do not always work for fluid power systems due to the nonlinear characteristics of fluid power components [65]. Advanced controllers such as adaptive and robust controllers may be necessary to satisfy stability and transient response requirements. A review of fluid power system controller design was given in [65], in which the author pointed out the importance of fluid power system modeling software for controller design [66], [67].

Control bandwidth is an important metric for mobile applications since timely response is needed to make the system function in a desired way. Control bandwidth is determined by both the mass and the power of the system.

## Chapter 2

# Power Density Analysis of Small Scale Hydraulic Systems

*This chapter was published in Journal of Mechanical Design, vol. 135, no. 9, pp. 1-11, 2013.*

### 2.1 Introduction

Hydraulic fluid power systems are well known for their high power density [41, 68]. This advantage is best illustrated in applications such as excavators and heavy manufacturing equipment that require extremely large power and force. Hydraulics is the only practical way to attain these levels of force and power while at the same time being relatively light weight compared to the equivalent electromechanical system. One reason for the high power density of hydraulics is that fluid power cylinders are inherently low-velocity, high-force actuators, which is a good match to the requirements for construction, agricultural and manufacturing heavy equipment. Contrast this with electric motors, which are high-velocity, low torque actuators, that require a transmission such as a gear head or a lead screw to match their optimal operating point to the application. At high forces and torques, the weight of the transmission ends up being a significant fraction

of the actuator package weight. A second reason for the high power density is that exceptionally high pressures can be generated. For example, the hydraulic pistons on an excavator operate as high as 380 bar (5500 psi).

An advantage of hydraulics is that the source of pressurized fluid can be housed in a base station and flexible hoses used to transport the fluid to light weight cylinders located at the periphery of the machine. For example, an excavator has actuators to control the boom, stick and bucket with bulky power supply, reservoir and accumulators placed in the house. The proximal actuators carry the load of the distal. When the excavator arm is fully extended, the bucket actuator at the end of the arm causes large moments at the joint connecting the boom to the house, which requires a powerful boom actuator. If the bucket actuator is a cylinder, the weight of the actuator is small compared to the bucket. If the bucket actuator is electromechanical, the weight of the electric motor and its associated transmissions, both of which must be placed at the joint, can be significant.

The power density of electromechanical systems has an upper limit because of inherent characteristics such as magnetic saturation. In contrast, the power density of hydraulic systems has no inherent upper limit and can be increased by simply increasing the pressure. The maximum power density in a hydraulic system is largely determined by the design of the containing structures and the seals.

There has been recent interest in portable, wearable powered systems including powered exoskeletons and powered orthotics [69, 70]. Examples of mobile systems in the 10 to 100 W range include ankle foot orthotics, small robots and powered hand tools. These devices are usually powered by electromechanics, typically a lithium-ion battery, DC motor and transmission. Little work has been done on using hydraulics for these applications because off-the-shelf tiny hydraulic components do not exist.

Love [7] demonstrated an application of small scale hydraulics by prototyping a prosthetic finger. Pressure as high as 138 bar (2000 psi) was used to operate 4 mm hydraulic cylinders. Another example is a novel endoscope[58]. Two systems were



studied, hydraulics and electric. The results showed that the hydraulic system had larger output force for the same space.

A barrier for increased hydraulic power density at reasonable efficiency is the seals. Too tight and friction dominates. Too loose and the pressurized fluid will leak past the seal. Volder et al. developed a ferrofluid seal for microactuators that was able to seal to 1.6 MPa (230 psi) without leakage[23, 24], but this approach does not work at higher pressures.

While microfluidics have advanced, they do not inform our problem as microfluidic systems operate well under 1 W and our systems of interest are 10 to 100 W. Reviews of microfluidics components are given in [71, 72, 73]. As shown in [73], micro fluid power cylinders can generate 1 to 10 N but their strokes are under 10 mm.

Designers might chose hydraulics for tiny, mobile powered systems because the same power density advantage of hydraulics over electromechanical should hold for a powered orthosis as it holds for an excavator. The story, however, is complex because the scaling laws are not intuitive. For example, in a cylinder, force is proportional to area while weight is proportional to volume. Surface effects such as friction drag of seals and viscous drag of gaps become significant at small bores and impact overall efficiency. On the other hand, the thickness, and thus the weight, of a cylinder wall required to contain a fixed pressure goes down with bore. The final weight of a hydraulic system at small scale cannot be determined by proportionally scaling the weight of a large system and determining for equal efficiency, which is lighter a fluid power or an electromechanical system for a tiny system cannot be answered using intuition.

The aim of this study was to use first principles to understand how the weight and other properties of hydraulic systems change with size and to answer the question, “When is a hydraulic solution lighter than an electromechanical solution for tiny, powered systems?” Our goal was to provide guidelines that mechanical designers could use at the early stages of evaluating architectures for small systems. Empirical and

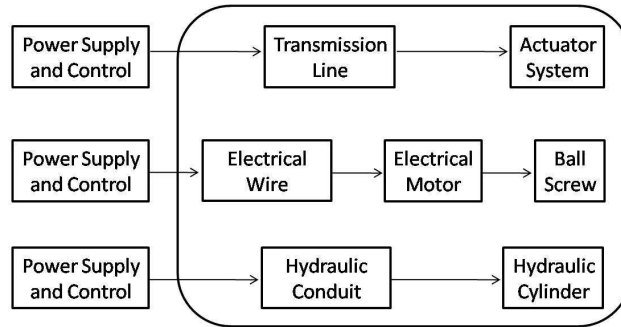


Figure 2.1: Architecture for powered actuation system. Top row is generic, middle row is electromechanical, bottom row is hydraulic.

analytical equations were used to model hydraulic and electromechanical systems, connecting the methods to real components wherever possible. The result of the analysis showed that for equal output power and system efficiency, a hydraulic solution will be lighter than an electromechanical solution only if the hydraulic system operates at high pressure.

## 2.2 Benchmark System

The top row of Fig. 2.1 illustrates the architecture of a generic mobile actuation system that contains a power supply, a means of control, a transmission line and an actuator located at the end-point. For this study, we considered systems that delivered force and velocity along a linear axis. For example, this could be a powered knee prosthesis with the joint driven by a linear actuator mounted behind the knee or a tiny powered gripper driven by a linear actuator.

The electromechanical realization (middle row of Fig. 2.1) includes a battery power supply, a PWM motor controller, wire, a brushed or brushless DC electric motor and a ball screw to convert the high velocity, low torque output of the motor to a low velocity, high force linear output. The ball screw was chosen because it is lighter and more efficient than the equivalent gear box, and it converts rotary to linear motion, which

provides a fair comparison to the hydraulic system. The hydraulic version (bottom row of Fig. 2.1) includes a battery or internal combustion engine driven pump to generate pressured fluid, a servovalve, pipe or hose and a hydraulic cylinder. Other realizations are possible.

Our analysis only considered the transmission line plus actuator system, the circled components in Fig. 2.1. These are the parts of the system that must be located at the point of mechanical output where weight is of greatest concern. For example, for a portable hand tool, the power supply and control can be placed in a backpack or tool belt, but the transmission line and actuator system must be held in the hand. In a real mobile system, the power supply will contribute significantly to the weight and in a real system, the control means will contribute significantly to the efficiency. Comparing electromechanical and hydraulic endpoint components, however, still provides valuable information to the designer looking to minimize weight at the endpoint.

## 2.3 Hydraulic System Analysis

The objective of the hydraulic system analysis was to estimate the weight of an ideal hydraulic cylinder plus the weight of ideal conduit to predict the total weight for a hydraulic system that delivers a specified mechanical force and power output. The weight of components was estimated from a set of theoretical equations developed using basic physics of fluids and solid mechanics.

### 2.3.1 Hydraulic Cylinder

The simplified hydraulic cylinder used for analysis is illustrated in Fig. 2.2 and its associated parameters are defined in Table 2.1. The cylinder has bore  $B$ , stroke  $S$  and rated maximum pressure  $P_r$ . The piston is a disk of uniform thickness  $t_1$  and the cylinder housing is a capped tube with barrel wall thickness  $t_2$  and end cap thicknesses  $t_3$  and  $t_4$ . O-ring seals are assumed for piston and rod. While large hydraulic cylinders

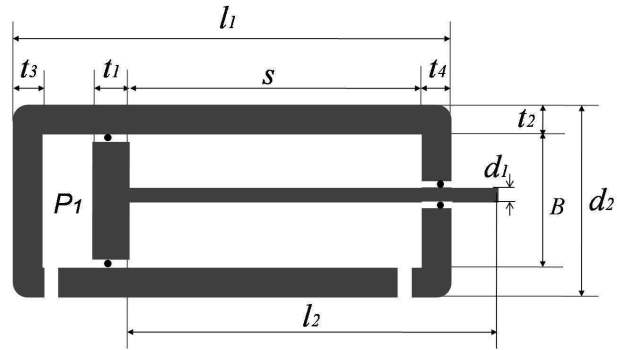


Figure 2.2: Ideal hydraulic cylinder used for analysis.

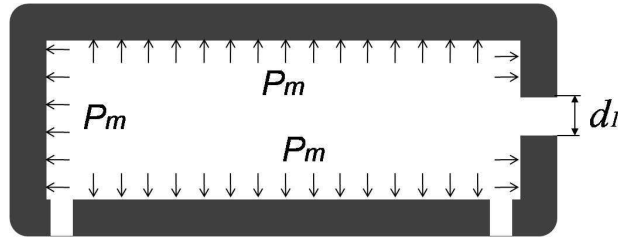


Figure 2.3: Wall loading scenario used to calculate wall thickness.

use a layered arrangement of cup and backing seals, for tiny cylinders, a simple O-ring is an appropriate design choice. Only uni-direction extension motion is considered with cap side pressure  $P_1$  and rod side pressure zero.

### Cylinder and Piston Wall Thickness

The pressure loading scenario to calculate the required cylinder wall and the piston thickness is shown in Fig. 2.3 where the cylinder rated pressure  $P_m$  acts everywhere on the wall. The end wall calculations assumed a fixed displacement boundary condition along the end wall circumference. The piston thickness calculation assumed that the rod was fixed and the  $P_m$  was distributed uniformly across the cap side of the piston and zero pressure on the rod side. These are all worst-case loading conditions.

The cylinder circumferential wall thickness was calculated using the equation for a

Table 2.1: Hydraulic cylinder parameters

| <i>VAR</i> | <i>DESCRIPTION</i>                      | <i>UNIT</i>       |
|------------|-----------------------------------------|-------------------|
| $B$        | bore                                    | m                 |
| $S$        | stroke                                  | m                 |
| $l_1$      | cylinder length                         | m                 |
| $l_2$      | rod length                              | m                 |
| $t_1$      | piston thickness                        | m                 |
| $t_2$      | cylinder circumferential wall thickness | m                 |
| $t_3$      | left end wall thickness                 | m                 |
| $t_4$      | right end wall thickness                | m                 |
| $d_1$      | rod diameter                            | m                 |
| $d_2$      | outer diameter                          | m                 |
| $P_m$      | maximum allowable fluid pressure        | Pa                |
| $P_1$      | cylinder left chamber pressure          | Pa                |
| $S_y$      | cylinder material yield strength        | Pa                |
| $E$        | cylinder material Young's modulus       | Pa                |
| $\rho$     | cylinder material density               | Kg/m <sup>3</sup> |
| $\nu$      | cylinder material Poisson's ratio       | —                 |
| $N$        | design safety factor                    | —                 |

thin-walled pressure vessel [74]

$$t_2 = \frac{N \cdot P_m \cdot B}{2S_y} \quad (2.1)$$

which is valid for  $t_2 < B/6$ . The cylinder end wall thicknesses  $t_3$  and  $t_4$ , and the piston thickness  $t_1$  were calculated using thin plate formulas [75]

$$t_1 = \sqrt{\frac{3NP_m G_1 \nu}{4S_y}} \quad (2.2)$$

$$t_3 = \sqrt{\frac{3\pi B^2 NP_m (1 + \nu)}{32\pi S_y}} \quad (2.3)$$

$$t_4 = \sqrt{\frac{3NP_m G_2}{4\nu S_y}} \quad (2.4)$$

where  $G_1$  and  $G_2$  are

$$G_1 = \frac{4B^4(1 + \nu)\log\frac{B}{d_1} + 4\nu B^2 d_1^2 + d_1^4(1 - \nu) - B^4(1 + 3\nu)}{4\nu(B^2 - d_1^2)}$$

$$G_2 = \frac{d_1^4(1-\nu) - 4d_1^4(1+\nu)\log\frac{B}{d_1} + B^2d_1^2(1+\nu)}{4B^2(1-\nu) + 4d_1^2(1+\nu)} + \frac{B^2}{4} - \frac{d_1^2}{2}$$

The thin plate formulas are valid for plate thickness that are less than 1/4 of the plate diameter. The formula used to determine  $t_4$  was that for a round plate containing a central hole.

Using the material yield strength <sup>1</sup> to determine the minimum thickness of a cylinder is a simplification. For larger cylinders, expansion of the cylinder when pressurized due to the elasticity of the material matters because a slight increase in bore will cause leakage past the piston seal. Therefore it is common practice to design walls that are thick enough for the expansion to be insignificant. As the bore size decreases, so does the expansion so for tiny cylinders with thin walls the increased leakage is insignificant.

### Rod Diameter

The rod must be sized so that it will not buckle under the maximum compressive load. The required rod diameter was calculated using Euler and JB Johnson buckling formulas [75], assuming that the rod was fully extended, loaded in compression and carrying the piston force at the maximum rated pressure. The slenderness ratio  $\frac{l_2}{\rho_1}$  dictates whether the Euler or the JB Johnson formula is appropriate. The critical rod slenderness ratio is

$$\left(\frac{l_2}{\rho_1}\right)_{\text{crit}} = \sqrt{\frac{2\pi^2 E}{S_y}} \quad (2.5)$$

where  $\rho_1 = d_1/4$  for a solid round rod. For a slenderness ratio less than the critical value the JB Johnson formula was used

$$d_1 = \sqrt{\frac{4NP_m\pi(B/2)^2\eta_f}{\pi S_y} + \frac{S_y l_2^2}{2\pi^2 E}} \quad (2.6)$$

---

<sup>1</sup> For dynamic applications with cyclic nature, the fatigue strength should be used to judge the strength of the cylinder wall and pipe, and in the case of the cylinder wall, stress concentrations must also be considered. Additionally, a higher safety factor such as 3 or 4 should be considered.

and for other cases, the Euler formula was used

$$d_1 = \left( \frac{32Nl_2^2 P_m \pi (B/2)^2 \eta_f}{\pi^3 E} \right)^{\frac{1}{4}} \quad (2.7)$$

### Cylinder Efficiency

The force in the rod is less than the pressure times the area of the piston because of the friction in the piston and rod seals. The cylinder force efficiency,  $\eta_f$  is

$$\eta_f = \frac{F_r}{P_1 A_1} \quad (2.8)$$

where  $F_r$  is the rod compressive force,  $P_1$  is the cap side pressure and  $A_1$  is the cap side piston area [10].

The velocity of the rod is less than the flow divided by the area of the piston because of the leakage through the piston and rod seals. The cylinder volumetric efficiency,  $\eta_q$  is

$$\eta_q = \frac{V_r}{Q/A_1} \quad (2.9)$$

where  $V_r$  is the rod velocity and  $Q$  is the flow into the cylinder [10].

Equations (2.10) and (2.11) are approximations that describe the seal friction [12] and leakage [37, 38] for a rubber O-ring seal with variables defined in Table 2.2.

$$F_s = f_s \cdot \pi \cdot D \cdot d \cdot E_s \cdot \epsilon \cdot \sqrt{2\epsilon - \epsilon^2} \quad (2.10)$$

$$Q_s = 2.99 \cdot \pi \cdot D \cdot \mu^{0.71} \cdot U_{hc}^{1.71} \cdot \delta_m^{-0.71} \cdot s_0^{0.29} \quad (2.11)$$

As described in references [12, 37, 38], the effect of pressure across the seal appears through  $f_s$ , which varies with pressure because the O-ring tends to extrude into the gap at higher pressure causing higher friction, and in the  $\delta_m$  and  $s_0$  terms for leakage.

Applying (2.10) and (2.11) for the piston and the rod yields the estimation of the cylinder force, volumetric and overall efficiency

$$\eta_f = \frac{P_1 A_1 - F_{sp} - F_{sr}}{P_1 A_1} \quad (2.12)$$

Table 2.2: Symbols used in (2.10) and (2.11)

| <i>VAR</i> | <i>DESCRIPTION</i>                  | <i>UNIT</i>       |
|------------|-------------------------------------|-------------------|
| $F_s$      | friction force piston with seal     | N                 |
| $f_s$      | O-ring seal friction coefficient    | —                 |
| $D$        | piston or rod diameter              | m                 |
| $d$        | O-ring cross-sectional diameter     | m                 |
| $E_s$      | O-ring Young's modulus              | Pa                |
| $\epsilon$ | O-ring squeeze ratio                | —                 |
| $Q_s$      | leakage across sealed piston or rod | m <sup>3</sup> /s |
| $\mu$      | hydraulic fluid dynamic viscosity   | Pa·s              |
| $U_{hc}$   | piston velocity                     | m/s               |
| $\delta_m$ | maximum O-ring contact stress       | Pa                |
| $s_0$      | O-ring contact width                | m                 |

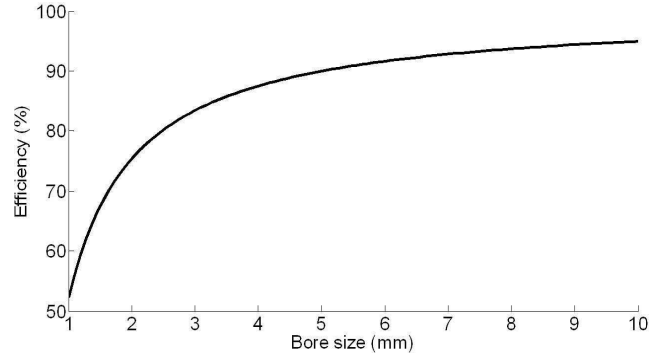


Figure 2.4: Cylinder efficiency as a function of bore size. The plot was generated assuming 500 psi operating pressure and 0.1 m/s rod speed.

$$\eta_q = \frac{V_r A_1}{V_r A_1 + Q_{sp} + Q_{sr}} \quad (2.13)$$

$$\eta_{hc} = \eta_f \cdot \eta_q \quad (2.14)$$

where  $F_{sp}$  is piston seal friction force,  $F_{sr}$  is rod seal friction force,  $V_r$  is rod velocity,  $Q_{sp}$  is piston seal leakage and  $Q_{sr}$  is rod seal leakage.

As shown in Fig. 2.4, cylinder efficiency is a strong function of bore size for smaller cylinders. This is because friction and leakage are a function of piston diameter while force and flow are a function of piston area.



## Cylinder Weight

The volume of the cylinder is

$$V_{\text{cyl}} = \frac{\pi}{4} \left[ (d_2^2 - B^2)l_1 + B^2(t_3 + t_1 + t_4) + d_1^2 t_2 - \Delta_V \right] \quad (2.15)$$

where  $\Delta_V$  are the adjustments to the volume due to the inlet, outlet and rod openings. For simplicity, only the rod opening volume will be included as the inlet and outlet openings is balanced by the volume of fittings.

$$\Delta_V = d_1^2 \cdot t_4 \quad (2.16)$$

Assuming the same material is used for the cylinder wall, piston and rod, the weight of the cylinder is

$$M_{\text{cyl}} = \rho \cdot V_{\text{cyl}} \quad (2.17)$$

## Validation

To validate the O-ring friction (2.10) and leakage (2.11) models, a test stand was built to collect corresponding experimental data for 4, 6 and 9 mm cylinders. A single O-ring seal was mounted on a ram, which was used to raise a constant load. The cylinder chamber underneath the ram was pressurized by a small hydraulic pump. When the cylinder reached full extension, the pump was shut off and a needle valve cracked to create different ram descending speeds at constant chamber pressure. The chamber pressure and the ram speed were sensed by a pressure transducer and a linear potentiometer whose output was conditioned and sampled at 100 Hz.

The comparison between the measured and the theoretical O-ring force efficiency for the 9 mm bore cylinder is shown in Fig. 2.5, and is representative of the data for the 6 mm and 4 mm cylinders. In Fig. 2.5, the minimum and maximum theoretical efficiency lines were generated using the maximum and the minimum reasonable friction coefficient

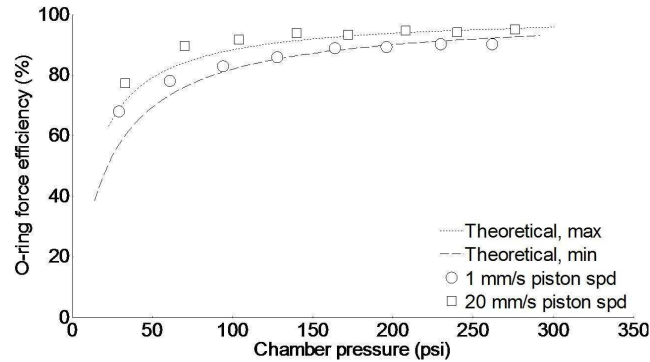


Figure 2.5: Experimentally determined cylinder force efficiency as a function of pressure for two rod speeds. The lines are the predicted efficiency curves from the O-ring model for the extremes of the coefficient of friction.

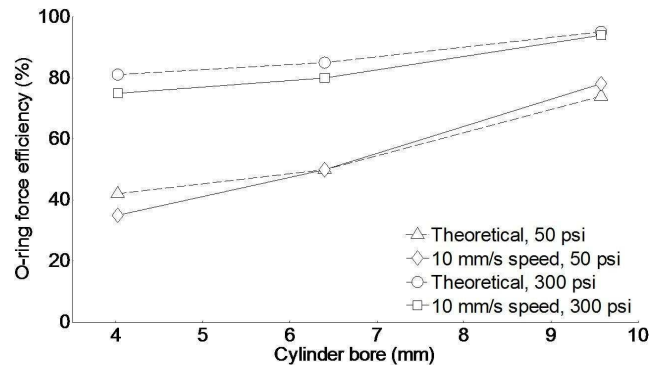


Figure 2.6: Experimentally determined cylinder force efficiency as a function of cylinder bore and two rod speeds. Overlaid are the equivalent results from the O-ring model.

$f_s$  between the O-ring and the cylinder wall. The higher piston speeds resulted in higher efficiency, which indicates that the lubrication between the O-ring and the cylinder wall shifted from mixed lubrication to hydrodynamic lubrication as the piston speed changed from 1 mm/s to 20 mm/s. Fig. 2.6 demonstrates that the O-ring force efficiency model is valid for different bore sizes and different chamber pressures.

Because leakage model (2.11) predicts essentially zero leakage for the experiment, it was not possible to quantify the dynamic leakage directly. Instead, two observations from the experiment served to validate the zero leakage prediction. First, no visible leakage was seen during the piston ascending and descending periods, and second, the

O-ring was leak free when the the cylinder was loaded because no motion was observed for 24 hours.

To validate the calculation of estimated cylinder weight based on the theory presented in the previous sections, (2.17) was used to predict the weight of commercially available cylinders. Catalog data for 187 hydraulic cylinders from several manufacturers (Airpot, Beily, Bimba, Hercules, Prince) were used to build a database of rated pressure, bore, stroke and weight for real products. For the analysis, the cylinder material was assumed to be 304 stainless steel, which provided the yield strength, Young’s modulus, Poisson’s ratio and material density for the equations. (A real cylinder would be fabricated from several materials.) The safety factor  $N$  was set to 2 as this was the value found in two of the vendor catalogs. Common parameters were used for O-ring seal and hydraulic oil: 10% for squeeze ratio, 10 MPa for O-ring Young’s modulus, 1 mm for O-ring seal cross-section diameter and 0.1 Pa·s for fluid viscosity. The pressure, bore, stroke, material properties and safety factor were used to calculate the theoretical wall thickness, volume and weight for the cylinder. The theoretical weight was then compared to the actual weight for the cylinder. Fig. 2.7 shows the results. If the theory held for real cylinders exactly, all data points would lie on the solid line. The figure shows that real cylinders are somewhat lighter than their predicted weight for heavier cylinders, and somewhat heavier than their predicted weight for lighter cylinders (see inset.) The latter is likely because for the smallest cylinders, the weight of fittings and mounting hardware, not accounted for by the theory, become a significant fraction of the total weight.

### 2.3.2 Hydraulic Conduit

For smooth pipes, the approximate fluid flow equations are [61]

$$P_2 - P_1 = \frac{f_p \cdot \rho_f \cdot V_p^2 \cdot L_p}{2 \cdot D_p} \quad (2.18)$$

$$A_p = \frac{\pi \cdot D_p^2}{4} \quad (2.19)$$

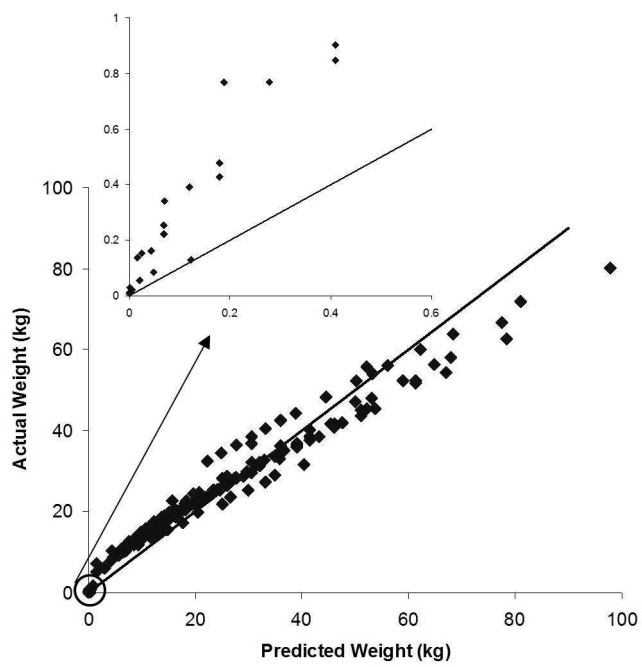


Figure 2.7: Comparison between the actual weight and the weight predicted from the theoretical analysis for 187 commercial cylinders. The solid line indicates an exact match between actual and predicted. The inset expands the data for light weight cylinders.

$$V_p = \frac{Q_p}{A_p} \quad (2.20)$$

$$Re = \frac{\rho_f \cdot D_p \cdot V_p}{\mu} \quad (2.21)$$

$$f_p = \begin{cases} 64/Re & \text{laminar flow} \\ 0.316/Re^{0.25} & \text{turbulent flow} \end{cases} \quad (2.22)$$

where  $P_2$  is pipe inlet pressure,  $P_1$  is pipe outlet pressure,  $f_p$  is pipe friction coefficient,  $\rho_f$  is fluid density,  $V_p$  is pipe flow velocity,  $L_p$  is pipe length,  $D_p$  is pipe inner diameter,  $A_p$  is pipe cross-section area,  $Q_p$  is pipe flow rate and  $Re$  is the Reynolds number.

Using (2.18)–(2.22), the pipe efficiency is

$$\begin{aligned} \eta_p &= \frac{P_1}{P_2} \\ &= \begin{cases} 1 - \frac{128\mu}{\pi} \cdot \frac{Q_p \cdot L_p}{D_p^4 \cdot P_2} & \text{laminar} \\ 1 - \frac{1.79\mu^{0.25} \cdot \rho_f^{0.75}}{\pi^{1.75}} \cdot \frac{Q_p^{1.75} \cdot L_p}{P_2 \cdot D_p^{4.75}} & \text{turbulent} \end{cases} \end{aligned} \quad (2.23)$$

These equations enable calculating the pipe i.d.  $D_p$  as a function of  $Q_p$ ,  $L_p$ ,  $P_2$  and  $\eta_p$ .

The pipe weight can be calculated once the pipe wall thickness is found using the thin-walled cylinder formula [74]

$$t_5 = \frac{N \cdot P_2 \cdot D_p}{2S_y} \quad (2.24)$$

where  $t_5$  is wall thickness,  $N$  is design safety factor, and  $S_y$  is pipe material yield strength. For this analysis we assumed that the pipes, like the cylinders, were fabricated from 304 stainless steel.

The weight of the pipe is

$$M_{\text{conduit}} = \pi \left( \left( \frac{D_p}{2} + t_5 \right)^2 - \left( \frac{D_p}{2} \right)^2 \right) L_p \rho_p \quad (2.25)$$

where  $\rho_p$  is the pipe density. The weight of the oil in the pipe is

$$M_{\text{ConduitOil}} = \pi \left( \frac{D_p}{2} \right)^2 L_p \rho_f \quad (2.26)$$

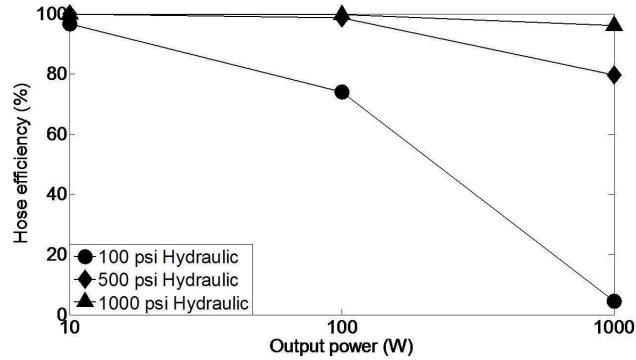


Figure 2.8: Hydraulic conduit efficiency at several pressures and levels of output power, showing that the efficiency of the conduit is high unless the pressure is low. Conduit length: 1 m, conduit inner diameter: 5 mm.

where  $\rho_f$  is the oil density.

The pipe efficiency  $\eta_p$ , inlet pressure  $P_2$  and fluid flow rate  $Q_p$  were calculated using

$$\eta_p = \frac{\eta_{sys}}{\eta_{cyl}} \quad (2.27)$$

$$P_2 = \frac{P_1}{\eta_p} \quad (2.28)$$

$$Q_p = \frac{F_r \cdot V_r}{\eta_{sys} \cdot P_2} \quad (2.29)$$

where  $\eta_{sys}$  is the desired overall efficiency,  $\eta_{cyl}$  is the cylinder efficiency,  $F_r$  is rod force and  $V_r$  is rod velocity.

Fig. 2.8 shows an example of the hydraulic conduit efficiency calculations. As expected, the efficiency of the hose only matters when running at high power and low pressure because under these conditions the flow rate is high, which results in a significant pressure drop. Our calculations (not shown) demonstrated that for most tiny hydraulic systems, the weight of the conduit is much smaller than the weight of the cylinder and can be ignored when doing approximate predictions of total system weight.

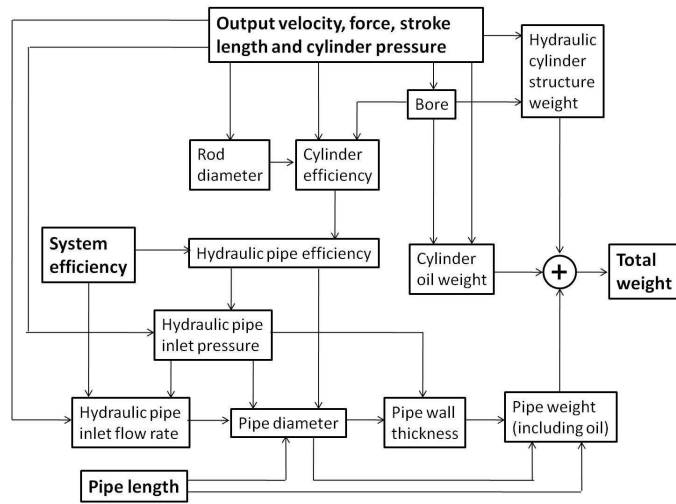


Figure 2.9: Method for calculating the weight of a hydraulic system.

### 2.3.3 Hydraulic System Weight

Fig. 2.9 illustrates how the weight of the hydraulic system is calculated. First, the output force, output velocity and stroke length are specified by the application requirements. Using this information, cylinder weight, efficiency, bore and rod diameter are calculated. Using the overall system efficiency of the equivalent electromechanical system, the hydraulic pipe inlet power and efficiency is calculated then hydraulic pipe inlet pressure is calculated for a given cylinder operating pressure. Next hydraulic pipe inlet flow rate is calculated using inlet power and pressure, then the hydraulic pipe diameter using inlet pressure, inlet flow rate, pipe efficiency and pipe length information, as shown in (2.23). With these numbers, pipe weight is calculated. Finally, total system weight is calculated by summing weights of the cylinder, pipe and hydraulic oil contained in the cylinder and pipe.

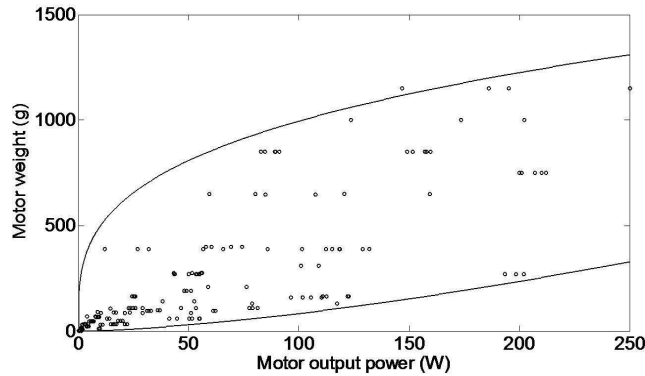


Figure 2.10: Motor weight vs. output power.

## 2.4 Electromechanical System Analysis

The electromechanical system includes wire for the transmission line, a DC electric motor and a ball screw. Unlike hydraulic components, electromechanical components for small-scale applications are readily available. Therefore, rather than using theoretical methods, the approach to estimating the total weight of an electromechanical solution was to develop a set of empirical equations that captured the scaling of component weight and efficiency with load or power based on the properties of high-end, commercially available electromechanical components captured from company catalogs.

### 2.4.1 DC Electric Motor

The key system-level parameters for DC electric motors are weight and efficiency. Brushless, permanent magnet DC motors were chosen because for small precision applications they have the highest efficiency and highest power density. Power, weight and efficiency data for 192 motors from two manufacturers (MicroMo Electronics Inc. and Maxon Motor) were collected. The power for a motor was taken as the peak continuous mechanical output power and the efficiency was the electrical power in to mechanical power out maximum efficiency at the nominal voltage. Fig. 2.10 plots motor weight versus motor power and Fig. 2.11 plots motor efficiency versus power for the motor data set.



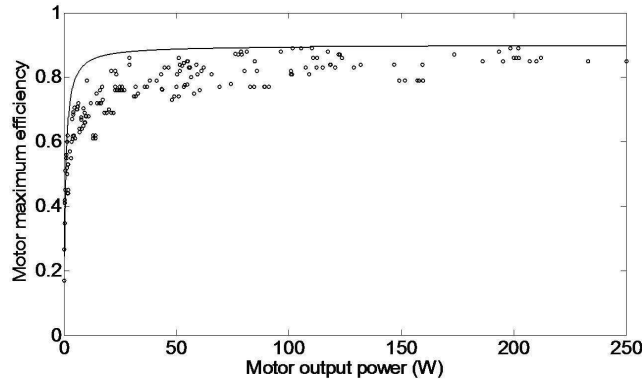


Figure 2.11: Motor efficiency vs. output power.

For modeling purposes, empirical equations were created to bound motor properties. The lower curve in Fig. 2.10 is the lower bound of motor weight. Using this curve in a system analysis means that one is looking for the lightest available motor for a given power. The upper curve in Fig. 2.11 is the upper bound of motor efficiency. Using this curve in an a system analysis means that one is looking for the highest efficiency motor for a given power. The two bounding curves are

$$W_m = \frac{P_m^{1.5}}{12} \quad (2.30)$$

$$\eta_m = 0.9 - 0.9 \cdot \frac{0.1}{0.15 \cdot P_m + 0.1} \quad (2.31)$$

where  $W_m$  is motor weight,  $\eta_m$  is motor efficiency and  $P_m$  is motor power.

### 2.4.2 Ball Screw

The ball screw converts the motor rotary power to low speed, high force linear power. The weight of a ball screw is related to its rated dynamic load and stroke length. Weight does not depend on rated velocity assuming the ball screw operates within its rated velocity. Rated dynamic load, stroke length and weight data were collected from catalog data for 82 ball screws from one manufacturer (Nook Industries). Fig. 2.12 shows weight as a function of rated load for two strokes, and an empirical equation for

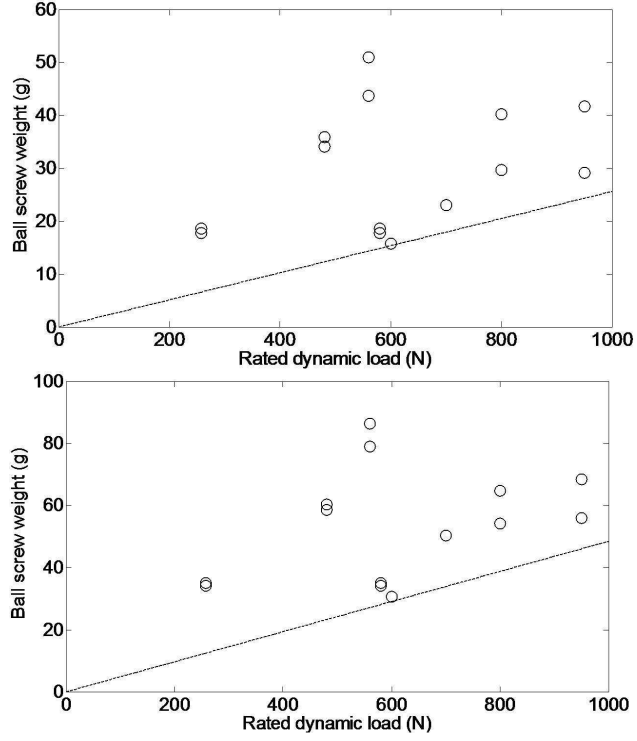


Figure 2.12: Ball screw weight vs. rated dynamic load at .01 m (top) and .04 m (bottom) stroke.

the lower bound of weight as a function of load and stroke was developed from the data

$$W_{bs} = F_{bs} \cdot \frac{180 + 3000 \cdot S_{bs}}{10000} \quad (2.32)$$

where  $W_{bs}$  is ball screw weight,  $F_{bs}$  is ball screw rated dynamic load, and  $S_{bs}$  is ball screw stroke length. The equation is the solid line in Fig. 2.12.

The transmission equations for the ball screw are

$$T_m = F_{bs} \cdot \frac{L_{bs}}{2\pi} \cdot \frac{1}{\eta_{bs}} \quad (2.33)$$

$$\omega_m = \frac{V_{bs}}{L_{bs}} \quad (2.34)$$

where  $T_m$  is motor shaft torque,  $F_{bs}$  is ball screw force,  $L_{bs}$  is the transmission ratio,  $\eta_{bs}$  is ball screw efficiency,  $\omega_m$  is motor shaft velocity and  $V_{bs}$  is ball screw linear velocity. The ball screw efficiency was assumed to be 90%, which is typical for a high performance

component. To simplify the electromechanical systems analysis, a fixed transmission ratio of 1 mm/rev was assumed for the ball screw.

### 2.4.3 Wire

The weight of wire can be significant when the wire is long, which would be the case when the battery is located some distance from the motor. High efficiency wire has large diameter but is heavy. The voltage drop across a length of electrical wire is [76]

$$\Delta U_w = \frac{4K_w}{\pi} \cdot \frac{P_w}{U_w} \cdot \frac{L_w}{D_w^2} \quad (2.35)$$

where  $K_w$  is wire specific resistance,  $P_w$  is wire input power,  $U_w$  is wire input voltage,  $L_w$  is wire length and  $D_w$  is wire diameter. Thus, wire efficiency is

$$\begin{aligned} \eta_w &= \frac{U_w - \Delta U_w}{U_w} \\ &= 1 - \frac{4K_w}{\pi} \cdot \frac{P_w}{U_w^2} \cdot \frac{L_w}{D_w^2} \end{aligned} \quad (2.36)$$

High wire efficiency results in a large wire diameter and thus a large wire weight. In contrast, low wire efficiency means the wire must dissipate a considerable amount of thermal energy, which can melt the insulation. To prevent the system level weight optimization algorithm from suggesting either extreme, the wire efficiency was fixed at 99%, which is realistic for many systems.

Inverting (2.36) provides an equation for wire diameter

$$D_w = \sqrt{\frac{4K_w}{\pi} \cdot \frac{P_w}{U_w^2} \cdot \frac{L_w}{(1 - E_w)}} \quad (2.37)$$

and the weight of the wire, without considering the insulation layer, is

$$W_w = \frac{\pi}{4} \cdot D_w^2 \cdot L_w \cdot \rho_w \cdot 1000 \quad (2.38)$$

where  $W_w$  is wire weight, and  $\rho_w$  is the density of the wire material. The analysis assumed copper wire with density 8960 kg/m<sup>3</sup> and specific resistance 17 nΩm.

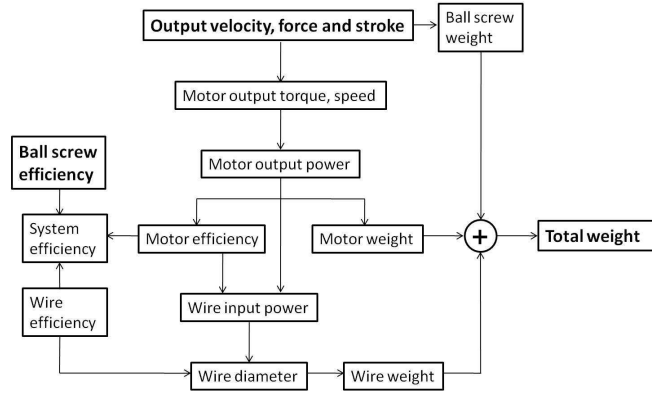


Figure 2.13: Method for calculating the weight of an electromechanical system.

#### 2.4.4 Electromechanical System Weight

Fig. 2.13 illustrates the approach for calculating the weight of the electromechanical solution. The application requirements set the ball screw output velocity, force and stroke. The ball screw weight is then calculated using (2.32). The electric motor shaft power is calculated from

$$P_m = \frac{T_m}{1000} \cdot 2\pi \cdot \omega_m = \frac{F_{bs} \cdot V_{bs}}{\eta_{bs}} \quad (2.39)$$

using (2.33) and (2.34). This determines the motor weight and efficiency according to (2.30) and (2.31). Next, the input power to the wire is determined from

$$P_w = P_m \cdot \frac{1}{\eta_m} \cdot \frac{1}{\eta_w} \quad (2.40)$$

and then the wire diameter and wire weight are calculated from (2.37) and (2.38). The system weight is the sum of the ball screw, motor and wire weights. The overall electromechanical system efficiency is

$$\eta_{esys} = \eta_{bs} \cdot \eta_m \cdot \eta_w \quad (2.41)$$

## 2.5 Method to Compare Hydraulic and Electromechanical Systems

With the ability to calculate hydraulic and electromechanical system weight and efficiency for a given application the two realizations can be compared to determine which will be lighter. The method used for the comparison was to: (1) Establish the design problem by specifying a system force and power (or force and velocity), and linear excursion. (2) Design an electromechanical solution using the empirical bounding equations as a stand-in for the best-available DC brushless motor and ball screw. (3) Calculate the efficiency of the resulting electromechanical system. (4) Design a comparable hydraulic system with the same force, power and stroke design requirements and the same efficiency. (5) Calculate and compare the weights of the electromechanical and hydraulic solutions. An application was implemented in Matlab to facilitate the calculations.

## 2.6 Results

Weight comparison examples are shown in Figs 2.14-2.21. Figs. 2.14-2.19 show system weight for a mechanical output power of 100 W and 10 W for various configurations of velocity, stroke length and transmission line length. The nominal voltage for the motors in the database ranged from 6 to 48 V but for this analysis 24 V motors were used. Motor voltage has some, but not a significant effect on the electromechanical system weight because as the voltage decreases, the system weight will increase due to the wire diameter increasing to accommodate the increase in current at the same efficiency.

Operating pressure has a significant influence on the weight of a hydraulic system. Fig. 2.20 shows the weights of hydraulic systems running at three pressures compared to the weight of the equivalent electromechanical system for three output power conditions with an output velocity of 10 mm/s. The 100 psi hydraulic system is heavier than the equivalent electromechanical system while the 500 psi and 1000 psi systems are

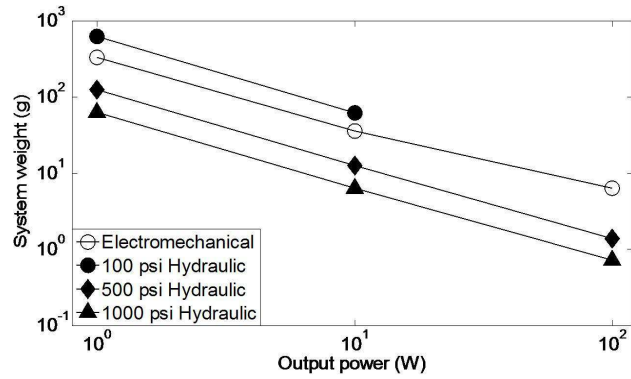


Figure 2.14: Hydraulic and electromechanical system weight at several output velocities. Output power: 10 W, stroke: 0.05 m, transmission line length: 0.1 m. The 100 psi, 100 mm/s data point is missing because there is no low pressure, high speed hydraulic system that can match the efficiency of the equivalent electromechanical system.

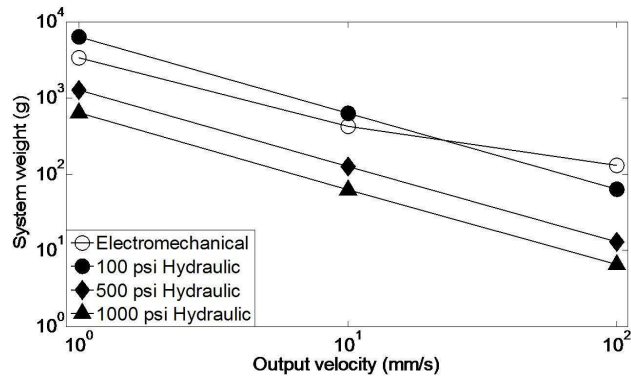


Figure 2.15: Hydraulic and electromechanical system weight at several output velocities. Output power: 100 W, stroke: 0.05 m, transmission line length: 0.1 m.

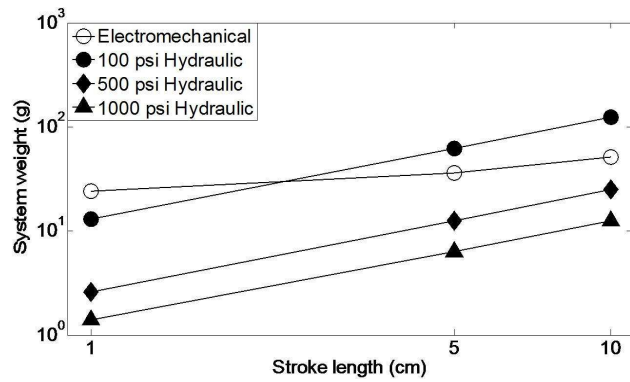


Figure 2.16: Hydraulic and electromechanical system weight at several stroke lengths. Output power: 10 W, velocity: 0.01 m/s, transmission line length: 0.1 m.

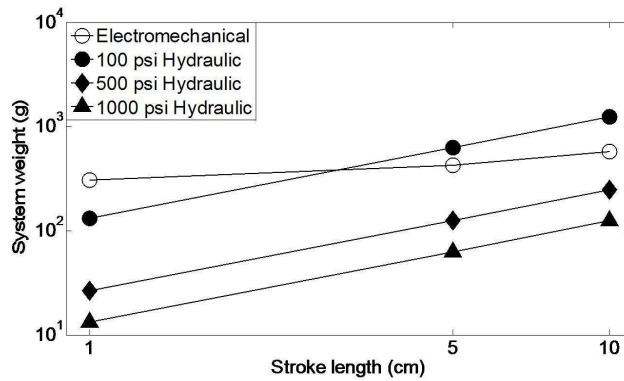


Figure 2.17: Hydraulic and electromechanical system weight at several stroke lengths. Output power: 100 W, velocity: 0.01 m/s, transmission line length: 0.1 m.

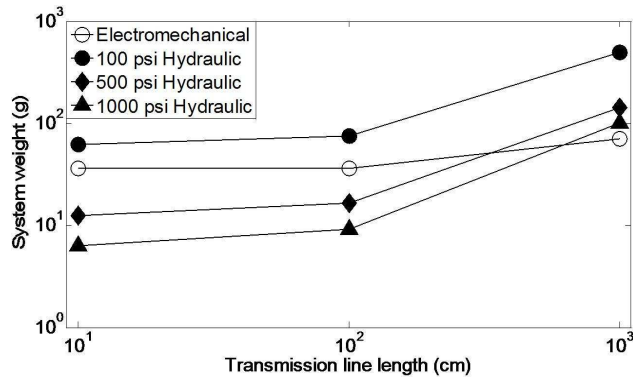


Figure 2.18: Hydraulic and electromechanical system weight at several transmission line lengths. Output power: 10 W, stroke: 0.05 m, velocity: 0.01 m/s.

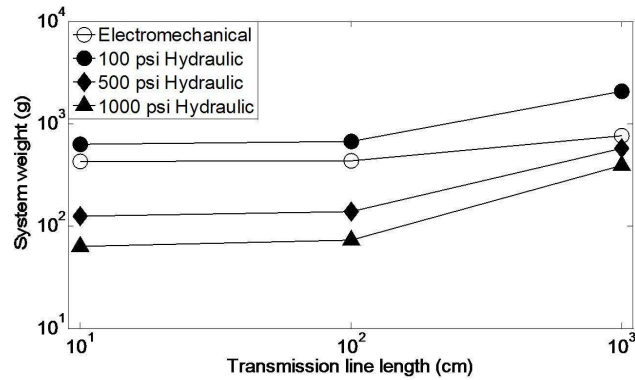


Figure 2.19: Hydraulic and electromechanical system weight at several transmission line lengths. Output power: 100 W, stroke: 0.05 m, velocity: 0.01 m/s.

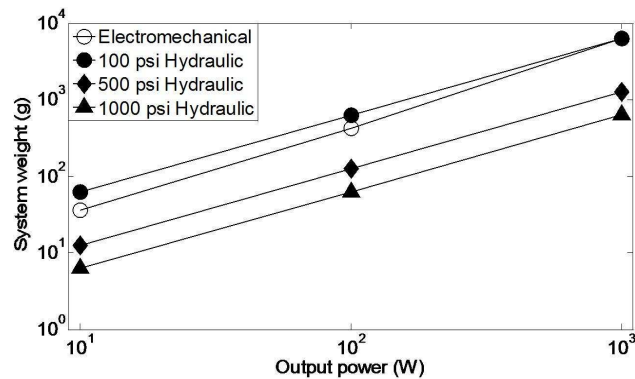


Figure 2.20: Hydraulic and electromechanical system weight at several output powers. Stroke: 0.05 m, velocity: 0.01 m/s, transmission line length: 0.1 m.

lighter. Fig. 2.21 shows the operating pressure required for the hydraulic system to have the same weight as the equivalent electromechanical system for three output powers. Pressures higher than the line will result in a lighter hydraulic system and pressures below the line will result in a heavier hydraulic system.

## 2.7 Design Example

A powered ankle foot orthosis (AFO) is a device that helps people with muscle deficiency to lift their toe or push off while walking [77]. The AFO was chosen as the design example



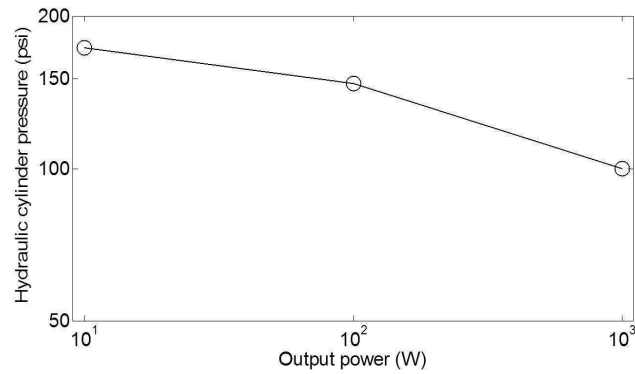


Figure 2.21: Operating pressure required for the hydraulic system to be the same weight as the equivalent electromechanical system at several output powers. Stroke: 0.05 m, velocity: 0.01 m/s, transmission line length: 0.1 m.

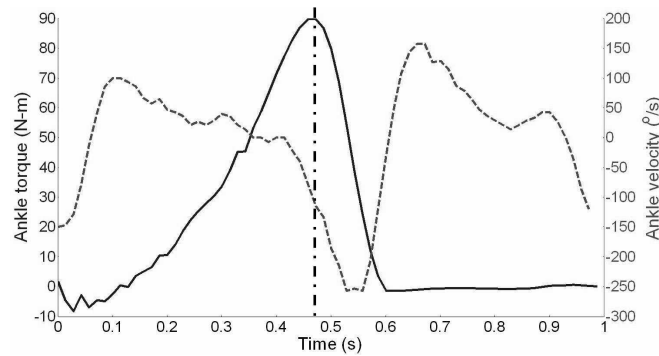


Figure 2.22: Ankle torque (solid) and velocity (dashed) for one step when walking at normal speed. The vertical dot-dash line marks the peak power point. Data from [3].

because of its challenging requirements. Large torque and large power is required during the push off phase of gait but the weight of the AFO on the ankle must be less than 2 kg to not influence leg swing dynamics. Fig. 2.22 shows ankle torque and velocity for one step when walking at normal speed. The vertical dot-dash line marks the point during the gait cycle where the ankle produces maximum power with torque 90 Nm and velocity 100 deg/s. This occurs just before toe-off and the AFO was designed to match this power.

Fig. 2.23 shows the placement of a single hydraulic cylinder for the conceptual

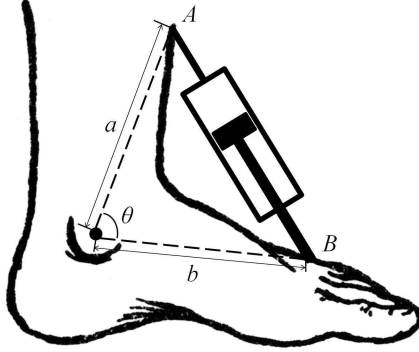


Figure 2.23: Conceptual design for a hydraulic AFO.

design of a powered AFO. The cylinder is oriented to extend for ankle plantar flexion to take advantage of the larger cap side piston area compared to the rod side. To reduce the AFO package size, in the neutral position, a moment arm of 8 cm was assumed. The ankle range of motion is  $20^\circ$  in dorsi-flexion and  $50^\circ$  in plantar-flexion for a total of  $70^\circ$  [78]. To minimize the weight carried on the ankle, the hydraulic power supply was assumed to be carried at the waist, separated from the actuator by a 1 m hydraulic hose.

The cylinder stroke length, maximum output force, maximum output velocity and maximum output power were derived from the geometry

$$S = S_f - S_i \quad (2.42)$$

$$S_i = \sqrt{a^2 + b^2 - 2 \cdot a \cdot b \cdot \cos(\theta_i)} \quad (2.43)$$

$$S_f = \sqrt{a^2 + b^2 - 2 \cdot a \cdot b \cdot \cos(\theta_f)} \quad (2.44)$$

$$F_{\max} = \frac{T_{\max}}{L_{\text{ma}}} \quad (2.45)$$

$$V_{\max} = \frac{\Omega_{\max}}{180^\circ} \cdot \pi \cdot L_{\text{ma}} \quad (2.46)$$

$$POW_{\max} = T_{\max} \cdot \Omega_{\max} \quad (2.47)$$

where  $S_i$  and  $S_f$  are the initial and final distance between the cylinder mounting point  $A$  and  $B$  (Fig. 2.23),  $\theta_i = 70^\circ$  and  $\theta_f = 140^\circ$  are the ankle angles corresponding to  $S_i$

Table 2.3: AFO systems weight comparison

| <i>System</i>      | <i>Component</i> | <i>Wt (g)</i> | <i>Total Wt (g)</i> |
|--------------------|------------------|---------------|---------------------|
| Electro-mechanical | Ball screw       | 44            | 241                 |
|                    | DC motor         | 192           |                     |
|                    | Wire             | 5             |                     |
| 200 psi hydraulics | Cylinder         | 210           | 248                 |
|                    | Hoses            | 38            |                     |
| 500 psi hydraulics | Cylinder         | 106           | 125                 |
|                    | Hoses            | 19            |                     |

and  $S_f$ , and  $a$  and  $b$  are fixed at 10 cm.

The system specifications from (2.42) - (2.47) were used in (2.1) - (2.41) along with the methods described in Section 2.5 to compute the theoretical weight of the electro-mechanical and hydraulic AFO components for the design example. The results are shown in Table 2.3. At 200 psi the hydraulic system will be about the same weight as the equivalent electro-mechanical system but at 500 psi it will be about one half the weight. While the 500 psi cylinder and hose must have thicker walls to accommodate the higher pressure, the bore size to achieve the same force is smaller at 500 psi resulting in overall lighter components.

## 2.8 Discussion

The key result of this study is that for applications where the output power is less than 100 W a hydraulic solution will be lighter than the equivalent electromechanical solution only if the hydraulics runs at high pressure. For example, Fig. 2.20 shows that a 100 W electromechanical system is predicted to weigh 428 g while a 100 W hydraulic system running at 1000 psi is predicted to weigh 63 g, about seven times lighter. While the exact numbers are system dependent (for example, as the power source is placed further away, the drag in small hydraulic lines become significant,) the conclusion is clear: for tiny, light hydraulic systems the operating pressure must be high.

There is an upper limit on the pressure. For equal force, the higher the pressure

the smaller the bore of the cylinder but Fig. 2.4 shows that efficiency rapidly drops if the bore becomes too small. Low efficiency is problematic because a large, heavy power source is needed to provide the energy required by the application and because the wasted energy results in heating that cannot be carried away by the tiny amount of circulating fluid. Thus, efficiency considerations lead to an effective lower limit on size, about 4 mm, and therefore an upper limit on pressure.

Because tiny high pressure hydraulic components are not available, small hydraulic systems are currently run at low pressures, often using pneumatic components that are small and light but generally limited to about 200 psi. (One exception is the small custom cylinder for the prototype prosthetic finger by Love [7].) Thus, there is a need for small components that operate at high pressures and are at the weight predicted by (2.17) and (2.25).

The limitation of this study is that it ignores the power supply and control means, which are significant components of the complete system. Analyzing only the distal components still provides guidance to the designer for two reasons. First, it is often the distally mounted components that are most weight sensitive and second, including the power supply and control would not change the main conclusion which is that tiny hydraulics should be run at high pressure to minimize weight.

Turning to the complete hydraulic system, hydraulic power supplies are typically large and heavy and traditional throttling control valves are inefficient. For truly lightweight, low power, mobile systems such as powered hand tools and powered orthotics, compact sources of high pressure fluid using pumps driven by battery powered electric motors or by tiny, high power density internal combustion engines are needed. Tiny cartridge piston pumps are available but have a modest efficiency of about 30% at 500 psi. There is also a need for tiny, high pressure, low flow hydraulic control valves that operate in an efficient on-off switching mode. The common PWM drivers for electric motors are efficient, and equivalent fluid power valves are under research [79]. Low-pressure, low flow digital MEMS valves are used in micro-fluidics, but are not

suitable for transmitting power in the one to 100 W range.

Other problems with tiny hydraulics for human-scale applications that must be solved include leakage of oil into the environment, which calls for developing low friction, leakless seals; cavitation of the fluid, which may be a significant problem for oil running through small passages at low pressure and high velocity; and creating designs that integrate structure, conduit, valving and cylinders to minimize weight by eliminating fittings.

## Chapter 3

# Modeling of Tiny Hydraulic Cylinders

*This chapter was published in 52nd National Conference on Fluid Power, Las Vegas, March 23-25, 2011.*

Objective: To investigate the efficiency of four hydraulic cylinder configurations with cylinder bore size between 1 and 10 mm. The configurations were: (1) no piston seal, no rod seal; (2) no piston seal, rod seal; (3) piston seal, no rod seal; (4) piston seal, rod seal. The influence of operating conditions, geometrical parameters and fluid properties on cylinder force efficiency, volumetric efficiency and overall efficiency were modeled. Methods: Empirical formulas were used to predict O-ring seal friction and leakage. Analytical solutions were used to predict viscous drag force and leakage of clearance seals. Results: With 10 micron clearance seal, cylinders with configuration (2) have higher overall efficiency than those with configuration (4). The difference increases as bore size decreases, and is significant for bores between 1 and 10 mm. The result reverses with 20 micron clearance seal. The cylinder force efficiency can be greater than one in some cases because of viscous drag forces on the piston. Discussion: Conventional cylinders have configuration (4) because most fluid power applications are

high power with large bore cylinders. Differences between configuration (2) and (4) are small for large bore size. For new fluid power applications such as medical devices, tiny bore size cylinders are needed. Configuration (2) is a useful design option in such applications because it not only saves a piston seal, but also improves cylinder efficiency. Configuration (1) is not feasible for hydraulic systems. However it may be viable for pneumatic systems. Commercial examples of configuration (1) exist.

### 3.1 Introduction

Hydraulic cylinders are commonly sealed by rubber seals to increase volumetric efficiency and to prevent hydraulic oil leaking into surrounding environment. There is a tradeoff between the cylinder volumetric efficiency and the cylinder force efficiency [10]. The higher the volumetric efficiency, the lower the force efficiency will be. With both cylinder piston and rod sealed by rubber seals, the room for further improving cylinder efficiency is physically limited. Furthermore, rubber seals produce detrimental friction force in tiny devices [22]. Alternatively, clearance seals can be used to replace rubber seals to reduce the sealing friction force [26]. Clearance seals are more favorable in tiny devices since viscous friction force dominates in these seals.

To explore new ways of improving the cylinder efficiency in tiny hydraulic cylinders, four cylinder configurations were conceived and compared side by side. The four cylinder configurations to be modeled are color-coded and labeled as (1) through (4) in Figure 3.1. The black dots in the figure represent O-ring seals. O-ring seals were chosen as the sealing elements due to its simplicity. Analytical solutions for O-ring seal friction and leakage exist in the literature ([12, 37, 38, 48]).

### 3.2 Cylinder Efficiency Modeling

Since piston seal was the focus of this study, only the outstroke was modelled. Parameters used in the modelling process are summarized in Table 3.1. The sealed element in

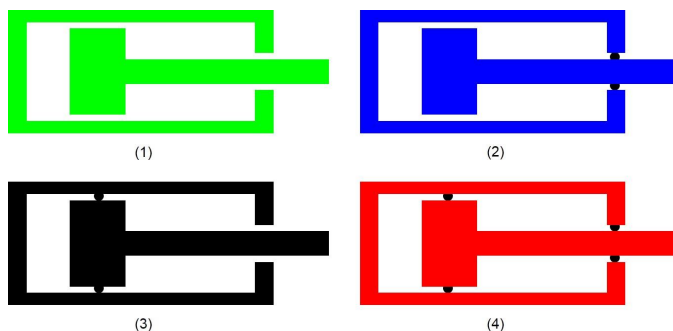


Figure 3.1: Four cylinder configurations with different sealing strategies.

the table refers to either piston or rod. The physical meaning of  $\delta$  and  $l$  is illustrated in Figure 3.2. O-ring squeeze ratio  $\epsilon$  is defined in (3.7).

Table 3.1: Parameters to be used in the modelling process

| VAR        | PHYSICAL MEANING              | UNIT |
|------------|-------------------------------|------|
| $P$        | Operating pressure            | MPa  |
| $D$        | Sealed element diameter       | mm   |
| $\mu$      | Fluid absolute viscosity      | Pa·s |
| $U$        | Sealed element velocity       | mm/s |
| $\delta$   | Clearance gap size            | m    |
| $l$        | Sealed element width          | mm   |
| $d$        | O-ring cross-section diameter | mm   |
| $E$        | O-ring Young's modulus        | MPa  |
| $\epsilon$ | O-ring squeeze ratio          | —    |

### 3.2.1 Clearance Seal Model

The viscous friction force and the leakage flow across a concentric clearance seal can be modelled with (3.1) and (3.2)

$$f_u = \frac{\pi \cdot \delta \cdot P \cdot D}{2} - \frac{\pi \cdot \mu \cdot U \cdot D \cdot l}{\delta} \quad (3.1)$$

$$q_u = \frac{\pi \cdot P \cdot D \cdot \delta^3}{12 \cdot \mu \cdot l} + \frac{\pi \cdot U \cdot \delta \cdot D}{2} \quad (3.2)$$



The sub-script  $u$  represents the unsealed situation, that is with a clearance seal. The meaning of other parameters is illustrated in Table 3.1 and Figure 3.2.

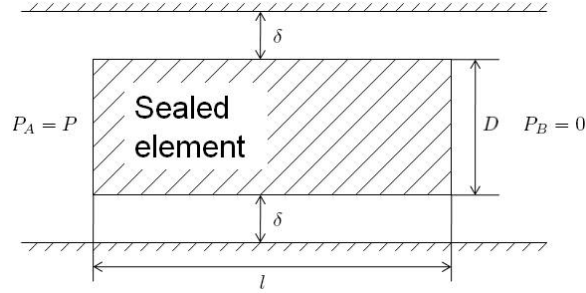


Figure 3.2: Parameters illustration for a clearance seal

The viscous friction force  $f_u$  can be treated as a super-imposition of pressure-induced and velocity-induced friction. If sealed element velocity  $U$  is zero, then only pressure-induced friction exists, and vice versa. Pressure-induced and velocity-induced gap flow velocity distribution is illustrated in Figure 3.3. Since the direction of viscous friction force is the same as gap flow velocity gradient [2], the pressure-induced friction is in the same direction as gap flow velocity, and the velocity-induced friction is in the opposite direction as gap flow velocity. Therefore the direction of  $f_u$  is determined by the relative magnitude of the operating pressure  $P$  and the sealed element velocity  $U$ . If pressure-induced friction is smaller than velocity-induced friction, then  $f_u$  is in the opposite direction as  $U$ , thus hindering sealed element movement. Conversely,  $f_u$  will be in the same direction as  $U$ , thus helping sealed element movement.

Since both pressure-induced and velocity-induced gap flows are in the same direction as the gap flow velocity, the leakage flow  $q_u$  is always in the same direction as  $U$ .

### 3.2.2 Rubber O-ring Seal Model

Reference [12] gives an analytical solution for rubber O-ring seal friction, as shown in (3.3), where sub-script  $s$  represents sealed situation, i.e., with an O-ring seal,  $\mu_f$  is the friction coefficient between the O-ring seal and the structural wall, and  $r$  is the O-ring

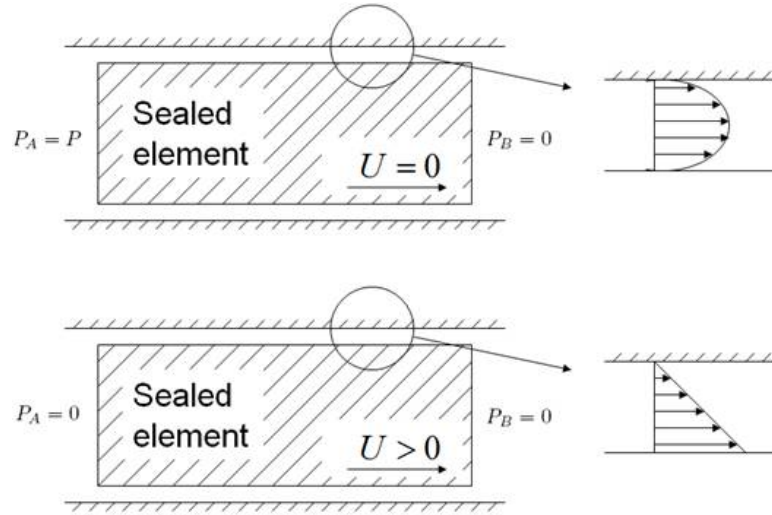


Figure 3.3: Pressure-induced (1st row) and velocity-induced (2nd row) gap flow velocity distribution

cross-sectional radius. Variables  $d$ ,  $d_1$  and  $d_2$  are defined in Figure 4.

$$f_s = 2 \cdot \pi \cdot \mu_f \cdot d_1 \cdot r \cdot E \cdot \left(1 - \frac{d_1 - d_2}{4 \cdot r}\right) \cdot \sqrt{1 - \frac{(d_1 - d_2)^2}{16 \cdot r^2}} \quad (3.3)$$

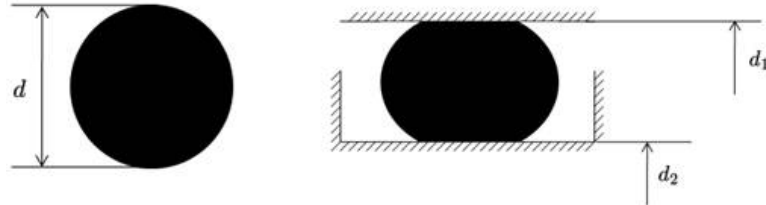


Figure 3.4: An O-ring seal before and after installation

To convert this solution to an expression that uses variables defined in Table 3.1. The following variables are defined

$$d = 2 \cdot r \quad (3.4)$$

$$g = \frac{d_1 - d_2}{2} \quad (3.5)$$

$$D = d_1 \quad (3.6)$$

$$\epsilon = \frac{d-g}{d} = 1 - \frac{d_1 - d_2}{4 \cdot r} \quad (3.7)$$

Substituting (3.4) - (3.7) into (3.3) following results in

$$f_s = \pi \cdot \mu_f \cdot D \cdot d \cdot E \cdot \epsilon \cdot \sqrt{2 \cdot \epsilon - \epsilon^2} \quad (3.8)$$

In the hydrodynamic lubrication domain,  $\mu_f$  can be expressed as [48]

$$\mu_f = C \cdot \sqrt{\frac{\mu \cdot U}{P}} \quad (3.9)$$

where  $C$  is a constant related to operating conditions.

Moreover,  $\mu_f = 0.3 \sim 0.5$  for well finished and sufficient lubricated sealed surfaces [12]. If  $\mu_f = 0.4$ ,  $\mu = 0.1$  Pa·s,  $U = 0.1$  m/s and  $P = 10$  MPa are nominal operating conditions, then

$$\mu_f = \begin{cases} 12650 \cdot \sqrt{\mu \cdot U / P} & \text{if } P \neq 0 \\ 4 \cdot \sqrt{\mu \cdot U} & \text{if } P = 0 \end{cases} \quad (3.10)$$

Equations (3.8) and (3.10) provide a set of equations for O-ring seal friction estimation.

Pressure-energized seals such as O-ring seals are normally designed to operate in a fully lubricated condition [15]. The seal rides on a thin film of lubricant which provides the final sealing barrier, retained in position by the surface tension of the film. Reference [37] gives an experimental formula for O-ring sealing film thickness  $h_c$

$$\frac{h_c}{s} = 2.99 \cdot \left( \frac{\mu \cdot U}{\sigma_m \cdot s} \right)^{0.71} \quad (3.11)$$

where  $s$  is the O-ring contact width, and  $\sigma_m$  is the maximum O-ring contact pressure. Figure 3.5 further illustrates the definition of these two variables. The parameters used

to achieve this formula spanned a wide range:  $U = 20 \sim 300$  mm/s,  $P = 1 \sim 15$  MPa,  $\mu = 0.47$  &  $0.08$  Pa s,  $E = 3.9 \sim 20.5$  MPa,  $\epsilon = 0.07 \sim 0.17$ , and  $d = 3$  &  $5.5$  mm.

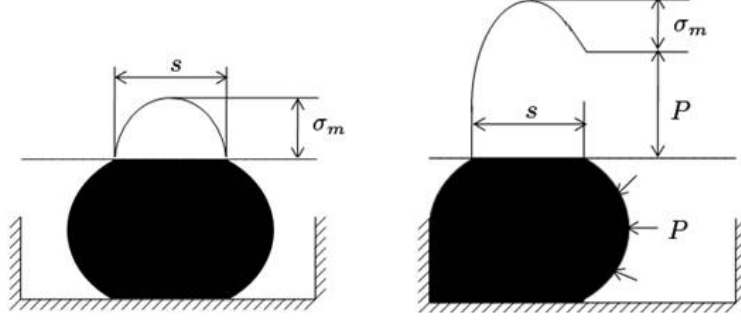


Figure 3.5: Illustration of O-ring contact width and maximum contact pressure

Since the gap flow has a linear velocity distribution at  $h_c$  [12], the average leakage flow velocity equals to half of the sealed element velocity. Therefore the leakage flow across the sealed element is

$$q_s = \pi \cdot D \cdot h_c \cdot \frac{U}{2} \quad (3.12)$$

Substituting (3.11) into (3.12) gives

$$q_s = 1.495 \cdot \pi \cdot D \cdot \mu^{0.71} \cdot U^{1.71} \cdot \sigma_m^{-0.71} \cdot s^{0.29} \quad (3.13)$$

In a loaded situation the O-ring contact width  $s$  and the maximum contact pressure  $\sigma_m$  can be expressed as [38]

$$s = d \cdot (2 \cdot \epsilon + 0.13) + d \cdot T \quad (3.14)$$

$$\sigma_m = 0.67 \cdot E \cdot (2 \cdot \epsilon + 0.13) + 3.6 \cdot P/\pi \quad (3.15)$$

where

$$T = \left[ \frac{0.39}{1 - \epsilon} - 0.5 \cdot (2 \cdot \epsilon + 0.13) \right] \cdot \left[ 1 - e^{-\frac{4.6 \cdot P}{E}} \right]$$

Equations (3.13) ~ (3.15) provides a set of equations for O-ring seal leakage estimation.

### 3.2.3 Cylinder efficiency model

Cylinder force efficiency and volumetric efficiency are defined as

$$\eta_f = \frac{F_{ar}}{F_{ir}} \quad (3.16)$$

$$\eta_v = \frac{Q_i}{Q_a} \quad (3.17)$$

where  $F_{ar}$  and  $Q_a$  are actual rod force and flow rate into cylinder chamber, and  $F_{ir}$  and  $Q_i$  are the ideal rod force and flow rate into cylinder chamber, defined as

$$F_{ir} = P \cdot \frac{\pi B^2}{4} \quad (3.18)$$

$$Q_i = U_{ar} \cdot \frac{\pi B^2}{4} \quad (3.19)$$

where  $B$  is cylinder bore size and  $U_{ar}$  is actual rod speed. Cylinder overall efficiency is

$$\eta = \eta_f \cdot \eta_v = \frac{F_{ar} \cdot U_{ar}}{P \cdot Q_a} \quad (3.20)$$

The force efficiency for configuration (1) through (4) can be expressed as

$$\eta_{f1} = \frac{F_{ir} + f_{up} + f_{ur}}{F_{ir}} \quad (3.21)$$

$$\eta_{f2} = \frac{F_{ir} + f_{up} - f_{sr}}{F_{ir}} \quad (3.22)$$

$$\eta_{f3} = \frac{F_{ir} - f_{sp} + f_{ur}}{F_{ir}} \quad (3.23)$$

$$\eta_{f4} = \frac{F_{ir} - f_{sp} - f_{sr}}{F_{ir}} \quad (3.24)$$

where

$$f_{up} = \frac{\pi \cdot \delta \cdot P \cdot D_p}{2} - \frac{\pi \cdot \mu \cdot U_{ar} \cdot D_p \cdot l}{\delta} \quad (3.25)$$

$$f_{ur} = -\frac{\pi \cdot \mu \cdot U_{ar} \cdot D_r \cdot l}{\delta} \quad (3.26)$$

$$f_{sr} = 4 \cdot \pi \cdot \sqrt{\mu \cdot U_{ar}} \cdot D_r \cdot d \cdot E \cdot \epsilon \cdot \sqrt{2\epsilon - \epsilon^2} \quad (3.27)$$

$$f_{sp} = 12650 \cdot \pi \cdot \sqrt{\frac{\mu \cdot U_{ar}}{P}} \cdot B \cdot d \cdot E \cdot \epsilon \cdot \sqrt{2\epsilon - \epsilon^2} \quad (3.28)$$

where  $D_p$  and  $D_r$  represent piston diameter and rod diameter respectively. The plus sign is used for clearance seal friction and the minus sign for O-ring seal friction. The reason is the direction of clearance seal friction depends on the relative magnitude of operating pressure and rod velocity, while the direction of O-ring seal friction is always in the opposite direction of rod speed.

The volumetric efficiency for configuration (1) through configuration (4) can be expressed as

$$\eta_{v1} = \eta_{v2} = \frac{Q_i}{Q_i + q_{up}} \quad (3.29)$$

$$\eta_{v3} = \eta_{v4} = \frac{Q_i}{Q_i + q_{sp}} \quad (3.30)$$

where

$$q_{up} = \frac{\pi \cdot P \cdot D_p \cdot \delta^3}{12 \cdot \mu \cdot l} + \frac{\pi \cdot U_{ar} \cdot \delta \cdot D_p}{2} \quad (3.31)$$

$$q_{sp} = 1.495 \cdot \pi \cdot B \cdot \mu^{0.71} \cdot U_{ar}^{1.71} \cdot \sigma_m^{-0.71} \cdot s^{0.29} \quad (3.32)$$

Since only outstroke was modelled, leakage across the piston seal determines the volumetric efficiency. Since leakage across both the clearance seal and the O-ring seal is in the same direction as rod speed, the plus sign is used before both leakage terms.

### 3.3 Simulation Results

Equations (3.16) - (3.32) were used to model the efficiency of cylinder configuration (1) through (4). Following nominal values were used in the simulations:  $P = 10$  MPa,  $\mu = 0.1$  Pa·s,  $U_{ar} = 0.1$  m/s,  $l = 10$  mm,  $d = 1$  mm,  $E = 10$  MPa and  $\epsilon = 0.1$ . Since configuration (1) and (3) do not have rod seals, they are not feasible for hydraulic cylinders. Following discussions emphasize on configuration (2) and (4).

Figure 3.6 and figure 3.7 show the cylinder overall efficiency versus bore size with 20 and 10 micron clearance gap sizes. The gap size modeling can be found in [80]. The results show that the difference between configuration (4) and (2) becomes bigger as bore size decreases, and the difference becomes significant for bore size smaller than 10 mm. With a 20 micron clearance gap size, configuration (4) has higher efficiency than configuration (2), but the situation reverses if 10 micron gap size is used. This means configuration (2) is a better option than configuration (4) if the clearance gap can be made small. The benefits of configuration (2) become more significant in small bore size cylinders.

Figure 3.8 shows cylinder force efficiency versus bore size. An interesting phenomenon is that the force efficiency of configuration (1) can be greater than one. This phenomenon does not contradict energy conservation laws because the cylinder overall efficiency is always smaller than one. Clearance seals can generate positive drag force, which assists the piston and rod movement. Because there is a trade-off between force efficiency and volumetric efficiency, a force efficiency being higher than one means that volumetric efficiency is sacrificed, which can be seen in Figure 3.9.

### 3.4 Conclusion

Four cylinder configurations were conceived, modeled and analyzed. Empirical formulas were used to model O-ring seals, and analytical solutions were used to model clearance seals. Simulation results showed taking piston seals out can improve hydraulic cylinder

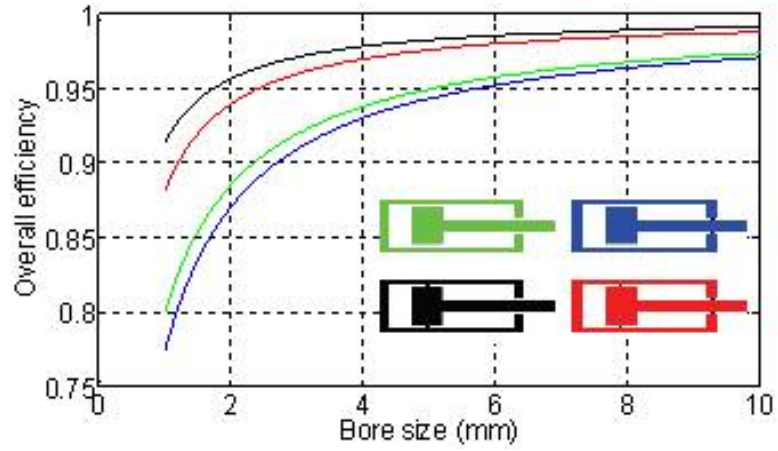


Figure 3.6: Cylinder overall efficiency vs. bore size ( $\delta = 20 \mu\text{m}$ )

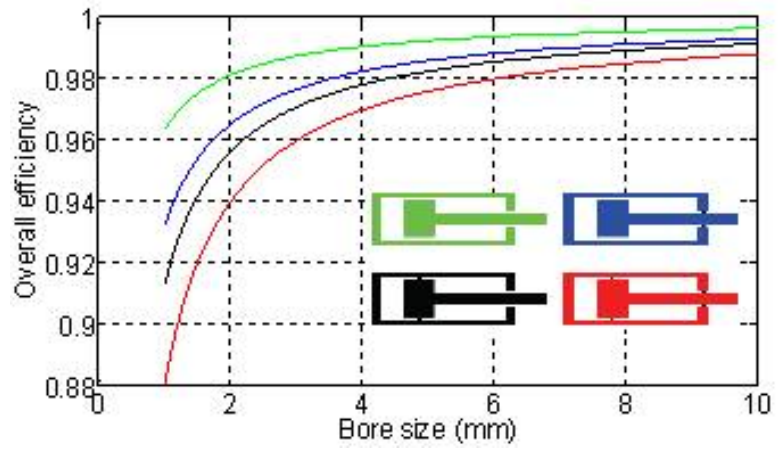


Figure 3.7: Cylinder overall efficiency vs. bore size ( $\delta = 10 \mu\text{m}$ )



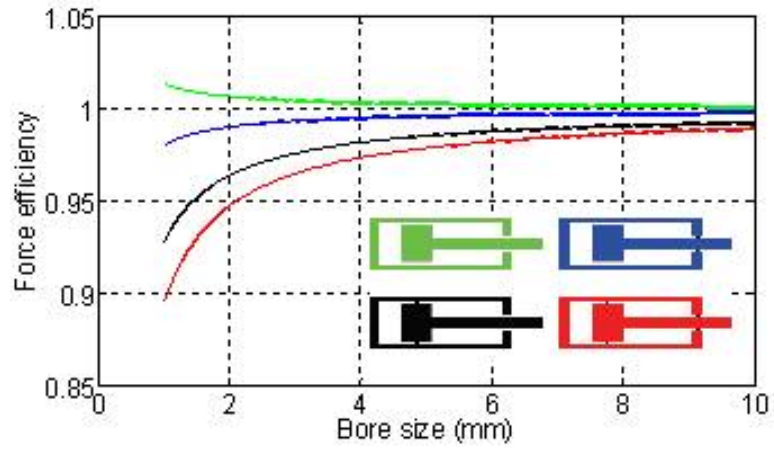


Figure 3.8: Cylinder force efficiency vs. bore size ( $\delta = 10 \mu\text{m}$ )

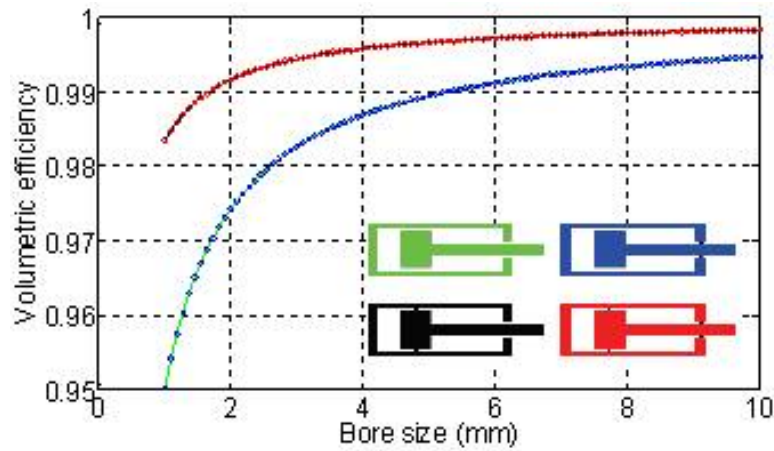


Figure 3.9: Volumetric efficiency vs. bore size ( $\delta = 10 \mu\text{m}$ )

overall efficiency if the clearance gap is small. The benefits of removing seals become significant as bore size decreases.

## Chapter 4

# Experimentally Validated Efficiency Models of O-ring Seals for Tiny Hydraulic Cylinders

*This chapter was published in Proceedings of ASME/Bath 2014 Symposium on Fluid Power & Motion Control, FPMP 2014, September 10-12, 2014, Bath, United Kingdom.*

### 4.1 Introduction

Large-scale hydraulic systems are well known for their high power density advantage compared to other technologies [39], which is why hydraulics are widely used in heavy-duty machines such as excavators. A recent study revealed that this power density advantage is maintained for tiny hydraulic systems [81], which makes hydraulic systems appealing for unthethered human-scale devices such as prostheses, orthoses and hand tools where high power and a small package are needed [7, 82].

Linear hydraulic cylinders are the most common actuators for a hydraulic system because they are simpler and far more efficient than rotary hydraulic motors. For most

systems, cylinder efficiency is not of concern because the overall system efficiency is dominated by the efficiency of pumps and valves. In small-scale systems, however, cylinder efficiency matters because while cylinder force varies with area, cylinder loss varies with diameter. Thus cylinder efficiency models are needed at the small scale to fully understand the overall efficiency of tiny hydraulic systems.

Analytical efficiency models for small-bore hydraulic cylinders were developed in a previous paper [83]. It was shown that cylinder efficiency degrades as bore decreases, and that efficiency drops precipitously when the bore drops below 1 cm, reinforcing the need for efficiency models at small sizes. Since validated models for a clearance gap seal are readily available [84], the purpose of this work was to validate a simple model for a rubber seal.

## 4.2 Cylinder Efficiency Model

### 4.2.1 Leakage

The fluid leakage across the O-ring was modeled as

$$q_l = 1.495 \cdot \pi \cdot B \cdot \mu^{0.71} \cdot U_r^{1.71} \cdot \sigma_m^{-0.71} \cdot s^{0.29} \quad (4.1)$$

where  $B$  is the cylinder bore size,  $\mu$  is the fluid viscosity,  $U_r$  is piston speed,  $\sigma_m$  is the maximum O-ring contact pressure and  $s$  is the O-ring contact width [37, 38].

### 4.2.2 Friction

The cylinder force efficiency is mainly determined by the O-ring squeeze ratio, which indicates how tight the seal is. The higher the squeeze ratio, the tighter the seal and the smaller the leakage. A tighter seal, however, means more friction, which degrades force efficiency. Because of its importance, the O-ring squeeze ratio model is presented first.

The O-ring cross-sectional diameter after it is placed in the piston groove, but before the piston assembly is inserted into the cylinder block is

$$d_s = d \cdot (1 - \delta) \quad (4.2)$$

where  $d$  is the original O-ring cross-sectional diameter, and  $\delta$  is the O-ring cross-sectional diameter reduction percentage, which can be read from a handbook chart [85]. The O-ring squeeze ratio  $\epsilon$  is then be calculated as

$$\epsilon = \frac{d_s - (B - D_g)/2}{d_s} \quad (4.3)$$

where  $B$  is the cylinder bore,  $D_g$  is the piston groove diameter and  $(B - D_g)/2$  is the O-ring cross-sectional diameter after installation.

The O-ring friction force was modeled as

$$f_s = \pi \cdot \mu_f \cdot B \cdot d \cdot E \cdot \epsilon \cdot \sqrt{2 \cdot \epsilon - \epsilon^2} \quad (4.4)$$

where  $\mu_f$  is the friction coefficient between the O-ring and the cylinder wall,  $B$  is the cylinder bore,  $d$  is the original O-ring cross-sectional diameter and  $E$  is Young's modulus for the O-ring material [12]. For O-ring seals,  $\mu_f = 0.3$  to  $0.5$  for well finished and sufficiently lubricated sealed surfaces [12] and a typical modulus for elastomeric seals is 10 MPa.

### 4.2.3 Force Efficiency

The pressure for an ideal cylinder is

$$P_i = \frac{M}{A_p} \quad (4.5)$$

where  $M$  is the load, and  $A_p$  is the piston area.

The actual pressure  $P_a$  in the cylinder is smaller than the ideal pressure because of the O-ring friction

$$P_a = \frac{M - f_s}{A_p} \quad (4.6)$$

Therefore, the cylinder force efficiency is

$$\eta = \frac{P_a}{P_i} \quad (4.7)$$

## 4.3 Methods

### 4.3.1 Test Apparatus

Three sets of pistons and matching cylinder blocks were fabricated for validation testing with bore sizes 4, 6 and 9 mm (Fig. 4.1). For high precision, the pistons were machined from tight-tolerance precision ground rod. The cylinder block inner wall was brought to its final dimension using a reamer. Piston grooves were machined into the piston rod with dimensions according to [85], except that the piston groove diameter was intentionally made larger than that specified in the handbook to achieve 14% squeeze ratio as defined by (4.3). Fillets with dimension 0.002” were cut on both the upper and lower portion of the groove to facilitate O-ring mounting. The rings were lubricated before mounting. The overall piston length was less than 10 times the bore to minimize rod bending [75] and a linear bearing was mounted at the top of the cylinder block to vertically constrain the motion of the piston and to minimize side loading on the seal.

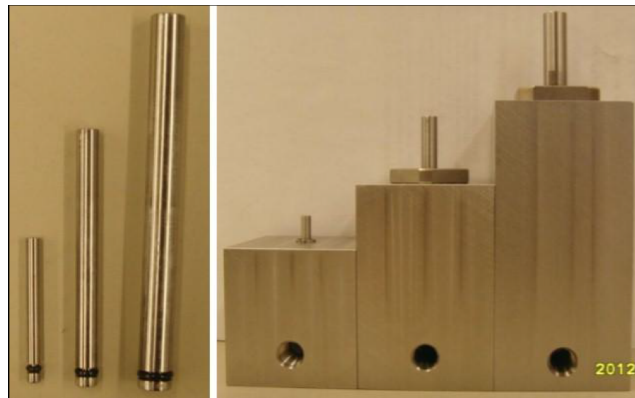


Figure 4.1: Pistons with O-ring seals and matching cylinder blocks

The cylinder block was fixed to a rigid frame (Fig. 4.2). A loading block whose mass

could be varied was suspended above the piston and was able to move up and down on a low-friction linear slide. The load block was carefully aligned to eliminate side loading on the piston and piston seal. The hydraulic chamber under the piston head was connected by tubing to a needle valve that could be adjusted to control the speed of descent of the load pressing down on the other end of the piston rod as hydraulic oil passed through the valve and into a reservoir that was open to atmosphere. Another set of valves connected the cylinder to a small hydraulic axial piston pump whose purpose was to run oil from the reservoir into the cylinder, extending the piston and raising the load for the start of a test. During testing, the pump was disconnected from the circuit.

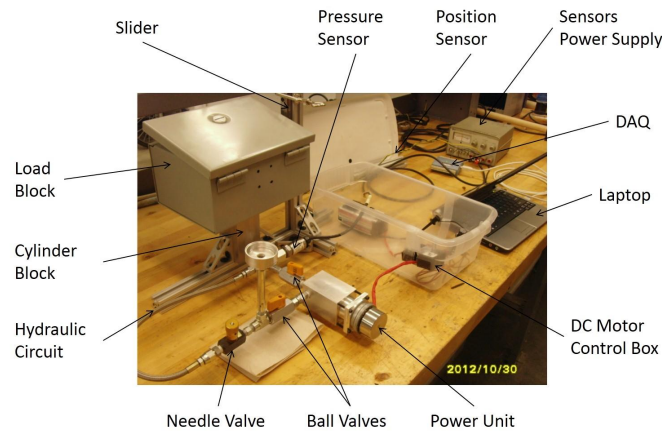


Figure 4.2: Cylinder efficiency test stand

An analog output pressure gauge (PX309-300G5V, Omega Engineering) was connected between the cylinder and the valve to measure cylinder pressure and a linear potentiometer (LCP12Y,ETI Systems) was attached to the load to measure piston position. Pressure and position sensor signals were digitized using a USB data acquisition system (USB-6008, National Instruments). The piston force was determined by measuring the weight of the load block using a digital scale.

### 4.3.2 Test Protocol

The test protocol involved collecting data during a steady state descent of the load whose speed was determined by setting the needle valve. Test conditions covered a range of loads and a range of descent speeds. The advantages of using this protocol were that the motion was smooth compared to the flow ripple that results from pump-driven motion and that slow speeds could be attained through minimal cracking of the valve. An example cylinder pressure measurement during a load descent trial is shown in Fig. 4.3, which demonstrates essentially constant output. An example of slow speed motion is shown in Fig. 4.4 where the velocity is about 1 mm/s and the staircase profile of the position record is caused by ADC quantization.

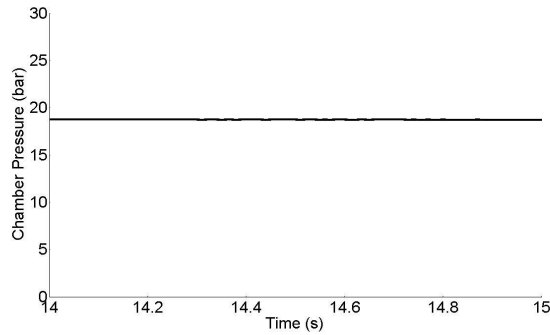


Figure 4.3: Pressure recorded during a typical characterization trial where the load was descending

A trial started by moving the load to its raised position using the pump after which the pump was disconnected from the circuit by closing the pump valve. Weights were added to the load block to reach the desired test condition. The needle valve was opened to the desired position and position and pressure sensors were sampled as the load descended. The position record was fit to a straight line to estimate piston velocity. The force on the piston was calculated from the load weight and the cylinder pressure from the pressure sensor. The corresponding O-ring efficiency for that test condition was calculated using (4.7). Loads were applied to produce cylinder pressures from about



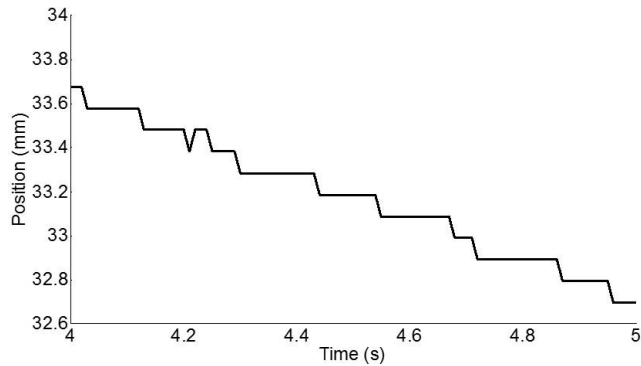


Figure 4.4: Piston position during a slow (1 mm/s) load descent

3.5 to 20.7 bar and speeds were set from about 1 to 20 mm/s. Before each set of tests, the system was bled to eliminate dissolved air. This was done by leaving the system under load for 24 hours.

To measure O-ring leakage, the piston was extended to its maximum height and loaded with the maximum weight with all valves closed, locking the piston in place. The initial position was estimated by collecting data from the position sensor for 5 minutes. At the 2.5 hour mark, the position sensor was sampled for 5 minutes. At the 64 hour mark (to completely eliminate air bubbles), another 5 minutes of position data was sampled. At the 88 hour mark, a final 5 minutes of position data was collected.

## 4.4 Results

Figs. 4.5 through 4.8 compare the cylinder force efficiency as a function of pressure calculated from experiment data (the markers) to the efficiency predicted by the model (the lines) for the three sizes of cylinders and two piston speeds. The friction coefficient  $\mu_f$  between the O-ring and the cylinder wall depends on the lubricating condition and because lubrication can only be estimated, we show the model as upper (dotted line) and lower (dashed line) bounds using the minimum and maximum values of  $\mu_f$  friction coefficient. Fig. 4.8 shows efficiency as a function of bore size for two cylinder pressures.

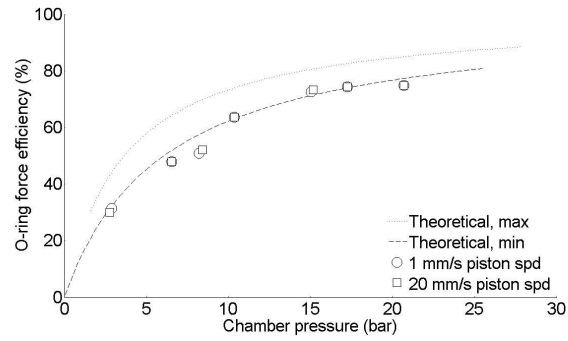


Figure 4.5: Cylinder force efficiency with pressure, 4 mm bore

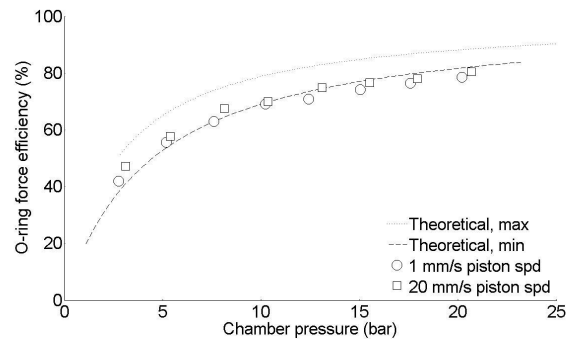


Figure 4.6: Cylinder force efficiency with pressure, 6 mm bore

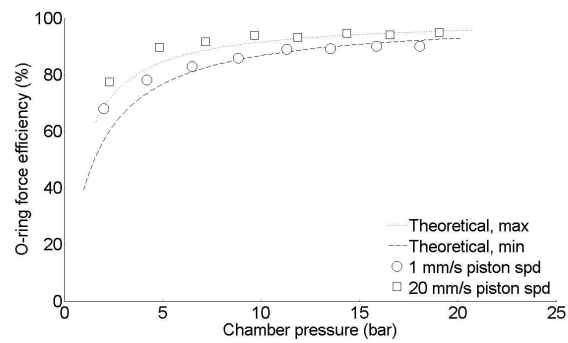


Figure 4.7: Cylinder force efficiency with pressure, 9 mm bore

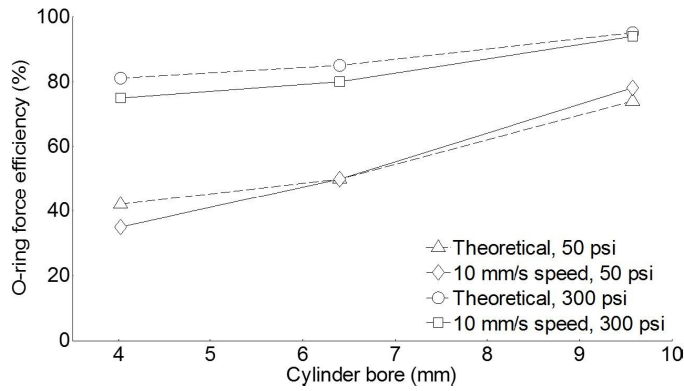


Figure 4.8: Cylinder force efficiency with bore size

Fig. 4.9 shows the position of the cylinder during the leak test with the initial position set to 0 microns. At 2.5 hours, the data is oscillating between -100 and -200 microns because escaping air bubbles in the fluid causing noise on the position signal. At 64 and 88 hours, the position is fixed at -200 microns.

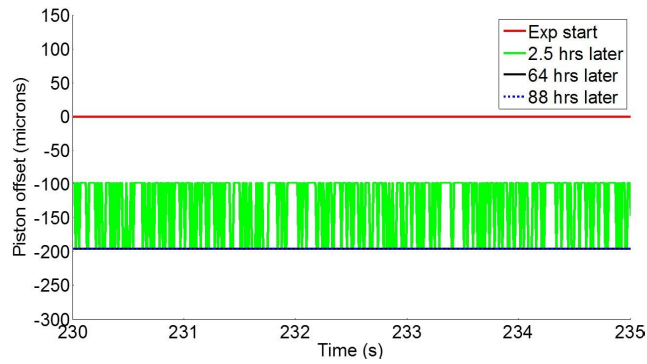


Figure 4.9: Piston position during O-ring leak test

## 4.5 Discussion

### 4.5.1 Seal Leakage

The leakage model in (4.1) predicts leakage by a moving seal, however, because the leakage is small, measuring the flow rate out the cylinder and the piston velocity with

the required precision was not feasible. The experiment did show (Fig. 4.9) that leakage is insubstantial as the piston did not move over many hours of being under load. From this we conclude that in our case the cylinder volumetric efficiency is essentially 100% and that the overall efficiency for small bore cylinders is dominated by the seal friction.

### Seal Friction

The results show that the friction model of (4.4) predicted the measured piston force efficiency for all three sizes and across the entire tested operating range as can be seen most clearly in Fig. 4.8.

Typically, an O-ring squeeze ratio between 7%-15% is an acceptable range for the O-ring to perform well [15]. A 14% squeeze ratio was selected for the cylinders tested in this study to ensure there would be sufficient friction to measure in the experiment. Figs. 4.5 - Fig. 4.7 show that the piston efficiency is close to 100% when the pressure is high, despite the high O-ring squeeze ratio, and that efficiency rolls off with lower pressure as expected. In applications where low friction was paramount, it would be possible to fabricate a cylinder with a lower squeeze ratio seal which would raise efficiency at lower pressures. Using a squeeze ratio over 15% is not recommended as the friction goes up substantially and the O-ring may become stretched. The O-ring stretch percentage is

$$\sigma = \frac{D_g - D_i}{D_i} \cdot 100 \quad (4.8)$$

where  $D_g$  is the mounting groove diameter, and  $D_i$  is the O-ring inner diameter. The stretch percentage is directly related to the squeeze ratio, and to avoid damage should not exceed the limit established by good design practice [85].

Equation (4.4) states that the seal friction does not change with piston velocity. This is approximately the case in Figs. 4.5 – 4.8 and implies that speed need not be taken into account when computing cylinder efficiency for cases where the seal is leak free or almost leak free.

Closer examination of the figures, and particularly Fig. 4.7 for 9 mm bore, reveals

that efficiency does depend somewhat on speed. This is because friction coefficient  $\mu_f$  in (4.4) changes, which can be explained by the Stribeck curve shown in Fig. 4.10 that shows the variation of the friction between two liquid lubricated surfaces [86]. In our experiment, cylinder efficiency improved with speed, which indicates that as speed increased, friction was likely moving down the Stribeck curve in the mixed friction region.

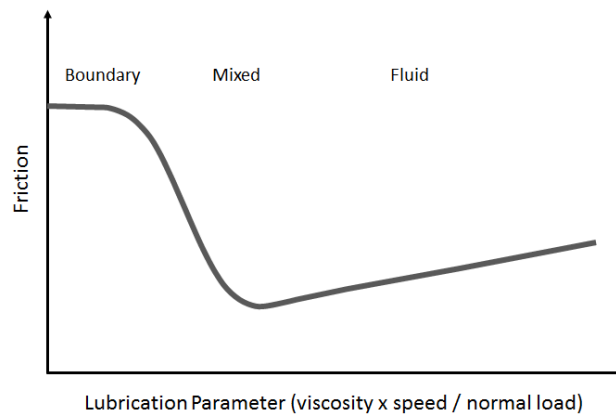


Figure 4.10: Typical Stribeck curve showing how friction depends on speed. Three friction regions are identified: boundary, mixed and fluid, or hydrodynamic. The pistons had lower friction (more efficient) at higher speeds, which indicates moving down the curve in the mixed friction region.

## 4.6 Conclusion

The main conclusion from this study is that a simple mathematical model for an O-ring is sufficient to describe the friction and leakage for a small hydraulic cylinder. Further, the experiments showed that for a small cylinder, an O-ring seal is essentially leak-free, which means that cylinder efficiency depends only on friction. Therefore, when developing system models for tiny hydraulic systems, small cylinders may be represented by a cylinder force efficiency modeled by (4.4). The experiments also showed that the simple model is not sufficient to describe detailed behavior such as the small changes in

friction that occur with piston speed.

## Chapter 5

# Efficiency Models for Small Hydraulic Pumps

### 5.1 Introduction

Human-scale devices such as prostheses, orthoses and hand tools require large force, slow speed, light weight and small size, which matches the high power density characteristics of hydraulic systems [87, 77]. Traditionally, human-scale devices have been driven by electro-mechanical systems since small-scale electric motors, gears and batteries are readily available. Hydraulic power systems, however, can provide higher power density than the equivalent electro-mechanical systems at human-scale power range [88], but small-scale hydraulic pumps, hoses and cylinders are not commercially available.

Since the pump is the heart of a hydraulic system, its size, weight and efficiency are of great concern for tiny mobile hydraulic systems. Existing models of pump efficiency typically contain empirical formulas [2] or are derived from finite element analysis [89]. The empirical models assume that pump efficiency is correlated to known parameters such as operating pressure, shaft speed, and fluid viscosity, then use experimental data to identify the unknown coefficients of the proposed efficiency model. While this method

is helpful in terms of analyzing the performance of existing pumps, it cannot predict the performance of new pumps, including new small-scale pumps. Finite element models can predict and optimize the performance of any proposed pump and are excellent for optimizing a design, but a detailed FEM analysis is time consuming and not suited for system level design decisions. Simplified analytical models based on the physics of mechanics and fluid flow have about the accuracy of empirical models and are easily integrated into system-level models.

The focus of this Chapter is to develop analytic efficiency models for two common types of hydraulic pumps. The first is the hydraulic vane pump, which is lighter than any other type of pump with the same displacement [90]. Balanced vane pumps (also called double-stroke vane pumps) are preferable than single-stroke vane pumps because they are more compact than single stroke vane pumps [2]. Additionally, balanced vane pumps have little side load on the pump shaft due to the hydraulic pressure balance. Small side load reduces friction torque, which increases pump mechanical efficiency.

The second type is the hydraulic piston pump, which has the highest efficiency among all pump types [2]. Although piston pumps are generally heavier than equivalent vane pumps, their high efficiency can offset the heavier weight because higher pump efficiency indicates a smaller and lighter prime mover to drive the pump. Axial piston pumps are less efficient than bent-axis piston pumps, but are lighter and structurally simpler [90].

## 5.2 Vane Pump Model

### 5.2.1 Geometry

The typical structure of a balanced vane pump is shown in Fig. 5.1 with the corresponding symbols identified in Table 5.1. The rotor-vane assembly rotates with the pump driving shaft within the elliptic cam ring. The pump has two inlet and two outlet diametrical ports, which balance the pressure load on the driving shaft [91]. When the



vanes are driven across the inlet ports, the fluid is sucked into the chamber between the vanes due to the chamber volume expansion and when the vanes are driven across the outlet ports, the fluid is squeezed out due to the chamber volume reduction.

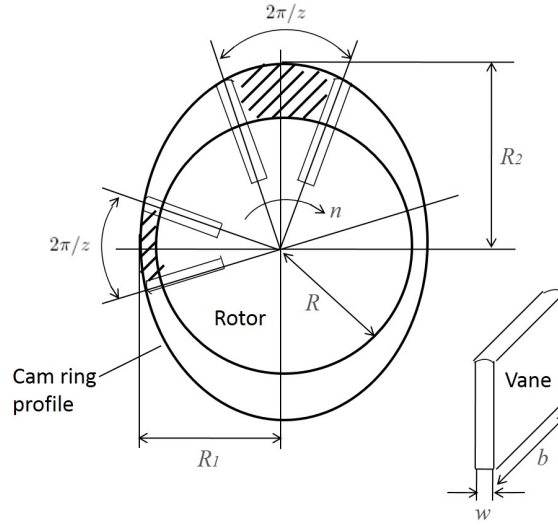


Figure 5.1: Layout of a hydraulic balanced vane pump.

For the vane pump shown in Fig. 5.1, the pump displacement without leakage is

$$V_{\text{th}} = 2 \cdot z \cdot b \cdot \left\{ \frac{\pi}{z} \cdot (R_2^2 - R_1^2) - w \cdot (R_2 - R_1) \right\} \quad (5.1)$$

For the case where  $w \cdot z / [\pi \cdot (R_2 + R_1)] \ll 1$ , which is true when the vanes are thin, the pump displacement can be simplified to

$$V_{\text{th}} = 2 \cdot \pi \cdot b \cdot (R_2^2 - R_1^2) \quad (5.2)$$

### 5.2.2 Mechanical Efficiency

The mechanical efficiency for a hydraulic balanced vane pump is

$$\eta_m = \frac{T_{\text{th}}}{T_{\text{th}} + T_n + T_b} \quad (5.3)$$

Table 5.1: Vane pump symbols.

| Var        | Description                                      | Unit |
|------------|--------------------------------------------------|------|
| $R_1$      | cam ring small radius                            | m    |
| $R_2$      | cam ring large radius                            | m    |
| $R$        | rotor radius                                     | m    |
| $z$        | number of vanes                                  | —    |
| $n$        | rotor speed                                      | rpm  |
| $w$        | vane thickness                                   | m    |
| $b$        | vane width                                       | m    |
| $\mu$      | fluid viscosity                                  | Pa·s |
| $\delta$   | gap height between rotor & side plate            | m    |
| $P_s$      | pump suction pressure                            | Pa   |
| $P_d$      | pump delivery pressure                           | Pa   |
| $\Delta P$ | pressure difference across pump ( $P_d - P_s$ )  | Pa   |
| $\lambda$  | friction coefficient between vane tip & cam ring | —    |

where  $T_{th}$  is the torque required to drive the pump shaft without considering friction,  $T_n$  is the torque required to overcome the friction between the vane tip and the cam ring, and  $T_b$  is the torque required to overcome the shaft bearing and oil seal friction.

Because  $T_b$  is independent of the pump operating pressure  $\Delta p$  [49] and because the shaft bearing friction can be balanced by a proper design of the pump inlet and outlet ports,  $T_b$  is not considered in (5.3). Therefore, the mechanical efficiency is estimated as

$$\eta_m = \frac{T_{th}}{T_{th} + T_n} \quad (5.4)$$

Using power conservation and the relation between pump torque and pressure (see [2] and [49]),  $T_{th}$  and  $T_n$  can be expressed as

$$T_{th} = \frac{V_{th}}{2 \cdot \pi} \cdot \Delta P \quad (5.5)$$

$$T_n = \lambda \cdot z \cdot \frac{R_1 + R_2}{2} \cdot \frac{w \cdot b \cdot \Delta P}{2} \quad (5.6)$$

where  $w \cdot b \cdot \Delta P / 2$  is the average fluid pressure force acting on each vane and  $(R_1 + R_2) / 2$  is the average moment arm.

### 5.2.3 Volumetric Efficiency

There are three causes of volumetric flow losses in a hydraulic balanced vane pump: the gap between the vane tip and the cam ring, the gap between the vanes and the rotor, and the gap between the rotor and the side plates. The gap between the vanes and the side plates is neglected because for most pumps it is small compared to the area between the rotor and side plates. The first loss is small since the pump can be designed so that the vanes press against the cam ring during the whole pumping cycle. The second factor is also small because long vane guides are generally used to reduce the side load on the vanes. Therefore, only the third factor will be used to estimate volumetric efficiency.

The flow between the rotor and the side plates can be modeled as a slip flow between two parallel flat plates [2], modified to the pump geometry

$$Q = \frac{U \cdot b \cdot d}{2} - \frac{b \cdot d^3}{12 \cdot \mu} \cdot \frac{dp}{dx} \quad (5.7)$$

where  $U$  is the upper plate travel velocity,  $b$  is the plate width,  $d$  is the gap height between the two plates and  $dp/dx$  is the pressure gradient along the  $x$  axis.

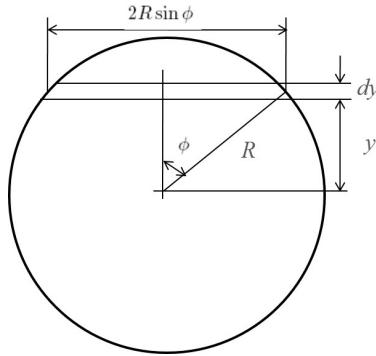


Figure 5.2: Illustration of the slip flow differential.

Assuming both the rotor and the side plate are fixed ( $U = 0$ ) the radial flow due to the centrifugal action is negligible. The slip flow taking place in the parallel channels of width  $dy$  and length  $2R \sin \phi$  (Fig. 5.2) can be determined by adapting (5.7) with

$U = 0$ ,  $b = dy$ ,  $y = R \cos \phi$ ,  $dx = 2R \sin \phi$ , and assuming  $d = \delta$  and  $dp = \Delta p$ , which results in

$$\begin{aligned} dQ_s &= -\frac{\delta^3}{24\mu} \cdot \frac{\Delta p}{R \sin \phi} \cdot dy \\ &= -\frac{\delta^3}{24\mu} \cdot \frac{\Delta p}{R \sin \phi} \cdot (-R \sin \phi) \cdot d\phi \\ &= \frac{\delta^3 \Delta p}{24\mu} \cdot d\phi \end{aligned} \quad (5.8)$$

The total slip flow through the gap between the rotor and the side plate is found by integrating the differential slip flow

$$Q_s = 2 \int_0^{\frac{\pi}{2}} \frac{\delta^3 \cdot \Delta p}{24 \cdot \mu} \cdot d\phi = \frac{\pi \cdot \delta^3 \cdot \Delta p}{24 \cdot \mu} \quad (5.9)$$

The pump flow rate if there were no leakage is

$$Q_{th} = V_{th} \cdot n/60 \quad (5.10)$$

where  $V_{th}$  is from (5.2) for thin vanes or (5.1) for thick vanes. Accounting for both two side plates, the pump volumetric efficiency is therefore

$$\eta_v = \frac{Q_{th} - 2 \cdot Q_s}{Q_{th}} = \frac{V_{th} - \frac{5\pi\delta^3\Delta p}{\mu}}{V_{th}} \quad (5.11)$$

#### 5.2.4 Overall Efficiency

The overall efficiency for a hydraulic balanced vane pump combines the mechanical and volumetric efficiencies and can be expressed as a function of cam lift  $CL$  and bearing number  $BN$

$$\eta = \eta_m \cdot \eta_v = \frac{CL - C/BN}{CL + \lambda \cdot z \cdot w/4} \quad (5.12)$$

where

$$CL = R_2 - R_1 \quad (5.13)$$

$$BN = \frac{\mu \cdot n}{\Delta p} \quad (5.14)$$

$$C = \frac{5 \cdot \delta^3}{2 \cdot b \cdot (R_2 + R_1)} \quad (5.15)$$

Equation (5.12) shows that pump efficiency can be improved by changing cam lift  $CL$ , the number of vanes  $z$ , the vane thickness  $w$  and the friction coefficient  $\lambda$  between the vane tip and the cam ring. Increasing cam lift, however, is constrained by the flow requirement for a specific application. Decreasing vane thickness is constrained by material stiffness and yield strength. The number of vanes must be even to balance the pressure force. The friction coefficient is fixed by the material property and the pressing force between the vane tip and the cam ring. Therefore, optimizing efficiency requires careful adjustment of these key design parameters.

Pump efficiency is a function of displacement with efficiency going down as displacement decreases, as shown in Fig. 5.3, which was derived from the efficiency model developed above. The reason the efficiency drops with pump size is that pump power is proportional to pump volume while pump leakage and friction losses are proportional to the pump surface area. As the size decreases the volume to surface area ratio increases, resulting in the efficiency drop. The drop is particularly pronounced at the smallest scale, which means that the design of miniature pumps is challenging and that below a certain size, pump loss will dominate system efficiency.

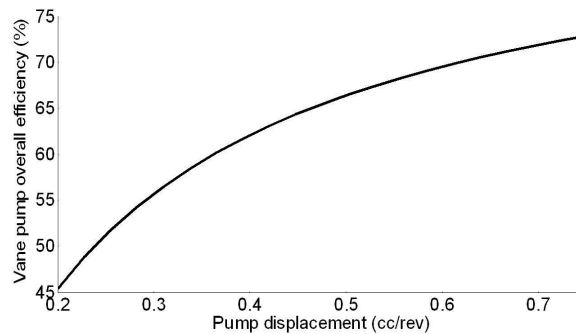


Figure 5.3: Efficiency as a function of displacement for a vane pump.

Fig. 5.4 shows the sensitivity of the pump efficiency model to several key design parameters. The nominal operating conditions used to generate these data were 2000 psi outlet pressure, 2000 rpm shaft speed, and mineral oil as the working fluid. The results will be different if different operating conditions are used. From the figure it can be

seen that vane pump efficiency is most sensitive to rotor radius and the vane material yield strength, which determines the vane thickness. The sensitivity to rotor radius is in line with the scaling law shown in Fig. 5.3, which is that for a fixed pump size, the bigger the rotor, the smaller the cam lift, and hence the lower the efficiency. Based on the sensitivity results, to maximize efficiency, one should minimize the rotor size and use fabricate vanes from a high yield-strength material. Note that the safety factor was used in the process of sizing the vane thickness.

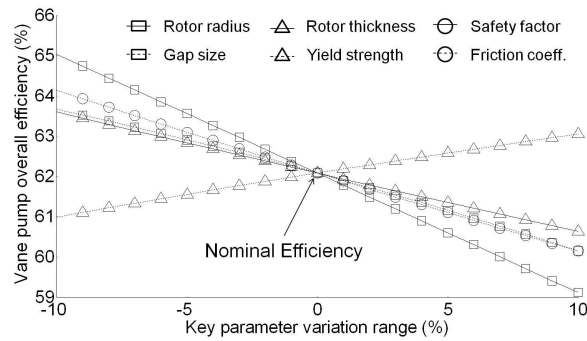


Figure 5.4: Sensitivity of the hydraulic balanced vane pump efficiency model.

### 5.2.5 Model Validation

The efficiency model was validated using data from the Eaton-Vickers V10/V20 line of pumps. Fourteen pumps with displacement ranging from 3.3 cc/rev to 42.4 cc/rev were analyzed. Internal dimensions and operating conditions were obtained from the pump manufacturer and used as parameters in the efficiency model to generate a theoretical efficiency for a particular pump. Catalog data for the measured efficiency of the same pump were used to generate the experimental efficiency. The results are shown in Fig. 5.5.

The modeled efficiency is 10 to 15% higher than the measured efficiency over the entire output power range. This is in line with the fact that minor losses such as that due to fluid compressibility, inlet suction and outlet delivery were not considered in

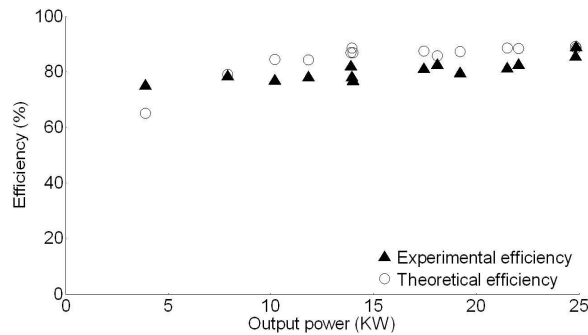


Figure 5.5: Validation of the efficiency model for the vane pump.

the model. Despite this difference, the model is sufficiently accurate to enable top-level design decisions.

## 5.3 Piston Pump Model

### 5.3.1 Geometry

The typical structure of a hydraulic axial piston pump and its key dimensions are shown in Fig. 5.6. The symbols definitions are provided in Table 5.2. The cylinder block and the pistons rotate together with the pump driving shaft while the slipper pads are in continual contact with the swash-plate. Like the vane pump, hydraulic fluid is sucked into and squeezed out of the pump through the valve plate due to the change in cylinder chamber volume as the pump rotates. The gaps between the slipper pads and the swash plate, between the pistons and the cylinder walls, and between the cylinder block and the valve plate allow the rotational and translational movements, while at the same time cause leakage and friction losses.

The analytical efficiency model of the axial piston pump is more complicated than that of the vane pump because both translational and rotational motions are involved during the pumping cycle, friction and leakage losses happen in three facing gaps, none of which can be neglected, and the piston may contact the cylinder wall due to the

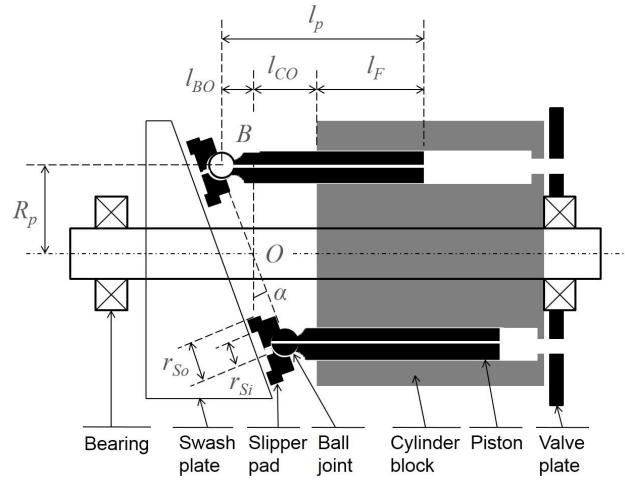


Figure 5.6: Key geometrical dimensions associated with the piston pump efficiency modeling.

Table 5.2: Piston pump symbols.

| Var      | Description                                     | Unit  |
|----------|-------------------------------------------------|-------|
| $d_p$    | piston diameter                                 | m     |
| $R_p$    | pitch radius                                    | m     |
| $l_p$    | piston length                                   | m     |
| $w$      | shaft speed                                     | rad/s |
| $z$      | number of pistons                               | —     |
| $\alpha$ | swash-plate angle                               | deg   |
| $P$      | operating pressure                              | Pa    |
| $\mu$    | fluid viscosity                                 | Pa·s  |
| $h_p$    | gap height between piston & cylinder wall       | m     |
| $h_s$    | gap height between slipper pad & swash-plate    | m     |
| $h_v$    | gap height between valve plate & cylinder block | m     |



centrifugal forces. Thus an average model over the pumping cycle is derived.

### 5.3.2 Basic Equations

Before formulating the mechanical and volumetric efficiencies, the basic equations that describe the piston pump operation are needed. Detailed derivations of the mechanical and volumetric efficiency of a hydraulic axial piston motor are found in references [50, 92, 90]. In this paper the appropriate transformations are used to adapt those models to a piston pump, aided by the basic equations derived in this section.

The piston cross-section area is

$$A_p = \frac{\pi}{4} \cdot d_p^2 \quad (5.16)$$

The distance between the origin O and the ball joint at the outer dead point (ODP) is

$$l_{BO} = R_p \cdot \tan \alpha \quad (5.17)$$

The pump displacement at ODP, which is the maximum single piston displacement, can be derived using eq. (A2) in [50]

$$V_{p_{max}} = \frac{A_p \cdot R_p \cdot \tan \alpha \cdot 2 \cdot \pi}{2 \cdot \sin[\pi/(2 \cdot z)]} \quad (5.18)$$

The pump displacement at ODP can also be expressed as

$$V_{p_{max}} = A_p \cdot (l_p - l_{BO} - l_F) \quad (5.19)$$

where  $l_p$ ,  $l_{BO}$  and  $l_F$  are defined in Fig. 5.6. Combining (5.18) and (5.19) gives the length of the piston guide at ODP

$$l_F = l_p - l_{BO} - \frac{\pi \cdot R_p \cdot \tan \alpha}{\sin[\pi/(2 \cdot z)]} \quad (5.20)$$

The distance between the origin O and the cylinder block can then be stated as

$$l_{CO} = l_p - l_F - l_{BO} \quad (5.21)$$

From [90], the outer and inner radius of the slipper sealing ring is estimated as

$$r_{So} = 1.25 \cdot d_p \quad (5.22)$$

$$r_{Si} = d_p \quad (5.23)$$

and the key valve plate dimensions shown in Fig. 5.7 can be approximated as

$$b_{v1} = 0.15 \cdot d_p \quad (5.24)$$

$$b_{v2} = b_{v1} \quad (5.25)$$

$$s = 2 \cdot [R_p \cdot \sin(180/z) - d_p/2] \quad (5.26)$$

$$r_{v4} = R_p + s + \frac{d_p}{2} \quad (5.27)$$

$$r_{v1} = R_p - s - \frac{d_p}{2} \quad (5.28)$$

$$r_{v3} = r_{v4} - b_{v2} \quad (5.29)$$

$$r_{v2} = r_{v1} + b_{v1} \quad (5.30)$$

where  $s$  is the minimum distance between the pistons. Finally, from [90] and [93], the typical friction coefficient between the piston and the cylinder block is  $f_p = 0.085$ .

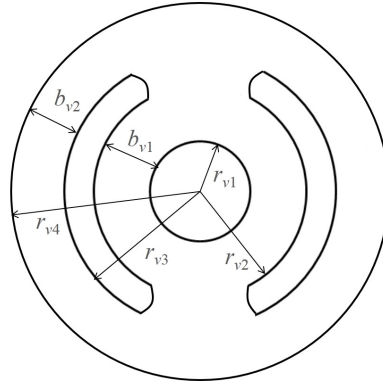


Figure 5.7: Key valve plate dimensions for a axial piston pump.

### 5.3.3 Mechanical Efficiency

Without friction, the average torque required to drive the pump shaft is

$$T_{pp} = \frac{P \cdot A_p \cdot R_p \cdot \tan \alpha \cdot z}{\pi} \quad (5.31)$$

Losses occur because of Coulomb and viscous friction acting between sliding surfaces. Coulomb friction can be neglected for surfaces separated by a small gap where hydrostatic balancing is present.

The average torque loss due to viscous friction between the pistons and the cylinder block is

$$T_{lvp} = \frac{\mu \cdot \pi \cdot d_p \cdot (R_p \cdot \tan \alpha)^2 \cdot (l_F + R_p \cdot \tan \alpha) \cdot w \cdot z}{2 \cdot h_p} + \frac{d_p \cdot h_p \cdot R_p \cdot \tan \alpha \cdot P \cdot z}{2} \quad (5.32)$$

The average torque losses due to Coulomb friction between the pistons and the cylinder block is [92]

$$T_{lfp} = \left[ \frac{B}{b} + \frac{A \cdot b - a \cdot B}{b \cdot \sqrt{a^2 - b^2}} \right] \cdot A_p \cdot P \cdot R_p \cdot \tan \alpha \cdot \frac{z}{\pi} \quad (5.33)$$

where

$$A = f_p \cdot \tan \alpha \cdot (l_p + l_{CO} - f_p \cdot d_p) \quad (5.34)$$

$$B = f_p \cdot \tan \alpha \cdot l_{BO} \quad (5.35)$$

$$a = l_p - l_{CO} - f_p \cdot \tan \alpha \cdot (l_p + l_{CO} - f_p \cdot d_p) \quad (5.36)$$

$$b = -(1 + f_p \cdot \tan \alpha) \cdot l_{BO} \quad (5.37)$$

The average torque loss due to viscous friction between the slipper and the swash plate is

$$T_{ls} = \frac{z \cdot \mu \cdot w \cdot R_p \cdot \pi \cdot (r_{So}^2 - r_{Si}^2) \cdot R_p}{h_s} \quad (5.38)$$

Finally, the average torque loss due to the viscous friction between the valve plate and the cylinder block is [90]

$$T_{lv} = \frac{\mu \cdot \pi \cdot w \cdot (r_{v4}^4 - r_{v3}^4 + r_{v2}^4 - r_{v1}^4)}{2 \cdot h_v} \quad (5.39)$$

The mechanical efficiency over one cycle can then be expressed as

$$\eta_m = \frac{T_{pp}}{T_{pp} + T_{lvp} + T_{lfp} + T_{ls} + T_{lv}} \quad (5.40)$$

### 5.3.4 Volumetric Efficiency

With no leakage, the average flow rate of the piston pump would be

$$Q_{vp} = w \cdot A_p \cdot R_p \cdot \tan \alpha \cdot \frac{z}{\pi} \quad (5.41)$$

The average leakage loss through the facing gap between the pistons and the cylinder block is

$$Q_{lp} = \frac{\pi \cdot d_p \cdot h_p^3 \cdot z \cdot P}{24 \cdot \mu \cdot \sqrt{(l_F + R_p \cdot \tan \alpha)^2 - (R_p \cdot \tan \alpha)^2}} + \frac{d_p \cdot h_p \cdot w \cdot R_p \cdot \tan \alpha \cdot z}{2} \quad (5.42)$$

The average leakage loss through the face gap between the slippers and the swash plate is

$$Q_{ls} = \frac{\pi \cdot h_s^3 \cdot z \cdot P}{12 \cdot \mu \cdot \log(r_{so}/r_{si})} \quad (5.43)$$

Finally, the average leakage loss through the face gap between the valve plate and the cylinder block is

$$Q_{lv} = \frac{h_v^3 \cdot \lambda_v \cdot z \cdot P}{24 \cdot \mu \cdot l_v} + \frac{h_v \cdot (b_{v1} + b_{v2}) \cdot R_p \cdot w \cdot z}{4} \quad (5.44)$$

where  $\lambda_v$  and  $l_v$  can be approximated as [90]

$$\lambda_v = 0.4 \cdot d_p \quad (5.45)$$

$$l_v = \frac{b_{v1} \cdot b_{v2}}{b_{v1} + b_{v2}} \quad (5.46)$$

The volumetric efficiency over one pumping cycle can then be expressed as

$$\eta_v = \frac{Q_{vp} - Q_{lp} - Q_{ls} - Q_{lv}}{Q_{vp}} \quad (5.47)$$

### 5.3.5 Overall Efficiency

The overall efficiency for a piston pump over one pumping cycle is

$$\eta = \eta_v \cdot \eta_m \quad (5.48)$$

As with the vane pump, the efficiency drops with pump displacement as shown in Fig. 5.8.

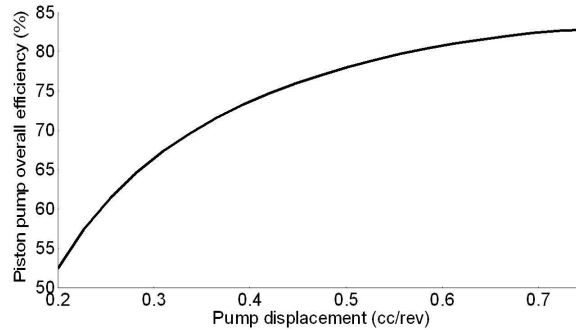


Figure 5.8: Efficiency as a function of displacement for a piston pump.

The sensitivity of pump efficiency to selected design parameters is shown in Fig. 5.9 for nominal operating conditions of 2000 psi outlet pressure, 2000 rpm shaft speed, and mineral oil as the working fluid. Fig. 5.9 reveals that the pump efficiency is most sensitive to the swash-plate angle and the gap between the slipper and the swash-plate. From (5.18), it can be seen that swash-plate angle  $\alpha$  is proportional to the pump displacement, which in turn is related to pump efficiency as shown in Fig. 5.8. Fig. 5.10 is the same as the previous figure except that the nominal slipper gap changes from 6  $\mu\text{m}$  to 8  $\mu\text{m}$ , demonstrating that sensitivity results are specific to the operating condition.

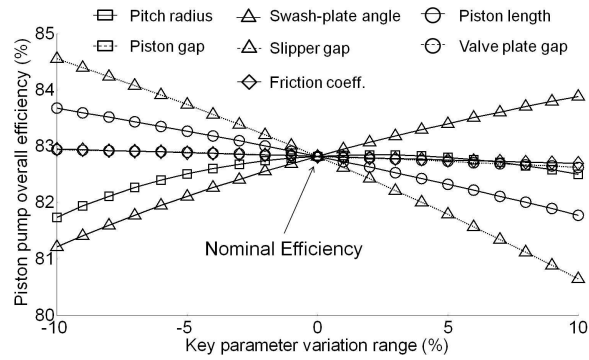


Figure 5.9: Sensitivity of the hydraulic axial piston pump efficiency model, slipper gap = 6  $\mu\text{m}$ .

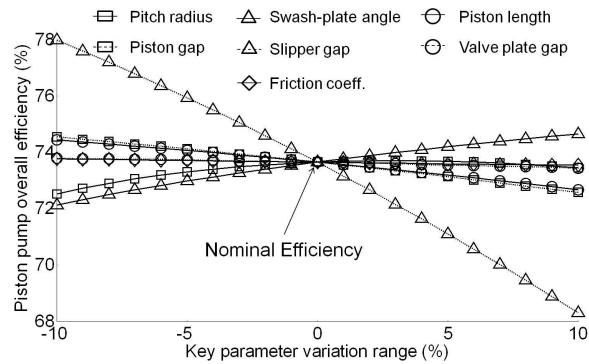


Figure 5.10: Sensitivity of the hydraulic axial piston pump efficiency model, slipper gap = 8  $\mu\text{m}$ .

### 5.3.6 Model Validation

The piston pump model for efficiency as a function of operating pressure was validated for a Takako Industries, Inc. axial piston pump with 0.4 cc/rev displacement. The predicted theoretical efficiency was determined by entering geometry data for the pump, obtained from the manufacturer, into the efficiency model. The measured efficiency for the pump was based on data from the manufacturer for output pressure and flow as a function of input shaft torque and speed.

The results are shown in Fig. 5.11. The modeled efficiency is 10 to 15% higher than the measured efficiency. One reason for the difference is that minor losses such as those due to fluid compressibility, inlet suction and outlet delivery were not considered in the model. Another reason is that geometry data for the gap height between the slipper pad and the swash plate and between the cylinder block and the valve plate were not provided by the manufacturer, so typical values for these parameters were used for the validation.

Despite the difference, as with the vane pump, the piston pump efficiency model is sufficiently accurate for making top-level system design choices, which is the long-range goal of this study.

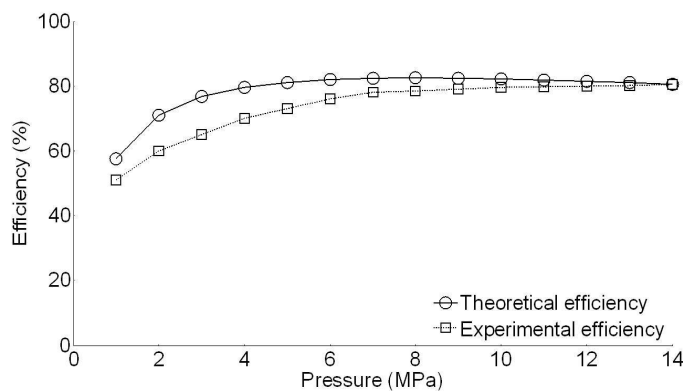


Figure 5.11: Piston pump efficiency model verification.

## 5.4 Design Case Study

The purpose of the efficiency models presented in this paper is to enable top-level decisions, particularly for designs involving miniature hydraulic systems. This section presents a case study that demonstrates the use of the efficiency models.

Our lab is developing an untethered ankle-foot orthosis (AFO) that is powered by tiny hydraulics [77, 94]. In [88] we demonstrated the weight advantage of hydraulic over electric motor actuation for small-scale if running at high pressures, but in that study did not consider the hydraulic power supply. In this case study, we address the question of whether the pressurized fluid should be delivered by a vane pump or a piston pump when the configuration of the power supply is Battery  $\rightarrow$  DC Electric Motor  $\rightarrow$  Hydraulic Pump. While vane pumps are lighter, their lower efficiency requires a larger electric drive motor and a larger battery.

The nominal operating conditions for the pump are 130 W of fluid power output at 69 bar (1000 psi), approximately what is needed for the AFO. Using nominal pump design parameters shown in Table 5.3, the efficiency model predicts that the vane pump has an overall efficiency of 47% while the piston pump has an efficiency of 70%.

Table 5.3: Pump nominal design parameters. Symbols are defined in Tables 5.1 and 5.2.

| VANE PUMP                                                                                                |                              |             | PISTON PUMP |                      |             |
|----------------------------------------------------------------------------------------------------------|------------------------------|-------------|-------------|----------------------|-------------|
| <i>Var</i>                                                                                               | <i>Nominal Value</i>         | <i>Unit</i> | <i>Var</i>  | <i>Nominal Value</i> | <i>Unit</i> |
| $P = 6.9 \text{ MPa}, n = 2000 \text{ rpm} (w = 209 \text{ rad/s}), \mu = 0.028 \text{ Pa}\cdot\text{s}$ |                              |             |             |                      |             |
| $R$                                                                                                      | 1                            | cm          | $d_p$       | 4.5                  | mm          |
| $R_1$                                                                                                    | $1.1 \times R$               | m           | $R_p$       | 7.8                  | mm          |
| $z$                                                                                                      | 8                            | —           | $l_p$       | 13.3                 | mm          |
| $b$                                                                                                      | 1                            | cm          | $z$         | 7                    | —           |
| $\delta$                                                                                                 | 30                           | micron      | $\alpha$    | 13                   | $^\circ$    |
| $\lambda$                                                                                                | 0.1                          | —           | $h_p$       | 13                   | micron      |
| $R_2$                                                                                                    | from (5.1)                   | m           | $h_s$       | 6                    | micron      |
| $w$                                                                                                      | from cantilever beam formula | m           | $h_v$       | 7.5                  | micron      |

The predicted weights of the vane and piston pumps are 45 gm and 129 gm. The



vane pump weight was estimated using a thin-walled pressure vessel formula, as shown in (2.1), to estimate the amount of material needed for the containment shell. The piston pump weight was estimated by fitting an empirical expression to published data for miniature piston pumps from Takako Industries, Parker Oildyne and a KIST research lab (Fig. 5.12).

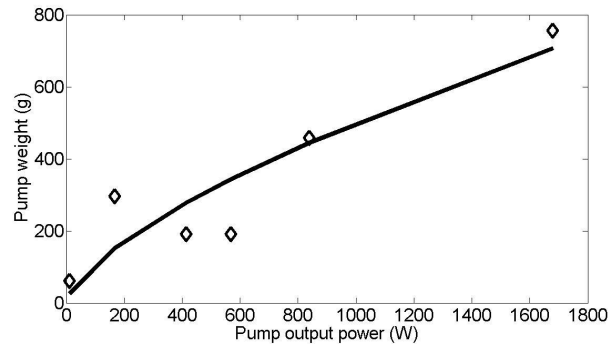


Figure 5.12: Piston pump weight vs output power.

The pump output power and efficiency set the required power of the DC electric motor, which means the electric motors needed to drive the vane and piston pumps must have a mechanical output power of 277 W and 186 W. From the analysis of DC electric motors presented in [88], the expected weights of these two motors will be 415 gm and 226 gm.

The weight of the battery is related to battery chemistry and capacity. The capacity is determined by the required electrical power output and the desired run time for the orthosis, where for this example, we assumed a 10,000 steps run time and 11 J of mechanical energy required per step [3]. To determine the energy density of the battery, we fit an empirical formula to published data for commercial LiPo batteries. As shown in Fig. 5.13, the density model is a constant of 148 Wh/Kg over all battery capacities and we used this constant to estimate the battery weight.

Finally, the estimated weight of the complete power supply was calculated, ignoring interconnects and enclosures. Table 5.4 shows the result, which is that to minimize the

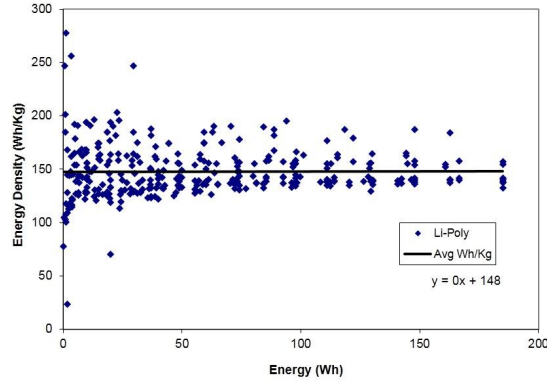


Figure 5.13: Energy density model of LiPo battery.

overall weight of the power supply for this application, a piston pump should be used.

Table 5.4: Power supply weight (gms) for vane and piston pump configurations.

| Component | Vane Configuration | Piston Configuration |
|-----------|--------------------|----------------------|
| Pump      | 45                 | 129                  |
| DC Motor  | 415                | 226                  |
| Battery   | 616                | 411                  |
| Total     | 1271               | 962                  |

## 5.5 Discussion

As demonstrated by the case study, the efficiency models developed in this paper are useful for making top level design decisions. Because of the model simplicity, however, more advanced modeling tools such as FEA should be used to design a pump optimized to a specific application. The limitations of the efficiency model include the following. First, the models only considered the leakage and friction related to the clearance gaps. Other factors such as pressure losses at suction and delivery distribution, and fluid compressibility were not considered, resulting in the model efficiencies that are higher than what can be actually attained. Second, the models assumed that the fluid temperature is regulated, so that the fluid viscosity is constant. In a real system, temperatures

can change and both mechanical and volumetric efficiencies are strong functions of the working fluid viscosity.

For small-scale mobile applications, pump size, weight and efficiency are particularly important. Because efficiency is a strong function of pump displacement and operating pressure, operating at high pressure and using a pump configuration with the highest possible displacement for the required size envelope should be the design drivers.

## Chapter 6

# Design Example: a Hydraulic Ankle Foot Orthosis

### 6.1 Introduction

An ankle-foot orthosis (AFO) is an orthosis or brace that encumbers the ankle and foot. AFOs are externally applied and intended to control position and motion of the ankle, compensate for weakness, or correct deformities. AFOs can be used to support weak limbs. They are also used to correct foot drop, a muscular pathology that causes the inability of a person to raise or lower his foot during walking. Patients with this type of impairment often swing their legs in large arcs or raise their knees higher than normal to walk [95]. Common brain and spinal disorders that lead to foot drop are multiple sclerosis, cerebral palsy and stroke.

A recent literature review [96] classified the AFO devices into three categories: passive, semi-active, and active. Passive AFOs are designed to hold the ankle in a pre-defined position, and are not capable of generating assistive torque. The semi-active AFOs [8, 97] contain capacitive components such as pneumatic springs, which are capable of harvesting and storing energy during the foot drop, so they are able to output

assistive torque, but this torque is limited since the semi-active AFOs don't use external energy. The active AFOs make use of technologies such as pneumatics [98, 99], electrohydraulics [100] and electromechanical systems [101, 102, 103] as external power source, and are capable of generating enough torque to aid the patients for normal walking.

The active AFOs presented in [98, 99, 100, 101] were designed for ankle rehabilitation or for research purposes, so they have a tethered power source, which means these devices cannot be carried around for daily walking. The active AFOs shown in [102, 103] are portable, but they are heavy at the ankle joint, which is not ideal for walking. As demonstrated by a previous study, a 2 kg load placed on each foot of a healthy adult can result in a 30% increase in the rate of oxygen uptake, whereas a 20 kg load placed on the trunk does not result in a measurable increase [104]. The PPAFO presented in [105] is portable and places reasonably light weight on the ankle joint, but it has only modest torque.

The goal of this work was to design a portable active AFO device that could be used for daily walking. This is a challenging task due to the size, weight, power, longevity and safety requirements. The size of the AFO needs to be compact, fitting underneath a loose-fitting pant, so that the patient wearing the AFO will not draw excessive attention from the crowd. The weight needs to be less than 1kg to minimize its impact on ankle dynamics [104]. The AFO also needs to be capable of generating 90 N-m torque and  $100^\circ/\text{s}$  angular velocity, which corresponds to the extreme operating condition during level ground walking [3, 95]. Additionally, the AFO needs to have sufficient energy to support 10,000 steps, which is equivalent to three miles continuous walking. Lastly, the AFO should be safe to use and easy to put on and take off.

To achieve these design goals, a system level analysis was carried out to identify the appropriate configuration, as presented in Section 6.2. Following the system configuration, the packaging options were explored and the optimal packaging was identified, as shown in Section 6.3. Then the efficiency and weight models of the key components were integrated, which enabled the sizing of these components, as detailed in Section

6.4.

## 6.2 AFO Configuration Selection

Rotary or linear actuators can be used to power an AFO, as shown in Fig. 6.1. The AFO configurations under consideration will be limited to fluid power and electro-mechanical due to the maturity and capability of these two technologies. Since sealing high pressure air is challenging and a portable power source for miniature pneumatic systems is not readily available [44], the focus for the following analysis was further reduced to hydraulic and electro-mechanical systems.

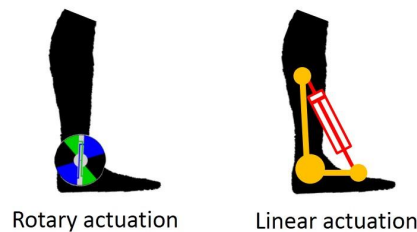


Figure 6.1: Both rotary and linear actuators can power an AFO.

A hydraulic motor and an electric motor & gearhead assembly can both produce rotary motion, but the latter one will not be considered for the AFO application because it would be too heavy. For example, a high end planetary gear head from Maxon Motor capable of outputting 90 N-m torque weighs 3 kg. Hydraulic vane and piston motors were chosen to study due to their light weight and high efficiency characteristics. A hydraulic cylinder and an electric motor & ball screw assembly can both generate linear motion and are light weight, so they could serve as candidates to power the AFO. By appropriately placing the cylinders, one can use either a single or dual cylinders.

There are nine candidates that could power the AFO, as summarized in Fig. 6.2: the hydraulic vane motor system, the hydraulic piston motor system, the single hydraulic cylinder system, the dual hydraulic cylinders system, and the electric motor & ball screw

system.

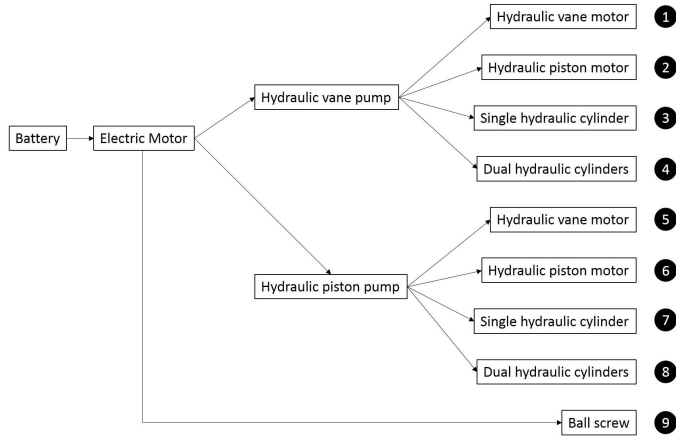


Figure 6.2: AFO configuration candidates.

The first step is to decide which system satisfies the size, weight, power, longevity and safety requirements. Weight and power are linked by power density, as defined in (6.1). The longevity of the AFO is proportional to the available energy, which is proportional to the weight of the energy source. So the longevity requirement is embedded in the system weight term in (6.1). This means the power density can assess the weight, power and longevity requirements together.

$$\text{Power Density} \triangleq \frac{\text{Input Power} \times \text{System Efficiency}}{\text{System Weight}} \quad (6.1)$$

The AFO requires a prime mover. Miniature internal combustion engines are not readily available [22], so a battery & electric motor assembly was used.

A system level analysis was carried out to assess the power density of the nine candidate configurations. In the analysis, each configuration was required to output a peak torque of 90 N-m at 100°/s angular velocity. The input power and the efficiency of each component were then calculated for a given operating condition. The weight of each component was estimated based on its power rating. The efficiency and the weight models were presented in Chapter 3 - cylinder efficiency, Section 2.3 - cylinder weight, Chapter 5 pump efficiency and weight, and Section 2.4 - electric motor and ball screw

efficiency and weight. The battery was sized to support 10,000 steps, where the energy per step was calculated based on the data provided in [3].

The results from this analysis are summarized in Fig. 6.3, which shows that the electro-mechanical system yields the highest power density, while the hydraulic piston motor system gives the lowest power density.

Both vane and piston pump driven systems were analyzed. The piston pump driven systems gave higher efficiency and lower weight for all hydraulic configurations. However, the relative weight and efficiency rankings among these configurations remain the same. This means different pumping elements such as vane, piston or gear will not change the design choice for the system configuration.

| Config No. | Pump Type     | Actuator        | Weight (g) |          |      |          |         | Efficiency (%) |          |      |          |         | Power Density (W/kg) |
|------------|---------------|-----------------|------------|----------|------|----------|---------|----------------|----------|------|----------|---------|----------------------|
|            |               |                 | Battery    | DC Motor | Pump | Actuator | Overall | Battery        | DC Motor | Pump | Actuator | Overall |                      |
| 1          | Balanced Vane | Vane Motor      | 757        | 534      | 49   | 995      | 2335    | 80             | 90       | 47   | 82       | 28      | 67                   |
| 2          | Balanced Vane | Piston Motor    | 643        | 418      | 45   | 9950     | 11056   | 80             | 90       | 46   | 98       | 32      | 14                   |
| 3          | Balanced Vane | Single Cylinder | 592        | 439      | 45   | 132      | 1208    | 80             | 90       | 49   | 100      | 35      | 130                  |
| 4          | Balanced Vane | Dual Cylinder   | 616        | 415      | 45   | 196      | 1272    | 80             | 90       | 47   | 100      | 34      | 123                  |
| 5          | Axial Piston  | Vane Motor      | 439        | 235      | 400  | 995      | 2069    | 80             | 90       | 80   | 82       | 47      | 76                   |
| 6          | Axial Piston  | Piston Motor    | 373        | 184      | 400  | 9950     | 10907   | 80             | 90       | 79   | 98       | 56      | 14                   |
| 7          | Axial Piston  | Single Cylinder | 374        | 196      | 410  | 132      | 1112    | 80             | 90       | 77   | 100      | 55      | 141                  |
| 8          | Axial Piston  | Dual Cylinder   | 393        | 237      | 430  | 196      | 1256    | 80             | 90       | 73   | 100      | 53      | 125                  |
| 9          | None          | Ball Screw      | 320        | 146      | 0    | 72       | 538     | 80             | 90       | 100  | 90       | 65      | 292                  |

Figure 6.3: Power density comparison of AFO candidates. The weight of the hydraulic motors is large since 68 cc/rev displacement is needed to achieve the desired ankle torque. The piston motor weight was estimated based on the vane motor weight.

The reason for the high power density of the electro-mechanical system is it only has one transmission, the ball screw, sitting in between the prime mover and the load. In contrast, the hydraulic systems have two transmission components, the pump and the actuator. Moreover, the hydraulic pump and hydraulic actuator have low efficiency compared to the ball screw.

Though the electro-mechanical system gives the highest system level power density, hydraulic systems are preferred for powering an AFO. The key reasons is the power unit of the hydraulic system can be separated from the actuation system, and hydraulic actuation systems gives higher power density than the electro-mechanical actuation systems



if the operating pressure is high [81, 106]. This is shown in Fig. 6.3: the electro-mechanical actuation system, the electric motor plus the ball screw, weighs 218 grams, which is heavier than the hydraulic cylinders. Another reason to choose hydraulic systems is: cylinders with different bore sizes can be used to match the power requirements for plantarflexion and dorsiflexion. Since the power required for plantarflexion and dorsiflexion are different [3], this feature is important to optimize the actuation system power density. Lastly, hydraulic systems can provide necessary compliance due to the fluid compressibility. For an electro-mechanical system, additional elements such as springs have to be used to achieve the equivalent compliance [102, 103].

Among those eight hydraulic configurations, the hydraulic cylinder systems are preferred due to their higher power densities. The single and dual hydraulic cylinder configurations gave comparable power densities, but the dual cylinder systems is preferred for the AFO application. First, a smaller cylinder can be used for dorsiflexion to further increase the power density; second, it is advantageous to place the actuators at the medial or lateral side of the ankle joint compared to sticking out behind the heel, which cannot fit under pants; lastly, flexible rods can be used in dual cylinders system, which helps prevent rod buckling and reduce packaging size. The flexible rods are feasible for the AFO application since both dorsiflexion and plantarflexion motions can be achieved by tension force. This is the same as human muscle, which can only generate pulling force [3].

The configuration chosen for the HAFO was the piston pump driven dual hydraulic cylinder systems. This configuration could best serve the size, weight, power, and longevity requirements at overall system and actuation sub-system levels.

### **6.3 HFAO Packaging and Integration**

Multiple options are available for where to place components of the HAFO system, as summarized in Fig. 6.4. Option 1 places the whole device on the ankle. This

option provides compact packaging, but the weight on the ankle will be heavy to carry, approximately 1.2 kg (2.6 lbs) as shown in Fig. 6.3. Option 2 places the battery at the hip, which reduces the weight on the ankle by about 30%. While this option allows integration of all hydraulic components, the weight on the ankle is still 863 grams (1.9 lbs). Option 3 places the cylinders on the ankle, and moves the power unit to the hip, with hydraulic hoses sitting in between the power unit and the cylinders. This option minimizes the weight on the ankle joint. From Fig. 6.3, the weight on the ankle is 196 grams, which is less than half pound. Since minimizing the weight on the ankle joint is important for long distance walking [104], option 3 was selected. The key disadvantage of option 3 is the long hydraulic hoses, which may pose pin hole leakage risk, cause discomfort during daily walking, and lead difficulty for dynamic control. These disadvantages will likely prevent the HAFO from becoming daily walking device.

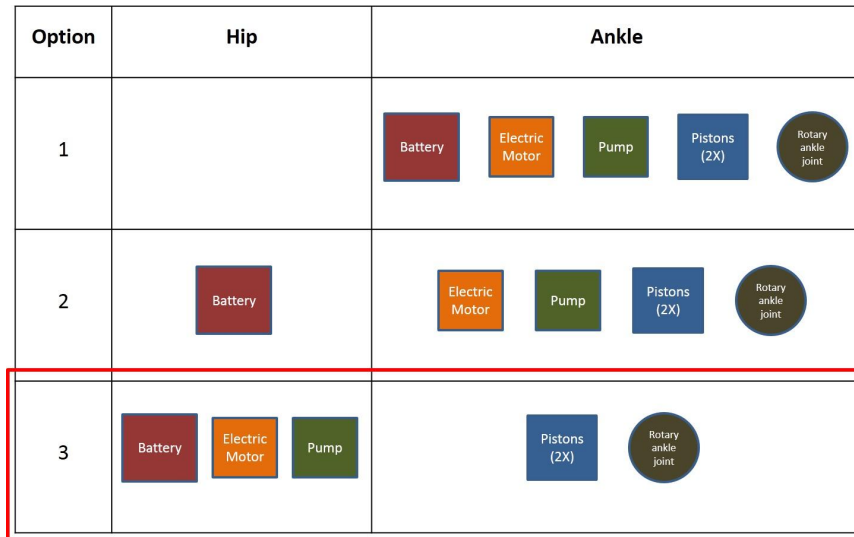


Figure 6.4: HAFO packaging options.

Based on AFO configuration and packaging decisions, a conceptual design was rendered, as shown in Fig. 6.5. Two cylinders provide the dorsiflexion and planterflexion torques. Two hoses rout along the user’s leg to separate the cylinders from the power unit, which consists of a battery, an electric motor, a gear head, a hydraulic pump and

several check valves.

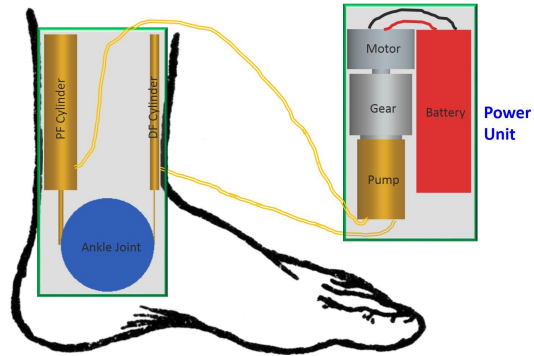


Figure 6.5: HAFO system rendering.

The components in the actuation system could be integrated to further increase the power density. Fig. 6.6 gives an example, where the cylinders and the reservoir were integrated into the AFO structural wall. A similar concept can be applied to the pump and the valves.

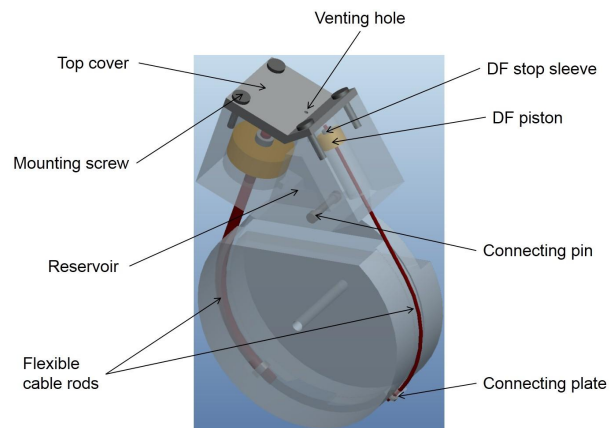


Figure 6.6: Conceptual rendering of an integrated HAFO actuation system.

## 6.4 HAFO Component Design

This section focuses on the design of the major components in the HAFO system. The auxiliary components such as hoses will be analyzed after a hydraulic circuit is designed, as presented in Chapter 7. These auxiliary components will not impact the system power density significantly, so neglecting them will not alter the design for the major components.

The HAFO must generate 90 N-m torque at  $100^\circ/\text{s}$  angular velocity, which corresponds to the extreme operating condition during level ground walking (Fig. 6.7) [3]. Additionally, the battery should provide energy to support 10,000 steps between charges. The components in the HAFO device need to be properly sized to fulfill the torque, velocity and energy requirements, and to optimize the power density at both overall system and actuation system levels.

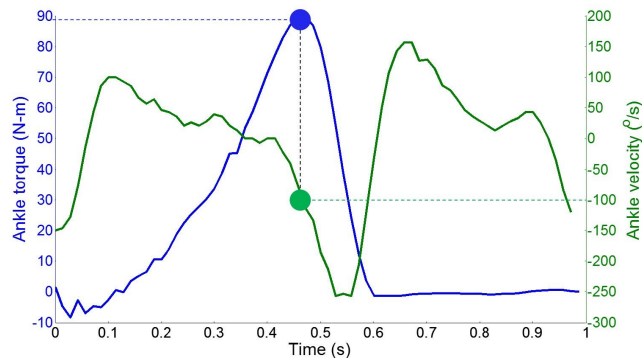


Figure 6.7: The extreme operating condition during level ground walking – the extreme torque in blue dot and the corresponding velocity in green dot [3].

### 6.4.1 HAFO Governing Equations

The key design variables for the HAFO system are the cylinder bore size, the pump displacement, the pump piston diameter, the pump operating pressure, the pump shaft speed, the gear head output torque, the electric motor output torque and the battery weight. Power conservation will be applied to connect these variables.

In the HAFO, the electromechanical sub-system including the battery, the electric motor and the gear head is coupled with the hydraulic sub-system. The design variables that link these two sub-systems are the pump operating pressure and its shaft speed, whose reasonable ranges are 500 to 3000 psi and 1000 to 3000 rpm. The low end of the pressure range was set according to the analysis presented in Chapter 2. The high end was determined by the maximum continuous operating pressure of off-the-shelf miniature axial piston pumps. The shaft speed range was set by leveraging the speed rating of an Oildyne 3-piston miniature axial piston pump. The rationale behind this speed range is: to form hydrodynamic lubrication, the shaft speed cannot be too low, as shown in Fig. 4.10; to avoid cavitation, the shaft speed should not go too high.

To size each component, those key design variables need to be expressed by the following four parameters: the HAFO output torque and velocity, and the pump operating pressure and shaft speed. The derivations for each component will be presented in the following sub-sections.

## Hydraulic Cylinders

The rod force and velocity can be formulated as

$$F_r = \frac{T_{out}}{L} \quad (6.2)$$

$$V_r = \omega_{out} \cdot L \quad (6.3)$$

where  $T_{out}$  and  $\omega_{out}$  are the output torque and velocity of the HAFO, and  $L$  is the moment arm.

Since the flexible rods are subject to tension force, rod yield formula [75] was used instead of rod buckling formula. The rod diameter and cylinder bore size were calculated as

$$D_r = \sqrt{\frac{4 \cdot N_c \cdot F_r}{\pi \cdot T_r}} \quad (6.4)$$

$$B_c = \sqrt{\frac{4 \cdot F_r}{\pi \cdot P_c \cdot \eta_{cm}}} + D_r^2 \quad (6.5)$$

where  $N_c$  is the safety factor,  $T_r$  is the tensile strength of the flexible rod,  $P_c$  is the cylinder operating pressure, and  $\eta_{cm}$  is the cylinder mechanical efficiency as shown in (3.22).

By substituting (6.2) and (6.4) into (6.5), the cylinder bore size becomes a function of the cylinder operating pressure, the cylinder efficiency and the HAFO output torque

$$B_c = \sqrt{\frac{4 \cdot T_{out}}{\pi \cdot P_c \cdot \eta_{cm} \cdot L} + \frac{4 \cdot N_c \cdot T_{out}}{\pi \cdot T_r \cdot L}} \quad (6.6)$$

where the cylinder operating pressure  $P_c$  is the same as the the pump outlet pressure, and the cylinder mechanical efficiency  $\eta_{cm}$  was modeled in Chapter 3. Since  $\eta_{cm}$  is a linear function of  $B_c$ , second-order equation solver is needed to solve (6.6).

Note that the cylinder volumetric efficiency was not a part of this section of the analysis and will be considered in next section when determining the required pump displacement.

## Hydraulic Pump

From power conservation, the pump output power times the cylinder efficiency gives the cylinder output power. Using this relationship the pump displacement  $V_p$  can be derived as

$$V_p = \frac{T_{out} \cdot \omega_{out}}{P_p \cdot \omega_p / 2\pi \cdot \eta_c} \quad (6.7)$$

where  $P_p$  is the pump outlet pressure,  $\omega_p$  the pump shaft speed, and  $\eta_c$  the cylinder overall efficiency.

The cross-sectional area of a pump piston is a function of the pump displacement and can be formulated as [50]

$$A_p = \frac{V_p}{2 \cdot z \cdot R_p \cdot \tan \alpha} \quad (6.8)$$

where  $z$  is the number of pistons,  $R_p$  the pitch radius and  $\alpha$  the swash-plate angle.

Substituting (6.7) into (6.8) and considering  $A_p = \pi/4 \cdot d_p^2$ , the piston diameter  $d_p$  can be expressed as

$$d_p = \sqrt{\frac{4 \cdot T_{out} \cdot \omega_{out}}{P_p \cdot \omega_p \cdot \eta_c \cdot z \cdot R_p \cdot \tan \alpha}} \quad (6.9)$$

Equations (6.7) and (6.9) show that the pump displacement and the piston diameter have been formulated as a function of the pump pressure, the shaft speed and the HAFO output torque and velocity.

The pump efficiency links the pump and the gear head, and it was formulated as [107]

$$\eta_p = f(P_p, \omega_p, V_p, A_p) \quad (6.10)$$

### Gear Head and Electric Motor

Considering power conservation, the output torque from the gear head is

$$T_g = \frac{T_{out} \cdot \omega_{out}}{\omega_g \cdot \eta_p \cdot \eta_c} \quad (6.11)$$

where  $\omega_g$  is the shaft speed of the gear head, which is the same as the pump speed,  $\eta_p$  is the pump efficiency, and  $\eta_c$  the cylinder efficiency. The output torque from the electric motor is

$$T_m = \frac{T_g}{N_g \cdot \eta_g} \quad (6.12)$$

where  $N_g$  is the gear ratio, and  $\eta_g$  the efficiency of the gear head.

$\eta_g$  can be estimated as a function of the gear ratio  $N_g$ , as shown in Fig. 6.8 and eq. (6.13). The red line represents the empirical model of the efficiency, which was established using the average efficiency of 840 commercial planetary and spur gear heads. A step response for a first-order dynamic system was used to do the line fitting. The equation for the red line is

$$\eta_g = 55 + \frac{35}{1 + 0.02 \cdot N_g} \quad (6.13)$$

This efficiency model was not derived from first principles, so it does not reveal the actual efficiency dependency. In practice the gear head efficiency will also be a function of torque and speed. Equation (6.13) simply represents a reasonable efficiency that can be achieved from state-of-the-art gear head design.

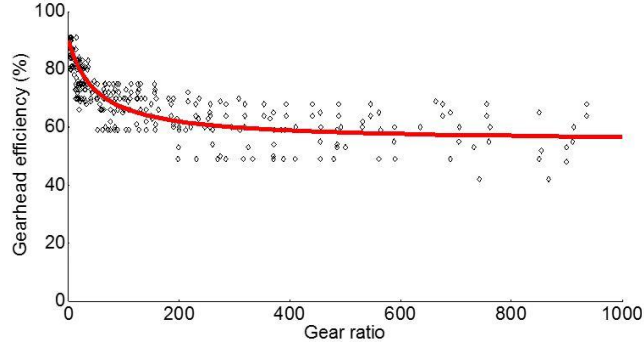


Figure 6.8: Gear head efficiency as a function of its gear ratio.

Combining (6.10)–(6.13) provides the output torque of the gear head and the electrical motor as a function of pump pressure, pump speed and HAFO output torque and velocity:

$$T_g = \frac{T_{out} \cdot \omega_{out}}{\omega_g \cdot \eta_c \cdot f(P_p, \omega_p, V_p, A_p)} \quad (6.14)$$

$$T_m = \frac{T_{out} \cdot \omega_{out}}{\omega_g \cdot \eta_c \cdot f(P_p, \omega_p, V_p, A_p) \cdot N_g \cdot (55 + \frac{35}{1+0.02 \cdot N_g})} \quad (6.15)$$

## Battery

Suppose the battery efficiency is  $\eta_b$  and the electric motor efficiency  $\eta_m$ , then the HAFO system efficiency is

$$\eta_{sys} = \eta_c \cdot \eta_p \cdot \eta_g \cdot \eta_m \cdot \eta_b \quad (6.16)$$

The electric motor efficiency  $\eta_m$  was modeled the same way as the gear head, as shown in Fig. 6.9 and (6.17). A total of 192 commercial electric DC motor data were



compiled to achieve this efficiency model:

$$\eta_m = 0.85 - \frac{0.85 \cdot 0.1}{0.05 \cdot P_m + 0.1} \quad (6.17)$$

where  $P_m$  is the output power of the electric motor.

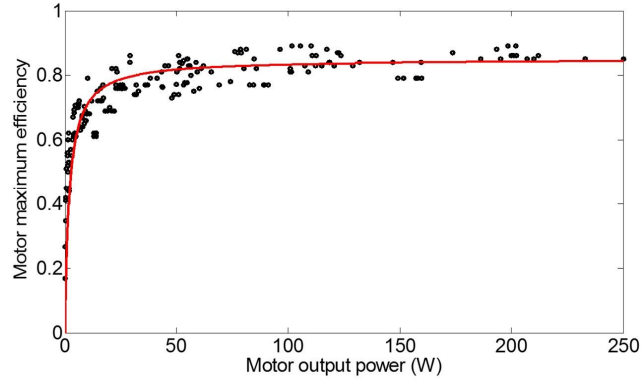


Figure 6.9: Electric motor efficiency as a function of its output power.

The energy required to support 10,000 steps was calculated as

$$E = \frac{E_{step} \cdot 10000}{\eta_{sys}} \quad (6.18)$$

where  $E_{step}$  is the energy required for each step, about 11 Joules [3]. Note that the energy calculation was based on the system efficiency at maximum HAFO output power. In practice the efficiency for each component degrades as its output decreases, as demonstrated in Fig. 4.7, 5.11 and 6.9, which means a larger battery is needed.

The energy density of the battery was modeled by analyzing the data of commercial LiPo batteries (Fig. 6.10), which is about 148 W·h/kg. Using this model, the battery weight was estimated as

$$W_b = \frac{E_{step} \cdot 10000}{148 \cdot \eta_c \cdot \eta_p \cdot \eta_g \cdot \eta_m \cdot \eta_b} \quad (6.19)$$

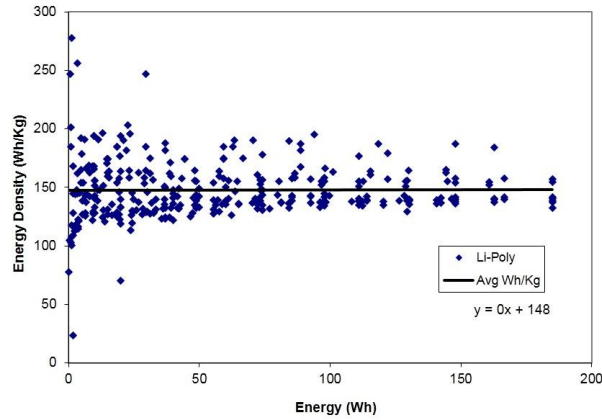


Figure 6.10: Energy density model of LiPo batteries.

### 6.4.2 HAFO Component Selection

To cover the pressure and speed range of the hydraulic pump, nine scenarios were selected to study, as shown in Fig. 6.11.

| Pump Operating Pressure (Mpa) |   |    |    |
|-------------------------------|---|----|----|
|                               | 7 | 14 | 21 |
| 1000                          | ① | ②  | ③  |
| 2000                          | ④ | ⑤  | ⑥  |
| 3000                          | ⑦ | ⑧  | ⑨  |

Figure 6.11: Pump operating conditions to be analyzed.

At this point, the gear ratio is still an open question. With a gear head, the electric motor can be downsized. But it is not clear if the electric motor weight reduction justifies the weight addition from the gear head and the battery. To address this question, three gear ratios will be analyzed: 1, 3 and 5. Gear ratio 1 means there is no gear head. It was decided to analyze those low gear ratios because the gear efficiency goes down as

the gear ratio increases, as shown in Fig. 6.8.

Nine pump operating conditions and three gear ratios give twenty-seven HAFO design choices. The corresponding weight of the actuator and the power unit are summarized in Fig. 6.12. All these design choices were required to output 90 N-m torque, 100°/s angular velocity, and to support 10,000 steps.

The weight of the cylinder and the electric motor was calculated using the models in Section 2.3 and 2.4. The weight of the pump was estimated using the data from Takako Industries, Parker Oildyne and KIST research lab, as shown in Fig. 6.13. Since the pump displacement is proportional to its volume, it was assumed that the pump weight is proportional its displacement. Equation (6.20) shows the formula for this approximation, the red line in Fig. 6.13. Similar to the empirical models of the electro-mechanical components, this model was not developed using first principles, so it does not reveal the actual dependency of the pump weight. Practically, the weight will also be a function of the pump pressure and speed.

$$W_p = 600 \cdot V_p \quad (6.20)$$

where  $V_p$  is the pump displacement in cc/rev, and  $W_p$  the pump weight in gram.

The goal of the HAFO design is to maximize the power density of the actuator and the power unit, but different pressure settings are needed to achieve these two goals. To maximize the actuator power density, high operating pressure is needed, as demonstrated in Chapter 2. At high operating pressure, all components are downsized, but a larger battery is needed considering the efficiency degradation with component size. This means there is an optimal pressure that maximizes the power density of the power unit. From Fig. 6.12, 21 MPa pump pressure gives the lightest actuator weight, while 14 MPa gives the lightest power unit weight. Considering the little weight difference between these two pressures, and the practical pressure limit for commercial miniature pumps (less than 21MPa for Takako 0.4 cc and Oildyne 0.3 cc pumps), 14 MPa operating pressure was selected.

| Gear Ratio = 1 |                |                 |                   |
|----------------|----------------|-----------------|-------------------|
| Pump Spd (rpm) | Pump Prs (Mpa) | Actuator Wt (g) | Power Unit Wt (g) |
| 1000           | 7              | 426             | 1570              |
|                | 14             | 331             | 1237              |
|                | 21             | 311             | 1241              |
| 2000           | 7              | 426             | 1113              |
|                | 14             | 331             | 957               |
|                | 21             | 311             | 991               |
| 3000           | 7              | 426             | 993               |
|                | 14             | 331             | 889               |
|                | 21             | 311             | 931               |

| Gear Ratio = 3 |                |                 |                   |
|----------------|----------------|-----------------|-------------------|
| Pump Spd (rpm) | Pump Prs (Mpa) | Actuator Wt (g) | Power Unit Wt (g) |
| 1000           | 7              | 426             | 1581              |
|                | 14             | 331             | 1248              |
|                | 21             | 311             | 1255              |
| 2000           | 7              | 426             | 1124              |
|                | 14             | 331             | 969               |
|                | 21             | 311             | 1005              |
| 3000           | 7              | 426             | 1005              |
|                | 14             | 331             | 901               |
|                | 21             | 311             | 945               |

| Gear Ratio = 5 |                |                 |                   |
|----------------|----------------|-----------------|-------------------|
| Pump Spd (rpm) | Pump Prs (Mpa) | Actuator Wt (g) | Power Unit Wt (g) |
| 1000           | 7              | 426             | 1591              |
|                | 14             | 331             | 1259              |
|                | 21             | 311             | 1268              |
| 2000           | 7              | 426             | 1135              |
|                | 14             | 331             | 980               |
|                | 21             | 311             | 1018              |
| 3000           | 7              | 426             | 1016              |
|                | 14             | 331             | 913               |
|                | 21             | 311             | 958               |

Figure 6.12: HAFO design candidates.

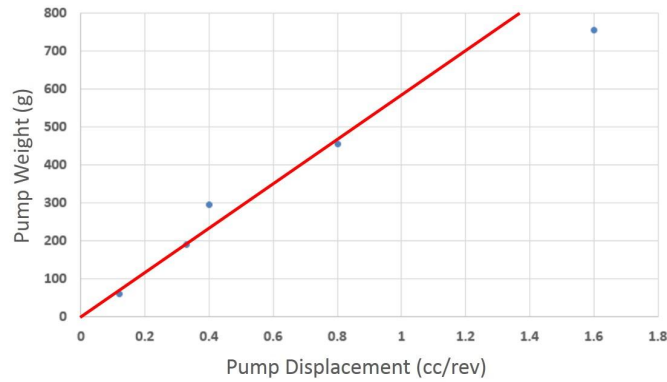


Figure 6.13: Weight model of axial piston pumps.

As to the pump speed, 3000 rpm gives the lightest power unit weight, but high speed raises cavitation concern. Takako 0.4 cc pump is rated for 2000 rpm, so the same speed was selected for the HAFO design. Another consideration for choosing 2000 rpm was to reserve some buffer for potential speed spikes due to the dynamic behavior of the HFAO device.

The next step is to select the gear ratio, Fig. 6.12 shows that the power unit weight increases with higher gear ratio, so direct drive between the electric motor and the pump is desired. This being said, 900 mN·m torque is needed for direct drive. The lightest electric motor from Maxon Motor that meets this torque requirement weighs 860 gram. This is more than three times heavier than the electric motor and gear head assembly as shown in Fig. 6.16. So for the HAFO device, a gear head is needed to maximize its power density.

The torque density for Maxon Motor products is plotted on Fig. 6.14, which shows that electronically commutated (EC) flat motors have the highest torque-to-weight and torque-to-volume ratios. So EC motors are preferred over other motor designs. One problem with the EC flat motors is their rated torque is less than what the HAFO needs. This further justifies the need of a gear head.

To pick a proper electric motor, the root mean square torque of a walking cycle was

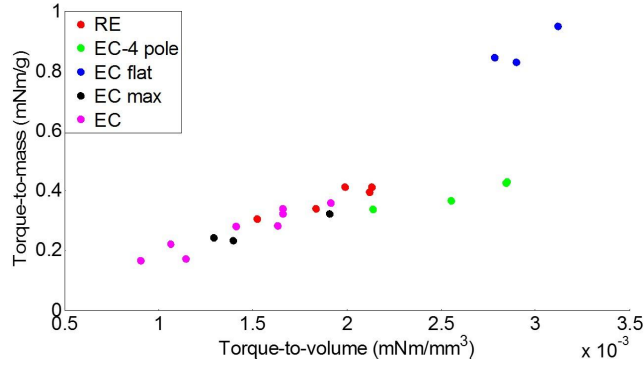


Figure 6.14: Electric DC motor torque density - Maxon Motor data only.

calculated, as shown in Fig. 6.15. The RMS torque is defined as

$$T_{RMS} \triangleq \sqrt{\frac{1}{t_{tot}} \cdot \Sigma(T^2(t) \cdot \Delta t)} \quad (6.21)$$

where  $t_{tot}$  is the total time for a walking cycle, and  $T(t)$  is the ankle torque at time  $t$ .

The RMS torque of the electric motor was then calculated as

$$T_{RMS_m} = \frac{T_{RMS}}{N} \quad (6.22)$$

where  $N$  is the transmission ratio of the HAFO system, defined as

$$N = N_g \cdot \eta_g \cdot \frac{\eta_p}{V_p} \cdot A_c \cdot \eta_c \cdot L \quad (6.23)$$

where  $N_g$  is the gear ratio,  $V_p$  is the pump displacement,  $A_c$  is the cross-sectional area of the cylinder piston,  $L$  is the moment arm, and  $\eta_g$ ,  $\eta_p$ ,  $\eta_c$  are the efficiencies of the gear head, the pump and the cylinder.

The rated maximum continuous torque of the electric motor must be larger than  $T_{RMS_m}$  to ensure that the motor winding will not melt during HAFO operation [108].

Another criteria when picking the electric motor is its extreme operating point ( $n_{max}$ ,  $T_{max}$ ) must lie underneath the motor speed-torque curve, which is defined as

$$n = K_n \cdot U - \frac{\Delta n}{\Delta T} \cdot T \quad (6.24)$$

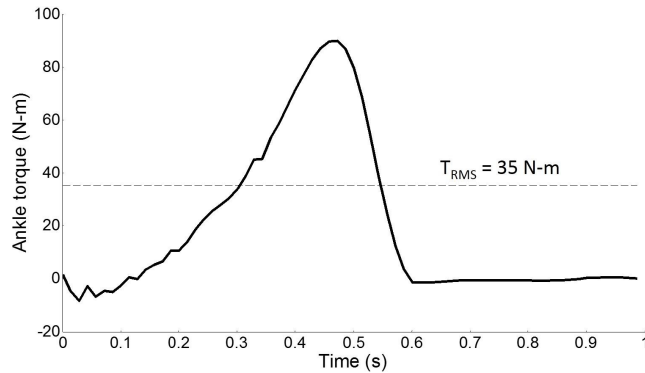


Figure 6.15: The average output torque of human ankle joint while walking [3].

where  $n$  is the electric motor speed,  $K_n$  is the motor speed constant,  $U$  is the motor voltage, and  $T$  is the motor torque. Since the motor torque-speed curve can move up and to the right with increasing motor voltage, it was assumed that the nominal voltage as specified on the motor data sheet was used to simplify the analysis.

The transmission ratio  $N$  is the torque amplification gain from the electric motor to the HAFO output. From (6.23), to achieve higher transmission ratio, it is preferred to have higher gear ratio, smaller pump displacement, larger piston bore, and longer moment arm. On the other hand, the gear and the pump efficiencies are working against these principles. Additionally, the cylinder and the moment arm cannot be too large due to the packaging space limitation.

Component choices for the HAFO system are shown in Fig. 6.16. The closest EC flat electric motor and planetary gear head from Maxon Motor was chosen to match the torque requirement corresponding to 2,000 rpm, 14 MPa psi and gear ratio 3.

## 6.5 Conclusion

The analysis in this Chapter showed that small-scale hydraulics is capable of achieving the design requirements of the AFO device as specified in Section 6.1. The results shown in Fig. 6.12 indicate that for applications where the overall system weight matters more,

| Actuator Package |             |            |                  |             |            |                 |
|------------------|-------------|------------|------------------|-------------|------------|-----------------|
|                  | Part Number | Wt (g)     | Predicted Wt (g) | Dia (mm)    | Len (mm)   | Other Specs     |
| PF Cylinder      | Customized  | 165        | 165              | 17.2        | 100        | 4.7 mm Rod dia. |
| DF Cylinder      | Customized  | 23         | 23               | 7           | 100        | 1.9 mm Rod dia. |
| <b>Total</b>     |             | <b>188</b> | <b>188</b>       | <b>24.2</b> | <b>200</b> |                 |

| Power Unit   |                |            |                  |               |            |                |
|--------------|----------------|------------|------------------|---------------|------------|----------------|
|              | Part Number    | Wt (g)     | Predicted Wt (g) | Dia (mm)      | Len (mm)   | Other Specs    |
| Pump         | Oildyne 642654 | 190        | 202              | 32            | 53         | 0.3 cc/rev     |
| Gear Head    | Maxon 166930   | 118        | 92               | 32            | 27         | 6 mm shaft dia |
| DC Motor     | Maxon 397172   | 141        | 274              | 45            | 27         | 4 mm shaft dia |
| Battery      | TP2700-6SPL25  | 465        | 405              | 50 x 34 x 102 |            | 24 V voltage   |
| <b>Total</b> |                | <b>914</b> | <b>973</b>       | <b>45</b>     | <b>107</b> |                |

Figure 6.16: HAFO system final design choice.

electro-mechanical systems should be considered.

For small-scale hydraulic systems, efficiency strongly influences weight. As shown in Fig. 6.3, vane pump driven HAFO systems weigh more than piston pump driven HAFO systems, for all configurations. This is because the vane pump efficiency is lower than piston pump, which requires a larger electric motor and a larger battery. Similarly, as shown in Fig. 6.12, gear ratio 1 - no gear in between the pump and the DC motor - gives the lightest overall system weight compared to higher gear ratios. This is because the inefficiencies from the higher gear ratio requires a larger battery, which cannot justify the weight reduction from the electric motor.

One limitation for the HAFO weight analysis is it was done for steady state. Considering the cyclic nature of the application, the fatigue yield strength and a larger safety factor should be used to refine the analysis. This will result in heavier system weight than the steady state analysis presented in this Chapter.



## Chapter 7

# Dynamic Analysis of HAFO Hydraulic Circuits, Fluids, and Hoses

### 7.1 HAFO System Hydraulic Circuit Design

With the key HAFO components being sized and selected, the next step is to design a proper hydraulic circuit to regulate the hydraulic fluid in the system. The hydraulic portion of the HAFO system is illustrated in Fig. 7.1. The hydraulic circuit design is challenging due to the following facts and requirements: first, the planterflexion (PF) and dorsiflexion (DF) cylinders were designed to have different bore sizes to optimize the actuator power density; second, the hoses routing in between the cylinders and the power unit are around 1 m long; third, the control valves need to consume minimal energy to maintain the system power density.

During plantar-flexion actuation, the PF chamber is pressurized. The PF piston runs at a slower speed than the DF piston, causing the flexible rods to become slack. Cable rod slackness leads to delay during pressure buildup. This means the HAFO system will

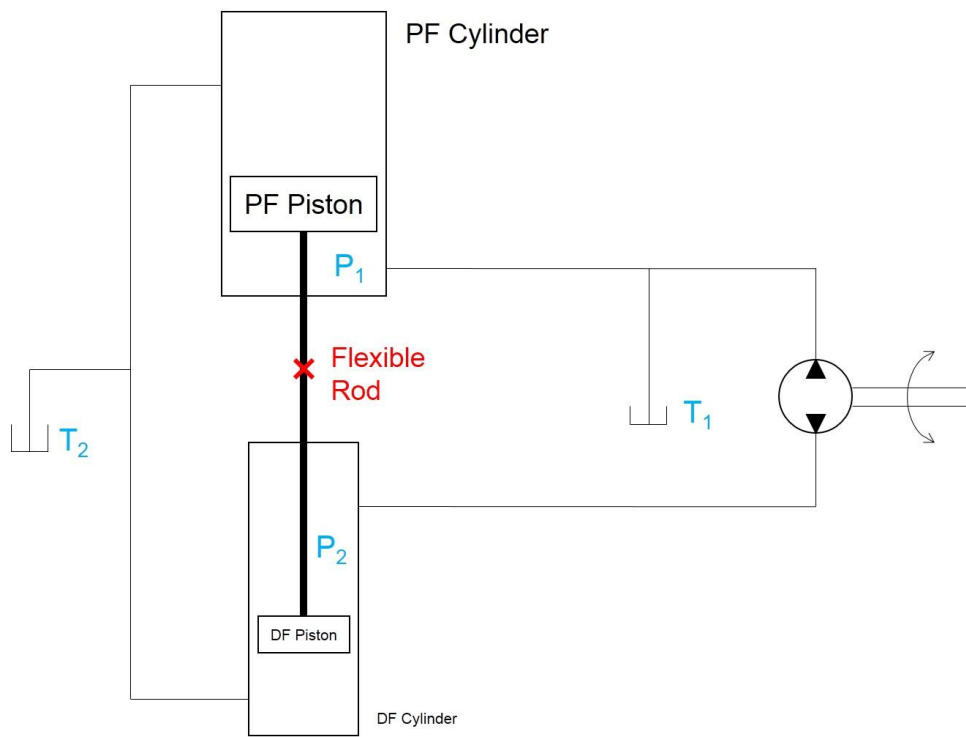


Figure 7.1: The hydraulic portion of the HAFO system.

not be as responsive as a system with rigid rods. During dorsi-flexion actuation, the DF chamber is pressurized. The DF piston runs at a faster speed than the PF piston, which requires excessive fluid coming out of the PF cylinder. These fluid needs to be handled properly by the hydraulic circuit. Otherwise, there will be pressure buildup in the PF cylinder that will resist the DF actuation.

To evaluate the performance of the hydraulic circuits, a dynamic simulation model was established in SimHydraulics as shown in Fig. 7.2. The cables sitting in between the PF and the DF cylinder were modeled using customized SimScape blocks. Details for the customized block are presented in Appendix 9.2. A closed loop PID controller was implemented to track the desired ankle position while compensating for the resistive torque from the ankle joint. The system was controlled by commanding the electric motor speed.

The desired ankle position is the ankle joint angle of an adult during level ground walking. The resistive torque is the ankle torque from the same adult. The torque is needed to overcome the load induced by the body weight and the ground friction. Data from [3] was used to represent the desired ankle position and the resistive torque. The control task for the HAFO system was to move the pistons to track the desired ankle position, and to generate proper chamber pressure to conquer the resistive force.

With the dynamic simulation model, the performance of the hydraulic circuit can be evaluated. Four hydraulics circuits were investigated. The goal was to enable the HAFO system to deliver the right amount of torque and speed at the right timing, to maximize the system efficiency and to consume minimal energy during the whole walking cycle.

### **7.1.1 Circuit 1: a Simplified EHA Circuit**

The initial circuit proposed, shown in Fig. 7.3, was based on simplifying the hydraulic circuit of a commercial electro-hydraulic actuator (EHA) system. It consists of a regular check valve  $CV_2$  and a pilot-operated check valve  $CV_1$ . This circuit works for the EHA system which only has one cylinder, but it does not work for the HAFO system where

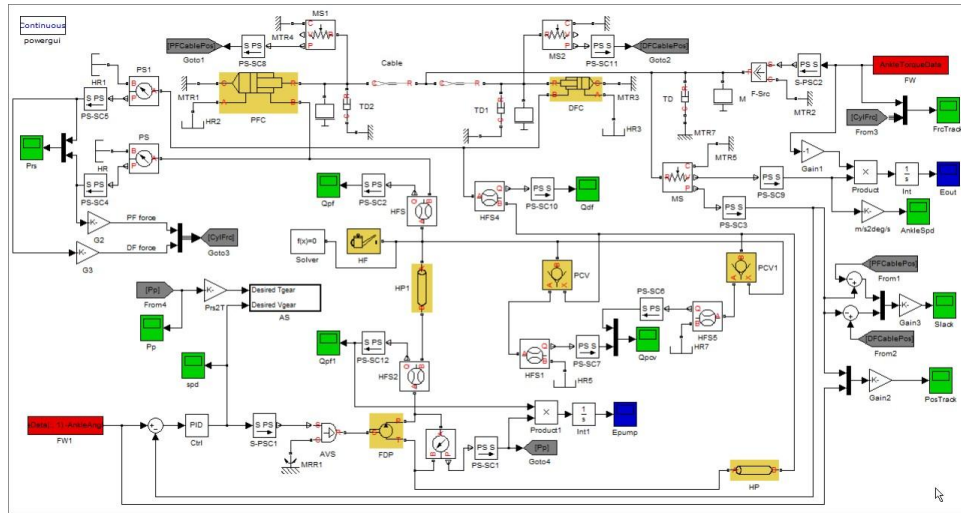


Figure 7.2: SimHydraulics model for the HAFO system. Full page image shown in Appendix 9.2.

two inter-connected cylinders and a flexible rod are needed.

The position tracking result for this circuit is shown in Fig. 7.4. The tracking performance is not satisfactory during the whole plantar-flexion phase. From 0.1 to 0.4 seconds, the ankle joint position (the position difference between the PF and the DF piston) increases, which means the PF piston runs faster than the DF piston.  $P_1$  tries to close the check valve  $CV_1$  by pushing the ball downwards, and  $P_2$  tried to open the same valve by pushing the ball upwards through the pilot line. As a result,  $CV_2$  will be on and off, which causes chattering effect for position tracking and spikes for load balancing, as shown in Fig. 7.4 and Fig. 7.5.

From 0.4 to 0.6 seconds, the rod position decreases, which indicates that the PF piston runs slower than the DF piston. In this process, only  $P_1$  becomes positive, while  $P_2$  equals to the atmosphere pressure due to the pumping action. Since there is no upwards pressure force acting on the ball, valve  $CV_2$  remains closed. As a result, the force profile in Fig. 7.5 does not show spike during this period. On the other hand, the position tracking showed a constant tracking error. The error was caused by the

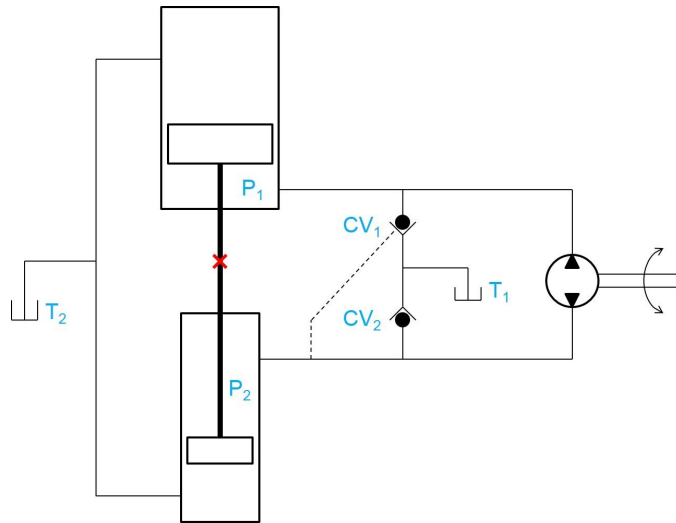


Figure 7.3: HAFO hydraulic circuit candidate - a simplified EHA circuit.

slackness of the flexible rod. With a slack rod, the PF piston tries to catch up with the DF piston and straighten the cable, but the cable remains slack due to the area difference between the PF and DF pistons.

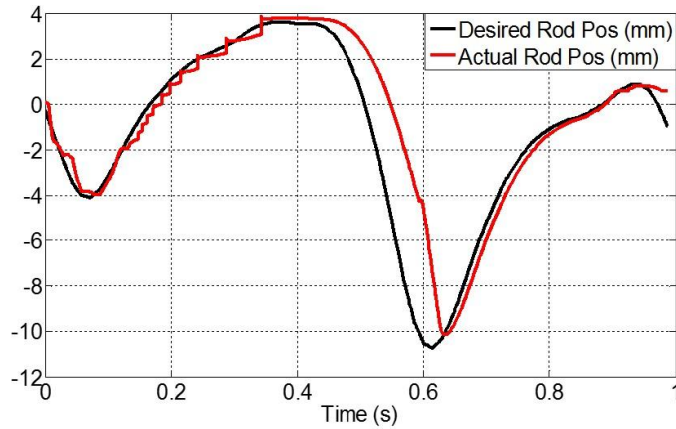


Figure 7.4: HAFO position tracking result - a simplified EHA circuit.

Due to the poor tracking performance of this circuit, it cannot be used to control the HAFO system. The following sections will present alternative circuit designs, aiming at providing better tracking performance and comparable circuit simplicity.

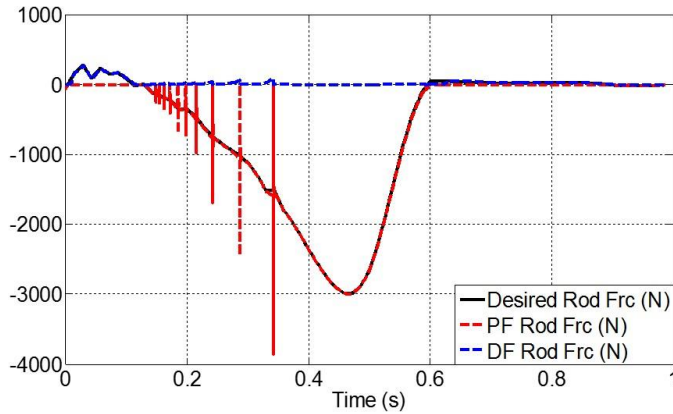


Figure 7.5: HAFO force balancing profile - a simplified EHA circuit.

### 7.1.2 Circuit 2: Directional Solenoid Valves

To improve the position tracking performance, the PF and the DF cylinders should not be pressurized at the same time. Ideally, at any time only one cylinder should be pressurized, while the other connected to the reservoir. Based on this requirement, the second circuit design places two directional solenoid valves  $DV_1$  and  $DV_2$  on the main hydraulic circuit line, as shown in Fig. 7.6. These two valves were controlled by feeding the desired rod force signals. During planter-flexion, valve  $DV_1$  will be closed and valve  $DV_2$  will be open. As the pump delivers fluid to the PF chamber, positive pressure will build up there. Since the DF chamber is connected to the reservoir,  $P_2$  will remain as zero. Similar operation principle will occur during dorsi-flexion.

The position tracking results for this circuit is shown in Fig. 7.7. By turning the proper valves on and off at the right timing, this circuit is capable of tracking the desired ankle position throughout the whole gait cycle. The glitches during valve switch is negligible. In the meantime, this circuit is also capable of compensating the resistive torque from the ankle joint, as shown in Fig. 7.8. The same type of glitches showed up as the valves switch.

While this circuit delivers better position tracking performance, it has the following two inherent disadvantages. First, the solenoid valves sit on the main circuit line -

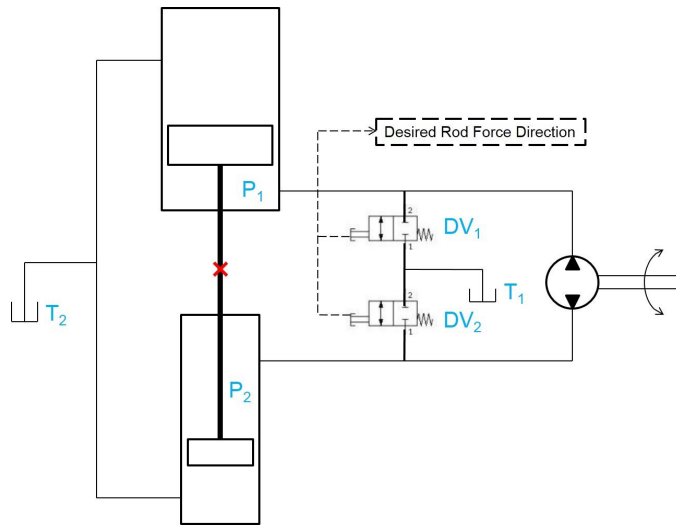


Figure 7.6: HAFO hydraulic circuit candidate - directional solenoid valves.

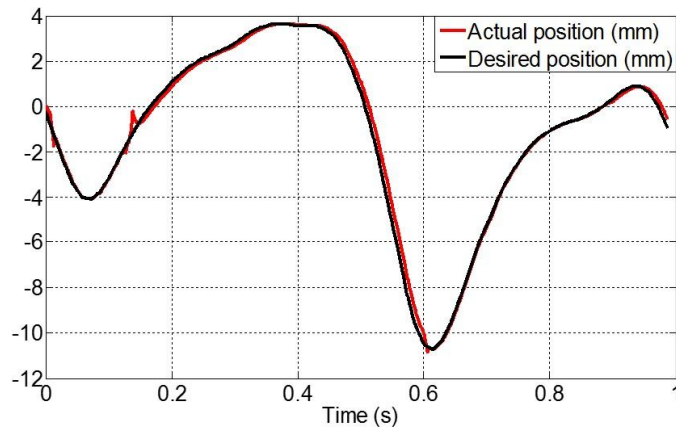


Figure 7.7: HAFO position tracking result - directional solenoid valves.

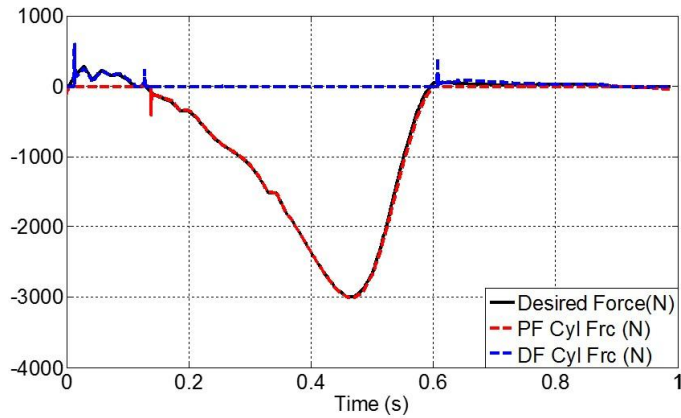


Figure 7.8: HAFO force balancing profile - directional solenoid valves.

the lines that connect the pump and the reservoir, and thus requiring large amount of external power to operate. This is not desired considering that power density is the key design requirement. Second, since there is no pilot lines in the system to control the valve solenoid, the valves require pre-defined force profile to open and close. Since the force profile changes from subject to subject and from one walking condition to another, this circuit may not function well for different subjects or different walking environment.

### 7.1.3 Circuit 3: Solenoid Valves and Pilot Check Valves

To downsize the solenoid valves, the third circuit design shifts the solenoid valves from the main hydraulic line to the pilot line, and adds two pilot-operated check valves. The operating principle for this circuit is similar to the second circuit. The desired rod force signals were fed into the circuit to control the solenoid valves, so that the check valves are on and off at proper timing. At any time there is one pressurized cylinder, while the other cylinder is connected to the reservoir.

Due to the similar operating principles, this circuit delivers similar position tracking results as the second circuit, as shown in Fig. 7.10. The dynamic response during valve switch is also comparable to the second circuit.

Though this circuit downsizes the solenoid valves, the following two reasons make



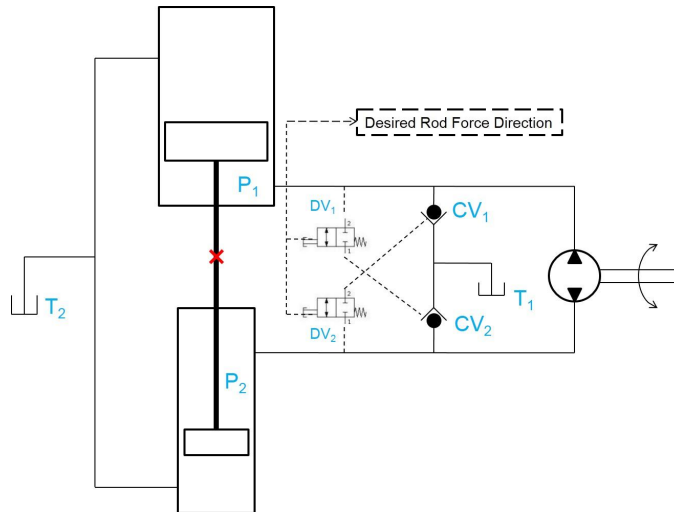


Figure 7.9: HAFO hydraulic circuit candidate - directional solenoid valves and pilot-operated check valves.

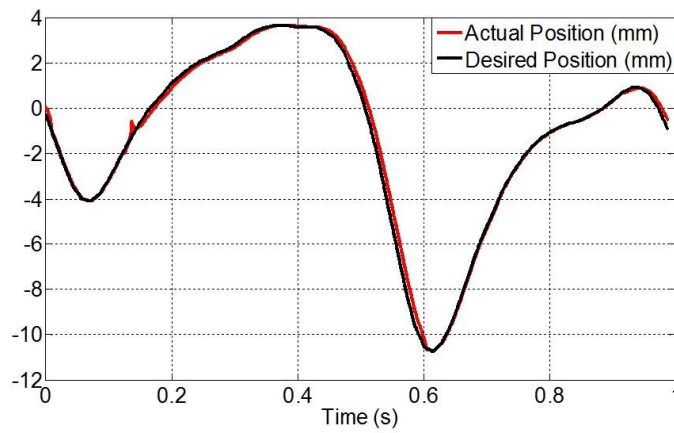


Figure 7.10: HAFO position tracking result - directional solenoid valves and pilot-operated check valves.

it hard to implement. First, commercial solenoid valves are large for pilot line control purpose, and valve customization is not only expensive, but challenging to do. Second, this circuit also requires pre-defined force profile to control the valves, so it may not function well for different subjects or different walking conditions.

#### 7.1.4 Circuit 4: Pilot-Operated Check Valves

The fourth circuit design, shown in Fig. 7.11, results from eliminating the disadvantages of the third circuit. First, eliminate the small solenoid valves so that no customization is needed. Second, use the chamber pressure to control the check valves automatically. During plantar-flexion actuation, the pump draws fluid from the DF chamber and delivers it to the PF chamber. As the pump routes more fluid to the PF chamber, the pressure starts to build up. Positive  $P_1$  will eventually close the pilot check valve pCV<sub>1</sub> and crack valve pCV<sub>2</sub> through the pilot line. Once pCV<sub>2</sub> is open, the DF chamber will be connected to the reservoir, thus creating a short circuit. During this process, the DF chamber pressure always stays at zero or negative due to the pump sucking action, so it cannot open pCV<sub>1</sub>. The same mechanism applies to dorsi-flexion actuation.

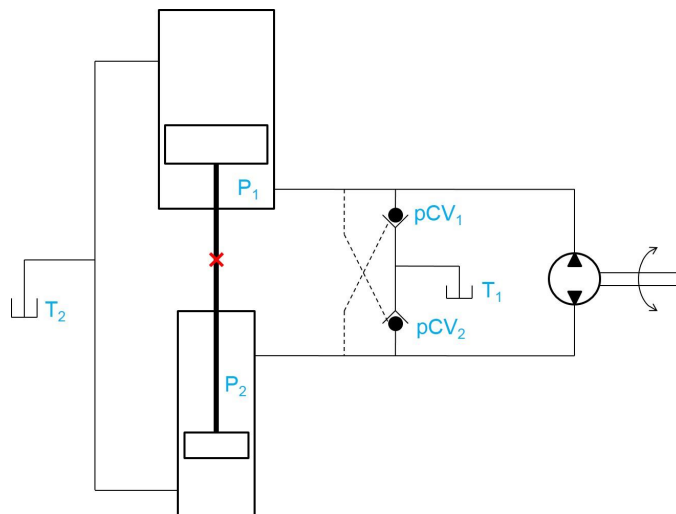


Figure 7.11: HAFO hydraulic circuit candidate - pilot-operated check valves.

The PF and DF cylinder chamber pressure profile during a gait cycle is shown in Fig. 7.12. At any time during the whole gait cycle, only one of the cylinders is pressurized. This means circuit 4 is capable of turning the check valves on and off automatically at the proper timing without an external command signal.

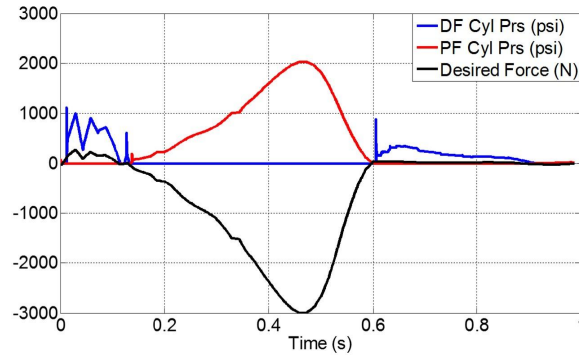


Figure 7.12: PF and DF cylinder chamber pressure profile during a gait cycle - pilot-operated check valves.

The ankle position tracking results from this circuit is shown in Fig. 7.13. The overall tracking performance is good, but the glitch shown in the gray circle is not ideal. The patient wearing the HAFO may experience a rough motion, so further investigation is needed to eliminate the undesired transient behavior.

The position tracking results shown in Fig. 7.7 and Fig. 7.10 did not have the glitch as highlighted in Fig. 7.13. The reason is circuit 2 and 3 use pre-defined force profile to control the valves, so that the valves open and close instantaneously. This quickens the pressure buildup in the DF chamber. On the other hand, circuit 3 uses the chamber pressure to control the valves. The chamber pressure has to be higher than some certain threshold to turn the valves on and off, which takes time. This slows down the pressure buildup, and thus causing delay in the position tracking.

Overall, circuit 4 is preferred over the other three. First, it is capable of tracking the ankle position throughout the whole gait cycle. Second, it doesn't consume any external energy. Third, the circuit is self-regulated, and doesn't require any pre-defined

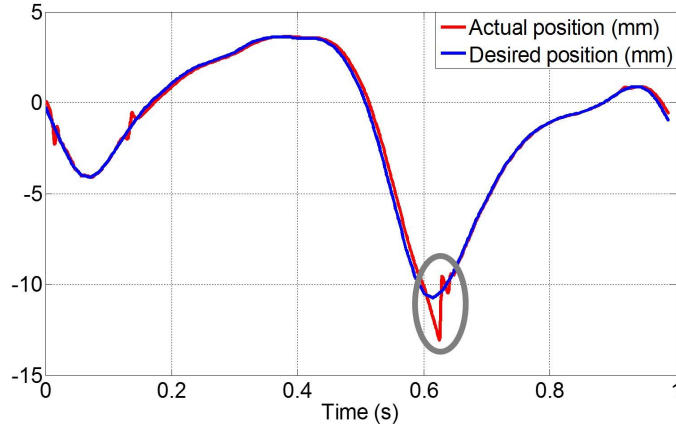


Figure 7.13: Position tracking result - pilot check valves. The gray oval highlights the glitch during the position tracking.

information to control the valves. Lastly, the circuit is as simple as the simplified EHA circuit, and off-the-shelf pilot-operated check valves can be used to construct this circuit.

Given these facts, circuit 4 was selected as the hydraulic circuit for the HAFO system. In the following sections, the hydraulic hose and the hydraulic fluid will be investigated, aiming at curing the glitches, shown in Fig. 7.13.

## 7.2 Hose Effects

To quantify the hose dimension impacts on the HAFO dynamic performance, the following index  $\zeta$  was defined

$$\zeta \triangleq \text{Glitch Height} \times \text{Maximum Pump Speed} \quad (7.1)$$

where maximum pump speed is the pump speed corresponding to the maximum glitch height. To improve the HAFO dynamic performance, it is desired to minimize the glitch height. To maintain the system efficiency and to avoid cavitation, small maximum pump speed is preferred.

Fig. 7.14 shows the height of the glitch as a function of the hose dimensions. From this result, short and slender hose is preferred to achieve the smallest glitch height. Short and slender hose gives the smallest fluid volume in the hose, which shortens the fluid transfer time and quickens the pressure buildup. Fast pressure buildup enabled the HAFO to track the desired position in a faster manner, thus small glitch height.

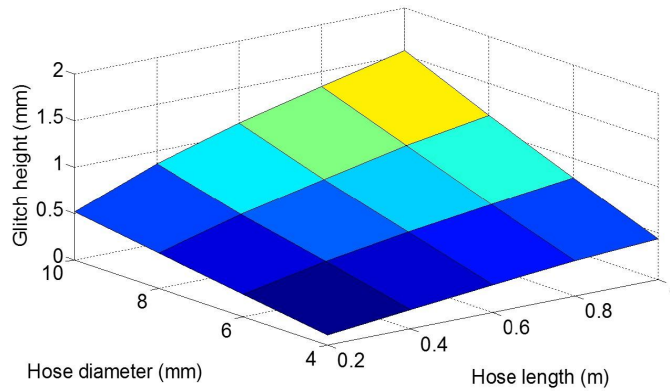


Figure 7.14: Glitch height as a function of hose dimensions.

Fig. 7.15 shows the maximum pump speed as a function of the hose dimensions. From this result, long and wide hose is preferred to achieve the minimal pump speed. Long and wide hose gives the smallest pressure drop across the hose, so the pump can work less harder to achieve the desired pressure, thus small pump speed.

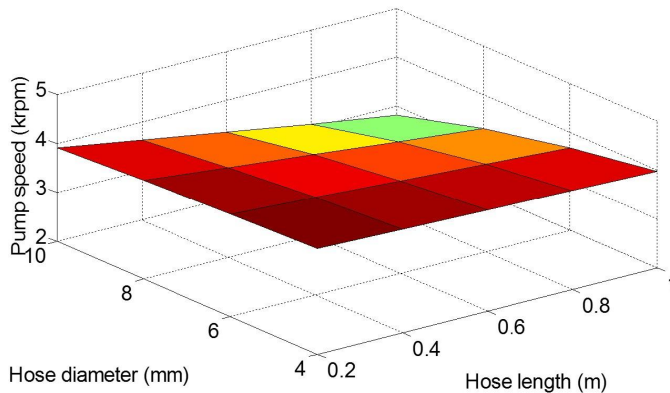


Figure 7.15: Maximum pump as a function of hose dimensions

Fig. 7.16 shows the index  $\zeta$  as a function of the hose dimensions. This trend is similar to the glitch height trend shown in Fig. 7.14. This is because the glitch height trend dominates the pump speed trend. The maximum over the minimum glitch height as shown in Fig. 7.14 is more than 15, while the maximum over the minimum pump speed as shown in Fig. 7.15 is less than 2. From Fig. 7.16, short and slender hose is preferred to achieve the smallest  $\zeta$ .

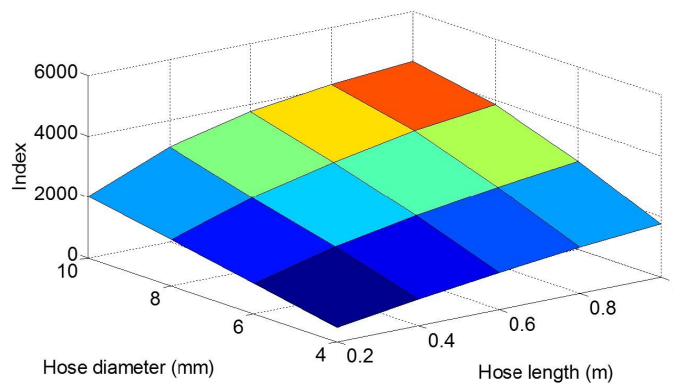


Figure 7.16: Index  $\zeta$  as a function of hose dimensions.

Since the hose length was pre-determined by the HAFO design, it needed to be fixed at 1 meter. As to the hose diameter, there is a lower limit that should not be exceeded. As shown in Fig. 7.17, with a 2 mm diameter hose, the large glitch shows up again in the HAFO position tracking. This is mainly driven by the pressure loss across the hose.

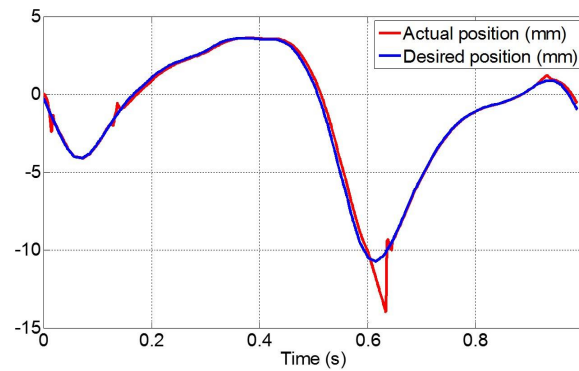


Figure 7.17: Position tracking results with 1 m long and 2 mm wide hoses.

Fig. 7.18 shows the pressure drop across the hose as a function of the hose dimensions. This result shows that the pressure drop becomes significant as the hose diameter goes smaller than 4 mm.

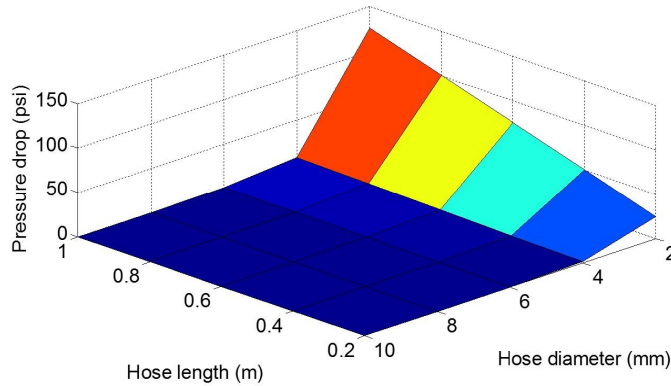


Figure 7.18: Hose pressure drop as a function of hose dimensions. Inlet pressure = 2000 psi. Inlet flow rate = 2000 rpm  $\times$  0.4 cc/rev.

Results shown in Fig. 7.16 and Fig. 7.18 indicate that 4 mm hose diameter is an appropriate hose diameter for the HAFO design. In the following analysis, 1 m long and 4 mm diameter hoses were used in the simulations.

### 7.3 Fluid Effects

To study the fluid effects on the HAFO dynamic performance, generic fluids with large range of viscosity and bulk modulus were simulated. The glitch height as a function of the fluid viscosity and bulk modulus is presented in Fig. 7.19. This result shows the bulk modulus has negligible impact on the glitch height. The dominating factor is the fluid viscosity. High viscosity fluid is hard to flow in the system, so it arrives at the desired location slower. This will delay the pressure buildup. When the necessary pressure cannot be provided timely, the desired force cannot be generated, so the glitch height will be large. On the other hand, fluid with low viscosity is easier to flow in the system, and is able to arrive at the desired location faster, and thus small glitch height.

This result shows low viscosity fluid is preferred to achieve small glitch height.

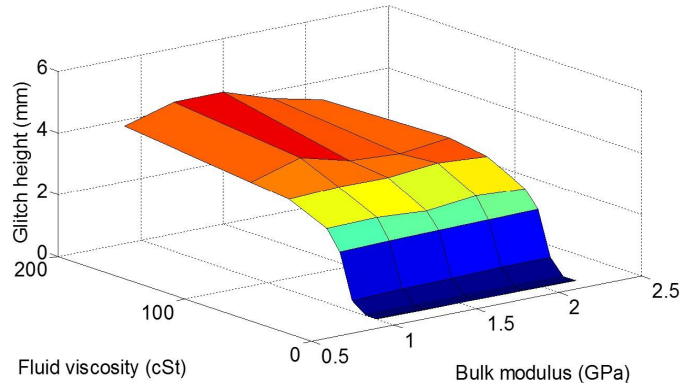


Figure 7.19: Glitch height as a function of fluid properties.

Fig. 7.20 shows the maximum pump speed (defined in (7.1)) as a function of fluid properties. Again, the bulk modulus impact is negligible. Fluid viscosity dominated the pump speed dependency on the fluid properties. With high viscosity fluid, the system volumetric efficiency is high. The pump doesn't need to spin as fast to move the desired amount of fluid to the destination. On the other hand, when the fluid viscosity is low, the pump has to work harder to compensate the low volumetric efficiency. From minimizing pump speed perspective, high viscosity fluid is desired.

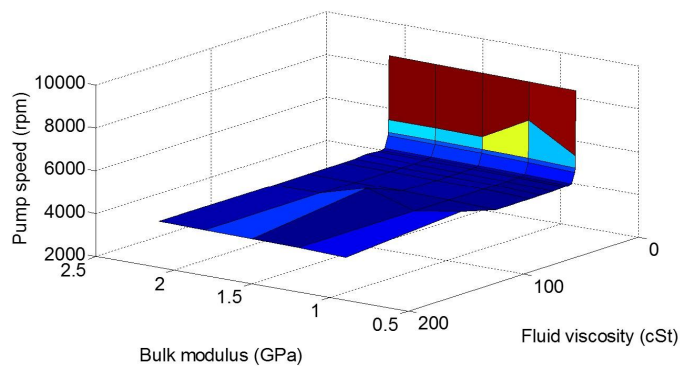


Figure 7.20: Maximum pump speed as a function of fluid properties.

Fig. 7.21 shows the index  $\zeta$  as a function of the fluid properties. Due to the opposite trend of the glitch height and the pump speed, fluids with medium viscosity gave the



lowest  $\zeta$  values, which can be more clearly seen in Fig. 7.22.

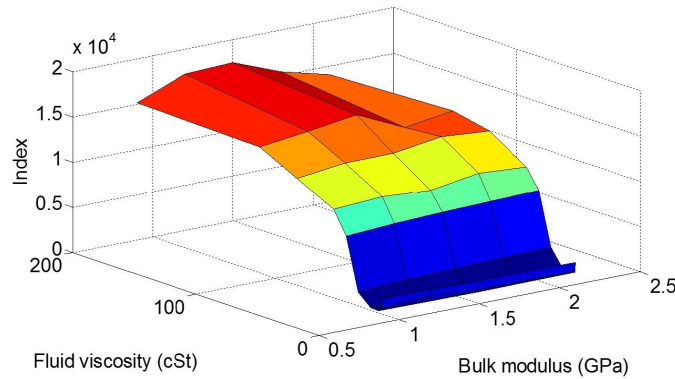


Figure 7.21: Index  $\zeta$  as a function of fluid properties.

Since bulk modulus is not playing a significant role, the following analysis will focus on the fluid viscosity. Fig. 7.22 shows the  $\zeta$  dependency on the fluid viscosity. It also maps the viscosity of the existing fluids in SimHydraulics library onto this curve. From this result, brake fluids and several aviation fluids give the lowest  $\zeta$  value. Since aviation fluids are expensive, brake fluids are preferred for the HAFO application.

Back to the position tracking results shown in Fig. 7.13, the reason for the glitch is mineral oil was used in the simulation. Mineral oil has a viscosity that is equivalent to fluid ISO VG 32 in Fig. 7.22, which has a high  $\zeta$  value.

Position tracking results using DOT 3 brake fluid and 50W oil are shown in Fig. 7.23 and Fig. 7.24. These results emphasize the importance of the fluid.

## 7.4 Cable Slackness

To confirm the cable slackness, 1 meter long, 4 mm diameter hoses and DOT 3 brake fluid were fed into the simulation model. With these desired parameter settings, the cable displacements were recorded in Fig. 7.25. Positive cable displacement means the cable is in compression. Since the cable is flexible, it cannot be subject to compression force. So positive displacement means the cable is slack. Conversely, negative displacement

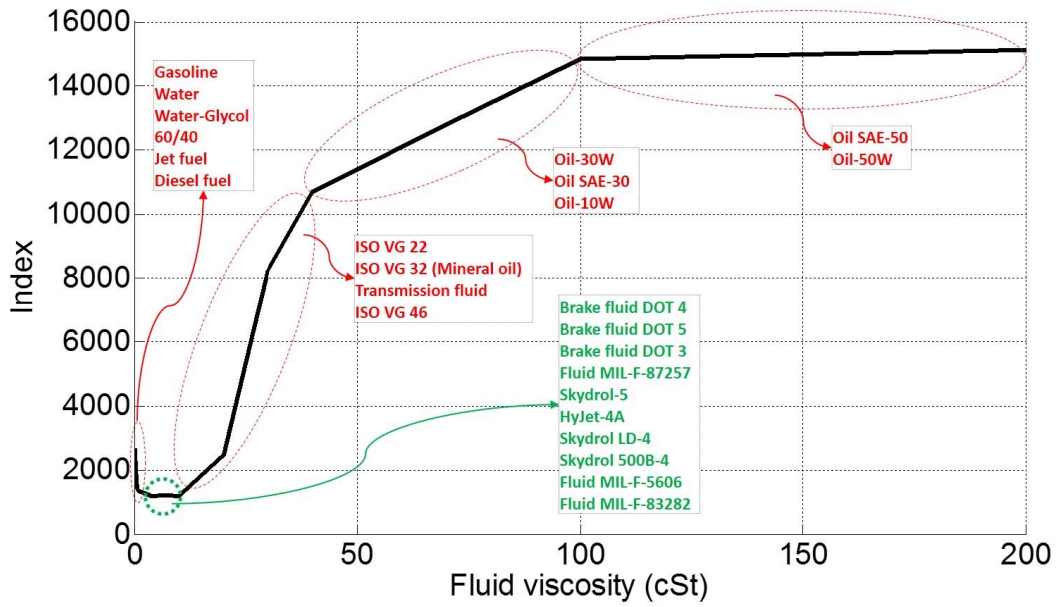


Figure 7.22: Index  $\zeta$  as a function of hydraulic fluids in SimHydraulics library

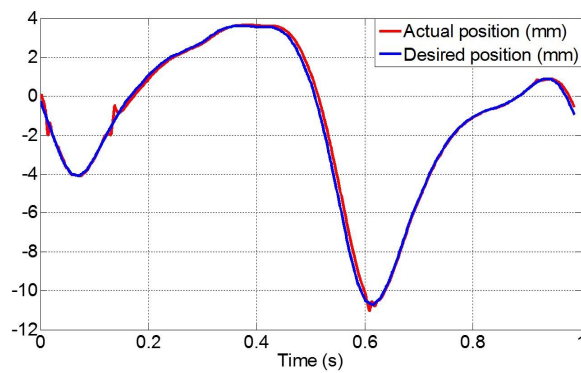


Figure 7.23: Position tracking result with DOT 3 brake fluid.

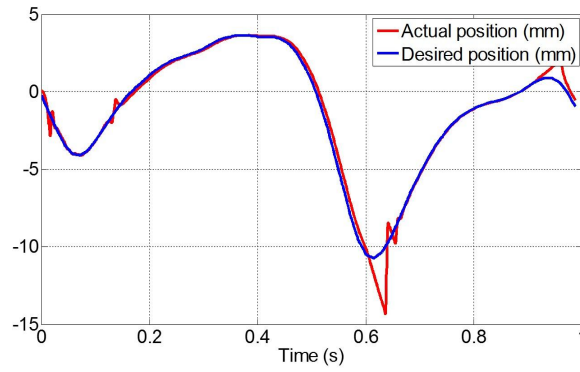


Figure 7.24: Position tracking result with 50W oil.

indicates tension in cable. This data confirms that the cable slackness does happen during the walking cycle.

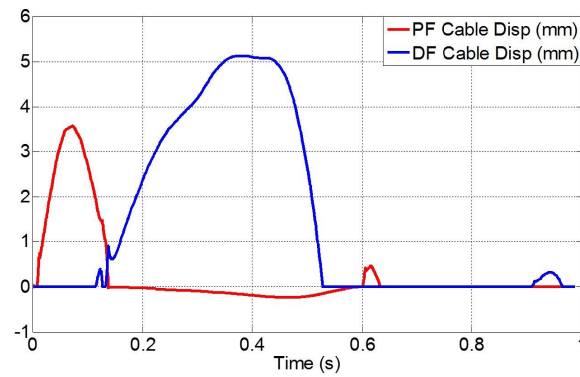


Figure 7.25: The cable displacements during HAFO operation.

## Chapter 8

# Design Guidelines for Small Scale Hydraulic Systems

To design small-scale hydraulic systems with desired performance, the analysis methods developed in this thesis have resulted in a set of design guidelines at the system and component levels.

### 8.1 Run at High Pressure

As shown in Fig. 2.20, high operating pressure is needed for small-scale hydraulic systems to weigh lighter than equivalent electro-mechanical systems. The pressure that is needed depends on the application requirements such as the output power, the stroke length and the transmission line length. The general rule is the smaller the system output power, the higher the pressure. As shown in Fig. 2.20, a 100 W electromechanical system is predicted to weigh 428 g while a 100 W hydraulic system running at 69 bar (1000 psi) is predicted to weigh 63 g, about seven times lighter.

Another reason for operating at high pressure is the component efficiency increases with higher pressure. As shown in Fig. 4.5, at 3 bar (50 psi), the O-ring efficiency is as low as 30%, but at 21 bar (300 psi), the efficiency goes up to 70%. The rationale

behind this is the pressure force increases at a faster rate than the friction force.

From the system perspective the operating pressure should not go too high. As shown in Fig. 6.12, 140 bar (2000 psi) gives the lightest HAFO system weight, while 70 bar (1000 psi) and 210 bar (3000 psi) yield heavier weight than 140 bar (2000 psi). This is primarily driven by the fact that thicker containing walls and more powerful prime movers are needed for high operating pressures. Base on these facts, 140 bar (2000 psi) was chosen for the HAFO system.

## 8.2 Small but not too Small

To make the system compact and portable, it is desired to use small components, but the component efficiency degrades as the components become smaller. The efficiency scaling law for hydraulic components is a nonlinear function of the component size. At large-scale, the efficiency changes slowly, while at small-scale it changes more drastically. There are some critical thresholds that designers should not exceed to avoid getting detrimental efficiencies.

The efficiency modeling results for small-scale hydraulic cylinders are shown in Fig. 3.7. For cylinders with 4 mm bore size, the efficiency is above 95%, but for cylinders with 1 mm bore size, the efficiency drops down to 88%. Similar scaling laws apply to small-scale hydraulic pumps, as shown in Fig. 5.8. For pumps with 0.4 cc/rev displacement, the efficiency is over 70%, but the efficiency drops down to 50% for a 0.2 cc/rev displacement. Lastly the hydraulic hoses obey the same scaling law. As shown in Fig. 7.18, hoses with diameter smaller than 4 mm will cause excessive pressure drop, thus smaller hose efficiency.

To maintain a reasonable system efficiency, the component should be sized as large as possible in a given design space. In case maximizing the component size (in the given design space) still cannot fulfill the efficiency requirement, new designs with different component configurations become necessary. Take a hydraulic cylinder for example, by

replacing the rubber piston seal with properly designed clearance gap seals, the overall efficiency can be improved, as shown in Chapter 3.

### 8.3 Efficiency Influences Weight

Both efficiency and weight affect the system power density, but for small-scale hydraulic systems, efficiency significantly affects system weight. As shown in Fig. 6.3, vane pump driven HAFO systems weigh more than piston pump driven HAFO systems, for all configurations. This is because the vane pump efficiency is lower than piston pump, which requires larger prime mover and batteries.

Another example is also from the HAFO design case study. As shown in Fig. 6.12, gear ratio 1 - no gear in between the pump and the DC motor - gives the lightest overall system weight compared to higher gear ratios. This is because the inefficiencies from the higher gear ratio requires a larger battery, which is more than the weight reduction from the electric motor.

### 8.4 Design Process Chart

It is recommended to follow the flow chart shown in Fig. 8.1 when designing a small-scale hydraulic systems. The same process has been applied and demonstrated in the HAFO design example, as detailed in Chapter 6 and 7.

**Step 1: Identify the application requirements and justify the usage of small-scale hydraulics.** The application requirements that need to be identified include the output power, the stroke length, the transmission line length and the power on hours. These parameters define the component size for a given set of operating conditions. Before the detailed design of the system, the usage of small-scale hydraulics needs to be justified. The general rule is for applications where the actuator weight matters the

most, small-scale hydraulics should be used. For applications where the overall system weight matters the most, electro-mechanical systems works better.

**Step 2: Determine the system configuration and packaging option.** On success of justifying the usage of hydraulics, the next step is to determine the system configuration. The designer needed to decide which type of pumps and actuators to use. Similar system level analysis as shown in Chapter 6 should be carried out to evaluate each configuration. Additional constraints such as the available packaging space should be taken into account when deciding the final configuration. After configuration, different packaging options should be evaluated. The key question to address is where to place the power unit, at the actuation point or not? The answer to this question determines the length of the hose, which is needed for subsequent dynamic simulation.

**Step 3: Define the design space, generate the design map and identify the component size.** For a electro-hydraulic system, the design space is defined by the range of the operating pressure, the pump shaft speed and the gear ratio. Previous design guidelines presented in Section 8.1 and 8.3 suggest high pressure and low gear ratio. Practical considerations such as cavitation constraints the shaft speed range. With the design space defined, the design map can be generated, which can be used to identify the optimal operating conditions and the component dimensions. The accomplishment of this step signifies the end of the static analysis.

**Step 4: Execute dynamic simulations and build prototype.** Before prototyping, the dynamic behavior of the system needs to be simulated to guide the detailed design of the hydraulic circuits, the hose dimensions and the hydraulic fluid. This can be achieved by feeding the operating conditions and the component dimensions to a dynamic simulation model. The accomplishment of this step signifies the end of the design steps, but to validate the paper design, prototypes should be built and evaluated.

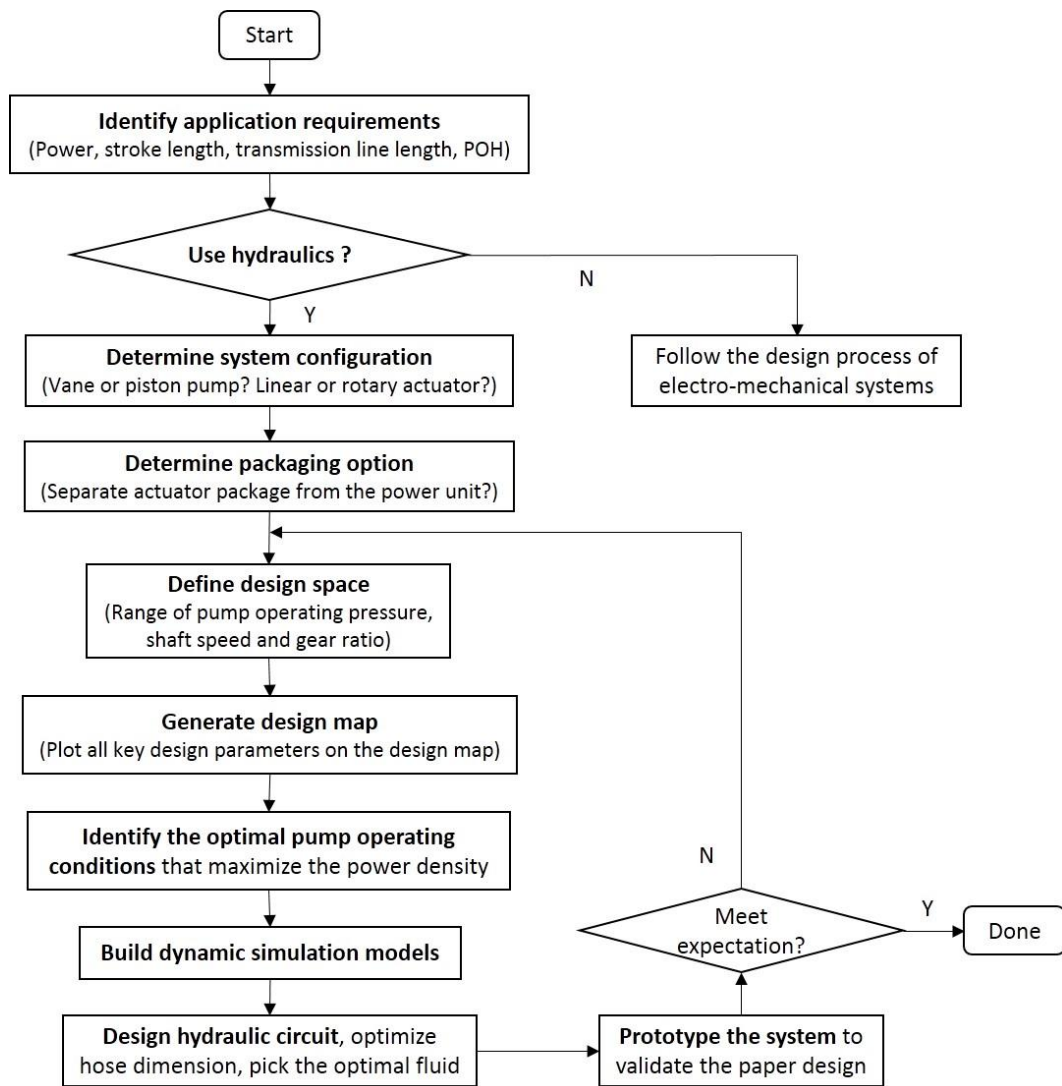


Figure 8.1: Design process chart for small-scale hydraulic systems.



# Chapter 9

## Conclusions

### 9.1 Limitations

While the work presented in this thesis can be used to design small-scale hydraulic systems, there are limitations that must be addressed in future work.

The power density analysis covered in Chapter 2 only considered the actuation sub-system. Though Chapter 6 demonstrated the benefit of hydraulics from the overall system perspective, it is constrained to the ankle-foot-orthosis application. Additionally, it was assumed that the actuation sub-system can be separated from the power unit. For an application where the power unit and the actuators have to co-locate, electro-mechanical systems should be considered. It would be useful to carry out power density comparison at an overall system level, and cover a wide range of output power, stroke lengths and transmission line lengths. This would justify or reject the usage of hydraulics for applications where the power unit and the actuation sub-system cannot be separated.

To simplify the analysis, this thesis only considered O-ring seals. For the same reason, all pressure and flow controls were shifted to the electric motor. The flow rate was controlled by regulating the electric motor speed, and the pressure was controlled by turning the electric motor on and off. To make the analysis more universal and

applicable to more design scenarios, it is necessary to model and validate the efficiency of other polymer seals, such as lip seals, and the efficiency and weight of hydraulic control valves. Accumulators should also be modeled and considered as an opportunity to further downsize the system and to increase the system power density. Though the accumulator and its associated valves add weight to the system, it downsizes other components. This is especially true for applications that have a peak power requirement and are cyclic in nature.

Model validation wise, it is recommended to validate the pump sensitivity charts (Fig. 5.4, 5.9, and 5.10) using prototyping testings. Also, it would be worthwhile to measure the overall system dynamic efficiency, and compare with the prediction from the dynamic simulation models. Additionally, the feasibility of the theoretical weight model of the hydraulic cylinders should be validated, especially at small-scale range. It is expected to reveal light weight component design opportunities by validating these weight models.

Another limitation is the HAFO weight analysis was done for steady state. Considering the cyclic nature of the application, the fatigue yield strength and a larger safety factor should be used to refine the analysis. This will result in heavier system weight than the original steady state analysis.

Lastly, the scope of this work is to analyze small-scale hydraulic system whose output power is in between 10 W and 100 W, so the benefit beyond this power range remains as a question. The first principle models developed in this thesis should work for any macro-scale power range, since they are all governed by continuum equations, but for those models that were derived from the catalog data, they are only applicable to the specific power range, and may not be extrapolated for different power regime.

## 9.2 Contributions

- Understood by using a system level analysis how the efficiency and weight of hydraulic components and systems scale in small-scale range. Analytical efficiency and weight models were developed for key hydraulic components including hydraulic cylinders, hoses and pumps. Empirical efficiency and weight models were developed for small-scale electro-mechanical components including gear heads, electric motors, wires and batteries.
- Designed, built and tested small-scale hydraulic components and systems to validate the models.
- Demonstrated the significance of the models by benchmarking a hydraulic ankle-foot-orthosis (HAFO) system. In the HAFO design example, these models enabled the identification of the optimal pump operating conditions and the sizing of the major functional components. They also enabled the hydraulic circuit design, the hose dimension optimization and the optimal fluid identification,

# References

- [1] Wikipedia contributors. *Energy Density*. Wikimedia Foundation, Inc., July 2012. Page Version ID: 500179221.
- [2] W. E. Wilson. *Positive-displacement Pumps and Fluid Motors*. Pitman Pub. Corp., 1950.
- [3] D. A. Winter. *Biomechanics and Motor Control of Human Movement*. John Wiley & Sons, Hoboken, N.J., 2005.
- [4] W. Back. The present and future of fluid power. *Proceedings of the Institution of Mechanical Engineers, Part I: Journal of Systems and Control Engineering*, 207(4):193–212, November 1993.
- [5] C. R. Burrows. Fluid Power-Progress in a key technology. *JSME International Journal Series B*, 37(4):691–701, 1994.
- [6] C. R. Burrows. Fluid power - some reflections. In *The 6th International Conference on Hydraulic Machinery and Hydrodynamics*, pages 51–56, Timisoara, Romania, October 2004.
- [7] L. J. Love, R. F. Lind, and J. F. Jansen. Mesofluidic actuation for articulated finger and hand prosthetics. In *Proceedings of the 2009 IEEE/RSJ International Conference on Intelligent Robots and Systems, IROS'09*, pages 2586–2591, Piscataway, NJ, USA, 2009. IEEE Press.

- [8] R. Chin, E. T. Hsiao-Wecksler, E. Loth, G. Kogler, K. S. Manwaring, A. Shorter, S. N. Tyson, and J. N. Gilmer. A pneumatic power harvesting ankle-foot orthosis to prevent foot-drop. *J. NeuroEng. Rehabil.*, 6(19):1–11, 2009.
- [9] W. Durfee and Z. Sun. *Fluid Power System Dynamics*. Center for Compact and Efficient Fluid Power, 2009.
- [10] N. Manring. *Hydraulic Control Systems*. John Wiley & Sons, 2005.
- [11] H. E. Merritt. *Hydraulic Control Systems*. Wiley, 1967.
- [12] F. M. M. Al-Ghathian and M. S. Tarawneh. Friction forces in o-ring sealing. *American Journal of Applied Sciences*, 2(3):626–632, 2005.
- [13] A. Bonchis, P. I. Corke, and D. C. Rye. A pressure-based, velocity independent, friction model for asymmetric hydraulic cylinders. In *Robotics and Automation, 1999. Proceedings. 1999 IEEE International Conference on*, volume 3, pages 1746–1751, Detroit, Michigan, 1999.
- [14] T. A. Stolarski and M. Tucker. Frictional performance of an o-ring type seal at the commencement of linear motion. *Tribology Letters*, 2(4):405–416, 1996.
- [15] M. W. Brown. *Seals and Sealing Handbook*. Elsevier Advanced Technology., 4th edition edition, 1995.
- [16] Parker Hannifin Corporation. *Parker O-Ring Handbook*. Parker Hannifin Corporation, 2009.
- [17] P. Beater. *Pneumatic Drives: System Design, Modelling and Control*. Springer, March 2007.
- [18] L. E. Schroeder and R. Singh. Experimental study of friction in a pneumatic actuator at constant velocity. *Journal of Dynamic Systems, Measurement, and Control*, 115(3):575–577, 1993.

- [19] N. B. Maser. *Numerical Model of a Reciprocating Rod Seal, Including Surface Roughness and Mixed Lubrication*. Master thesis, Georgia Institute of Technology, August 2006.
- [20] R. F. Salant, N. Maser, and B. Yang. Numerical model of a reciprocating hydraulic rod seal. *Journal of Tribology*, 129:91–97, January 2007.
- [21] H. K. Muller and B. S. Nau. *Fluid Sealing Technology: Principles and Applications*. CRC Press, July 1998.
- [22] I. Sher, D. Levinzon-Sher, and E. Sher. Miniaturization limitations of HCCI internal combustion engines. *Applied Thermal Engineering*, 29(2-3):400–411, February 2009.
- [23] M. D. Volder, F. Ceysens, D. Reynaerts, and R. Puers. A PDMS lipseal for hydraulic and pneumatic microactuators. *Journal of Micromechanics and Microengineering*, 17(7):1232–1237, July 2007.
- [24] M. De Volder and D. Reynaerts. Development of a hybrid ferrofluid seal technology for miniature pneumatic and hydraulic actuators. *Sensors and Actuators A: Physical*, 152(2):234–240, June 2009.
- [25] Airpot Corporation. *Cylinders with Clearance Gap Seals*. Airpot Corporation, July 2012.
- [26] N. Meikandan, R. Raman, M. Singaperumal, and K.N. Seetharamu. Theoretical analysis of tapered pistons in high speed hydraulic actuators. *Wear*, 137(2):299–321, May 1990.
- [27] N. Meikandan, R. Raman, and M. Singaperumal. Experimental study of friction in hydraulic actuators with sealless pistons. *Wear*, 176(1):131–135, July 1994.
- [28] M. De Volder and D. Reynaerts. A ferrofluid seal technology for fluidic microactuators. In *SPIE*, volume 6415, pages 1–10, 2006.

- [29] B. S. Nau. An historical review of studies of polymeric seals in reciprocating hydraulic systems. *Proceedings of the Institution of Mechanical Engineers, Part J: Journal of Engineering Tribology*, 213(3):215–226, March 1999.
- [30] G. K. Nikas. Eighty years of research on hydraulic reciprocating seals: Review of tribological studies and related topics since the 1930s. *Proceedings of the Institution of Mechanical Engineers, Part J: Journal of Engineering Tribology*, 224(1):1–23, January 2010.
- [31] G. J. Field and B. S. Nau. A theoretical study of the elastohydrodynamic lubrication of reciprocating rubber seals. *A S L E Transactions*, 18(1):48–54, 1975.
- [32] H. L. Johannesson. Calculation of the pressure distribution in an o-ring seal contact. In *Proceedings of the Fifth LeedsLyon Symposium on Tribology*, pages 379–387, 1978.
- [33] H. L. Johannesson. Oil leakage and friction forces of reciprocating o-ring seals considering cavitation. *Journal of Lubrication Technology*, 105:288–296, April 1983.
- [34] Y. Hori. *Hydrodynamic Lubrication*. Springer, December 2005.
- [35] A. Karaszkiwicz. Hydrodynamics of rubber seals for reciprocating motion. *Ind. Eng. Chem. Prod. Res. Dev.*, 24(2):283–289, 1985.
- [36] A. Karaszkiwicz. Hydrodynamics of rubber seals for reciprocating motion, lubricating film thickness, and outleakage of o-seals. *Ind. Eng. Chem. Res.*, 26(11):2180–2185, 1987.
- [37] A. Karaszkiwicz. Hydrodynamic lubrication of rubber seals for reciprocating motion; leakage of seals with an o-ring. *Tribology International*, 21(6):361–367, December 1988.

- [38] A. Karaszkievicz. Geometry and contact pressure of an o-ring mounted in a seal groove. *Ind. Eng. Chem. Res.*, 29(10):2134–2137, 1990.
- [39] A. Akers, M. Gassman, and R. J. Smith. *Hydraulic Power System Analysis*. CRC Press, April 2006.
- [40] J. F. D. Marsh and R. D. McLeish. A Self-Contained hydraulic power source for artificial upper limbs. *Biomedical Engineering, IEEE Transactions on*, BME-22(4):322–326, July 1975.
- [41] J. J. Pippenger and T. G. Hicks. *Industrial Hydraulics*. Gregg Division, McGraw-Hill, 3rd edition edition, January 1979.
- [42] M. F. Ashby. *Materials Selection in Mechanical Design*. Elsevier, September 2010.
- [43] M. Goldfarb, E. J. Barth, M. A. Gogola, and J. A. Wehrmeyer. Development of a hot gas actuator for self-powered robots. In *Robotics and Automation, 2003. Proceedings. ICRA '03. IEEE International Conference on*, volume 1, pages 188 – 193, Taipei, Taiwan, September 2003.
- [44] L. Tian. *Miniature Homogeneous Charge Compression Ignition Free-Piston Engine Compressor*. Thesis, University of Minnesota, 2013.
- [45] L. Tian, D. B. Kittelson, and W. K. Durfee. Miniature HCCI free-piston engine compressor for orthosis application. In *Proceedings of the SAE Small Engine Technology Conference*, Penang, Malaysia, 2009.
- [46] N. D. Manring. Friction forces within the cylinder bores of Swash-Plate type Axial-Piston pumps and motors. *Transactions of the ASME, Journal of Dynamic Systems, Measurement, and Control*, 121:531–537, September 1999.
- [47] A. Pourmovahed. Uncertainty in the efficiencies of a hydrostatic Pump/Motor. In *Winter Annual Meeting*, Ahaheim, CA, November 1992.



- [48] X. Shi and N. D. Manring. A torque efficiency model for an axial-piston, swash-plate type, hydrostatic pump. In *Bath Workshop on Power Transmission and Motion Control*, 2001.
- [49] Y. Inaguma and A. Hibi. Vane pump theory for mechanical efficiency. *Proceedings of the Institution of Mechanical Engineers, Part C: Journal of Mechanical Engineering Science*, 219(11):1269–1278, November 2005.
- [50] H. S. Jeong. A novel performance model given by the physical dimensions of hydraulic axial piston motors: Model derivation. *Journal of Mechanical Science and Technology*, 21(1):83–97, January 2007.
- [51] J.M. Bergada, S. Kumar, D.Ll. Davies, and J. Watton. A complete analysis of axial piston pump leakage and output flow ripples. *Applied Mathematical Modelling*, 36:1731–1751, 2012.
- [52] L. D. Mauck and C. S. Lynch. Piezoelectric hydraulic pump development. *Journal of Intelligent Material Systems and Structures*, 11(10):758–764, October 2000.
- [53] D. D. Shin, K. P. Mohanchandra, and G. P. Carman. Development of hydraulic linear actuator using thin film SMA. *Sensors and Actuators A: Physical*, 119(1):151–156, 2005.
- [54] R. T. Deam, E. Lemma, B. Mace, and R. Collins. On scaling down turbines to millimeter size. *Journal of Engineering for Gas Turbines and Power*, 130(5):1–9, 2008.
- [55] Eaton Corporation. *Vickers Industrial Hydraulics Manual*. Eaton Corp. Training, November 1992.
- [56] D. Wu, R. Burton, and G. Schoenau. An empirical discharge coefficient model for orifice flow. *International Journal of Fluid Power*, 3(3):13–18, 2002.

- [57] A. Pourmovahed, S. A. Baum, F. J. Fronczak, and N. H. Beachley. Experimental evaluation of hydraulic accumulator efficiency with and without elastomeric foam. *Journal of Propulsion and Power*, 4(2):185–192, 1988.
- [58] J. Peirs, D. Reynaerts, and H. Van Brussel. Design of miniature parallel manipulators for integration in a self-propelling endoscope. *Sensors and Actuators A: Physical*, 85(1-3):409–417, August 2000.
- [59] M. Ivantysynova, O. Kunze, and H. Berg. Energy saving hydraulic systems in aircraft—a way to save fuel. In *Proceedings of 4th Scandinavian International Conference on Fluid Power*, pages 1000–1014, Tampere, September 1995.
- [60] Parker Hannifin. *Commercial EHA example*. Parker Hannifin Corporation, July 2012.
- [61] D. F. Young, B. R. Munson, and T. H. Okiishi. *A Brief Introduction to Fluid Mechanics*. John Wiley & Sons, April 2004.
- [62] M. De Volder, J. Peirs, D. Reynaerts, J. Coosemans, R. Puers, O. Smal, and B. Raucent. A novel hydraulic microactuator sealed by surface tension. *Sensors and Actuators A: Physical*, 123-124(0):547–554, September 2005.
- [63] J. Zou, J. Zou, and J. Hu. Design and pressure control of high-pressure differential magnetic fluid seals. *Magnetics, IEEE Transactions on*, 39(5):2651 – 2653, September 2003.
- [64] M. Takaiwa and T. Noritsugu. Development of pneumatic walking support shoes using potential energy of human. *JFPS International Journal of Fluid Power System*, 2(2):51–56, 2009.
- [65] K. A. Edge. The control of fluid power systems - responding to the challenges. *Proceedings of the Institution of Mechanical Engineers, Part I: Journal of Systems and Control Engineering*, 211(2):91–110, March 1997.

- [66] Siemens PLM Software. AMESim, a simulation program for engineering applications. *International Journal of Fluid Power*, 1(1), 2000.
- [67] Dassault Systemes AB. Dymola and the component libraries HyLib and PneuLib. *International Journal of Fluid Power*, 7(1):67–76, 2006.
- [68] T. Hunt and N. Vaughan. *The Hydraulic Handbook*. Elsevier Science, 9th edition edition, 1996.
- [69] A. Dollar and H. Herr. Lower extremity exoskeletons and active orthoses: Challenges and state-of-the-art. *IEEE Transactions on Robotics*, 24(1):1 – 15, 2008.
- [70] C. Yang, J. Zhang, Y. Chen, Y. Dong, and Y. Zhang. A review of exoskeleton-type systems and their key technologies. *Proc. IMechE Part C: J. Mechanical Engineering Science*, 222:1599–1612, 2008.
- [71] D. Laser and J. Santiago. A review of micropumps. *Journal of Micromechanics and Microengineering*, 14(6):R35–R64, 2004.
- [72] K. Oh and C. Ahn. A review of microvalves. *Journal of Micromechanics and Microengineering*, 16(5):R13 – R39, 2006.
- [73] M. Volder and D. Reynaerts. Pneumatic and hydraulic microactuators: a review. *Journal of Micromechanics and Microengineering*, 20(4):043001, 2010.
- [74] S. Kannappan. *Introduction to Pipe Stress Analysis*. Wiley, May 1986.
- [75] M. Kutz. *Mechanical Engineers’ Handbook*. Wiley, 2nd edition edition, February 1998.
- [76] B. B. Singer and H. Forster. *Basic Mathematics for Electricity and Electronics*. McGraw-Hill, 6th edition edition, 1990.

- [77] K. A. Shorter, J. Xia, E. T. Hsiao-Wecksler, W. K. Durfee, and G. F. Kogler. Technologies for powered ankle-foot orthotic systems: Possibilities and challenges. *IEEE/ASME Transactions on Mechatronics*, 18(1):337–347, 2013.
- [78] K. Luttgens and N. Hamilton. *Kinesiology: Scientific Basis of Human Motion*. Brown & Benchmark, 9th edition edition, 1997.
- [79] H.C. Tu, M.B. Rannow, M. Wang, P.Y. Li, T.R. Chase, and J. D. Van de Ven. Design, modeling, and validation of a high-speed rotary pulse-width-modulation on/off hydraulic valve. *J. Dyn. Sys., Meas., Control.*, 134(6):061002:1–13, 2012.
- [80] K.A. Stelson and F. Wang. A simple model of piston-cylinder gap efficiency in positive-displacement hydraulic pumps and motors. In *Fluid Power and Motion Control*, 2010.
- [81] J. Xia and W. K. Durfee. Analysis of small-scale hydraulic actuation systems. *Journal of Mechanical Design*, 135(9):1–11, 2013.
- [82] K. A. Shorter. *The Design and Control of Active Ankle-Foot Orthoses*. Thesis, University of Illinois at Urbana-Champaign, 2011.
- [83] J. Xia and W. K. Durfee. Modeling of tiny hydraulic cylinders. In *52nd National Conference of Fluid Power*, pages 1–5, 2011.
- [84] W. E. Wilson. *Positive-Displacement Pumps and Fluid Motors*. Pitman Pub. Corp., New York, 1950.
- [85] Parker Hannifin. *Parker O-Ring Handbook*. Parker Hannifin Corp., Lexington, KY, 2007.
- [86] D. Dowson. *History of Tribology*. Professional Engineering Publishing, London and Bury St Edmunds, UK., 1998.

- [87] W. K. Durfee, J. Xia, and E. T. Hsiao-Wecksler. Tiny hydraulics for powered orthotics. In *IEEE International Conference on Rehabilitation Robotics (ICORR)*, pages 1–6, 2011.
- [88] J. Xia and W. K. Durfee. Analysis of small-scale hydraulic actuation systems. *Journal of Mechanical Design*, 135(9):1–11, 2013.
- [89] M. Pelosi, M. Zecchi, and M. Ivantysynova. A fully-coupled thermoelastic model for the rotating kit of axial piston machines. In *Fluid Power and Motion Control*, pages 217–234, 2010.
- [90] J. Ivantysyn and M. Ivantysynova. *Hydrostatic Pumps and Motors: Principles, Design, Performance, Modelling, Analysis, Control and Testing*. Tech Books International, 2003.
- [91] R. P. Lambeck and R. P. Lambeck. *Hydraulic Pumps and Motors: Selection and Application for Hydraulic Power Control Systems*. M. Dekker, New York; Basel, 1983.
- [92] H. Jeong and H. Kim. On the instantaneous and average piston friction of swash plate type hydraulic axial piston machines. *Journal of Mechanical Science and Technology*, 18(10):1700–1711, 2004.
- [93] H. Jeong and H. Kim. A novel performance model given by the physical dimensions of hydraulic axial piston motors: Experimental analysis. *Journal of Mechanical Science and Technology*, 21(4):630–641, April 2007.
- [94] B. Neubauer, J. Nath, and W. K. Durfee. Design of a portable hydraulic ankle-foot orthosis. In *Annual International Conference of the IEEE Engineering in Medicine and Biology Society*, 2014.

- [95] R. R. Neptune, S. A. Kautz, and F. E. Zajac. Contributions of the individual ankle plantar flexors to support, forward progression and swing initiation during walking. *J. Biomech*, 34(11):1387–98, 2001.
- [96] K. A. Shorter, J. Xia, E. T. Hsiao-Wecksler, W. K. Durfee, and G. F. Kogler. Technologies for powered ankle-foot orthotic systems: Possibilities and challenges. *Mechatronics, IEEE/ASME Transactions on*, 18(1):337–347, 2013.
- [97] S. Yamamoto, M. Ebina, S. Kubo, T. Hayashi, Y. Akita, and Y. Hayakawa. Development of an ankle-foot orthosis with dorsiflexion assist, part 2: Structure and evaluation. *J. Prosthetics Orthotics*, 11(2):24–28, 1999.
- [98] K. Bharadwaj, T. G. Sugar, J. B. Koeneman, and E. J. Koeneman. Design of a robotic gait trainer using spring over muscle actuators for ankle stroke rehabilitation. *J. Biomech. Eng.*, 127(6):1009–14, 2005.
- [99] D. P. Ferris, K. E. Gordon, G. S. Sawicki, and A. Peethambaran. An improved powered ankle-foot orthosis using proportional myoelectric control. *Gait Posture*, 23:425–428, 2006.
- [100] M. Noel, B. Cantin, S. Lambert, C. M. Gosselin, and L. J. Bouyer. An electrohydraulic actuated ankle foot orthosis to generate force fields and to test proprioceptive reflexes during human walking. *IEEE Trans. Neural Syst. Rehabil. Eng.*, 16(4):390–399, 2008.
- [101] A. Roy, H. I. Krebs, S. L. Patterson, T. N. Judkins, I. Khanna, L. W. Forrester, R. M. Macko, and N. Hogan. Measurement of human ankle stiffness using the anklebot, 2007.
- [102] J. A. Blaya and H. Herr. Adaptive control of a variable-impedance ankle foot orthosis to assist drop-foot gait. *IEEE Trans. Neural Syst. Rehabil. Eng.*, 12(1):24–31, 2004.

- [103] K. W. Hollander, R. Ilg, T. G. Sugar, and D. Herring. An efficient robotic tendon for gait assistance. *J. Biomech. Eng.*, 128:788–792, 2006.
- [104] R. L. Waters and S. Mulroy. The energy expenditure of normal and pathologic gait. *Gait & Posture*, 9(3):207–231, July 1999. PMID: 10575082.
- [105] K. A. Shorter, G. F. Kogler, E. Loth, W. K. Durfee, and E. T. Hsiao-Wecksler. A portable powered ankle-foot orthosis for rehabilitation. *J Rehabil Res Dev*, 48(4):459–472, 2011.
- [106] L. Love, E. Lanke, and P. Alles. Estimating the impact (energy emissions and economics) of u.s. fluid power industry. Report, U.S. Department of Energy, 2012.
- [107] J. Xia and W. K. Durfee. Analytical efficiency modelling and verification of hydraulic vane and axial-piston pumps. *to be submitted*.
- [108] O. Stemme and P. Wolf. *Principles and Properties of Highly Dynamic DC Miniature Motors*. Maxon Motor, 1994.

# Appendix

## Details for the HAFO Simulation Model

The HAFO Simulink simulation model is shown in Fig. 9.1. The hydraulic components are highlighted in yellow color, and the inputs to the simulation model in red color. The raw data for the desired ankle position profile and the ankle resistive force profile was imported from [3]. To model the weight and the damping of the cylinders and the ankle joint, mass and damper blocks were used in the model. To study the impact of the fluid viscosity and bulk modulus in a generic range, a custom hydraulic fluid block was used.

## Model for the Flexible Rod

The flexible cables sitting in between the PF and DF cylinders were modeled using a custom SimScape block. The SimScape script is shown in Fig. 9.2. The governing equations for the flexible rod are

$$F = \begin{cases} k \cdot x & \text{if } x \leq 0 \\ 0 & \text{if } x > 0 \end{cases} \quad (9.1)$$

where  $x$  is the cable displacement, defined as the displacement difference between node  $R$  and  $C$ . Negative  $x$  means the cable in tension, and positive  $x$  indicates the cable in compression. When in tension, its governing equation is the same as that for a mechanical spring. When in compression, the cable will be slack, and cannot be subject to compression force.



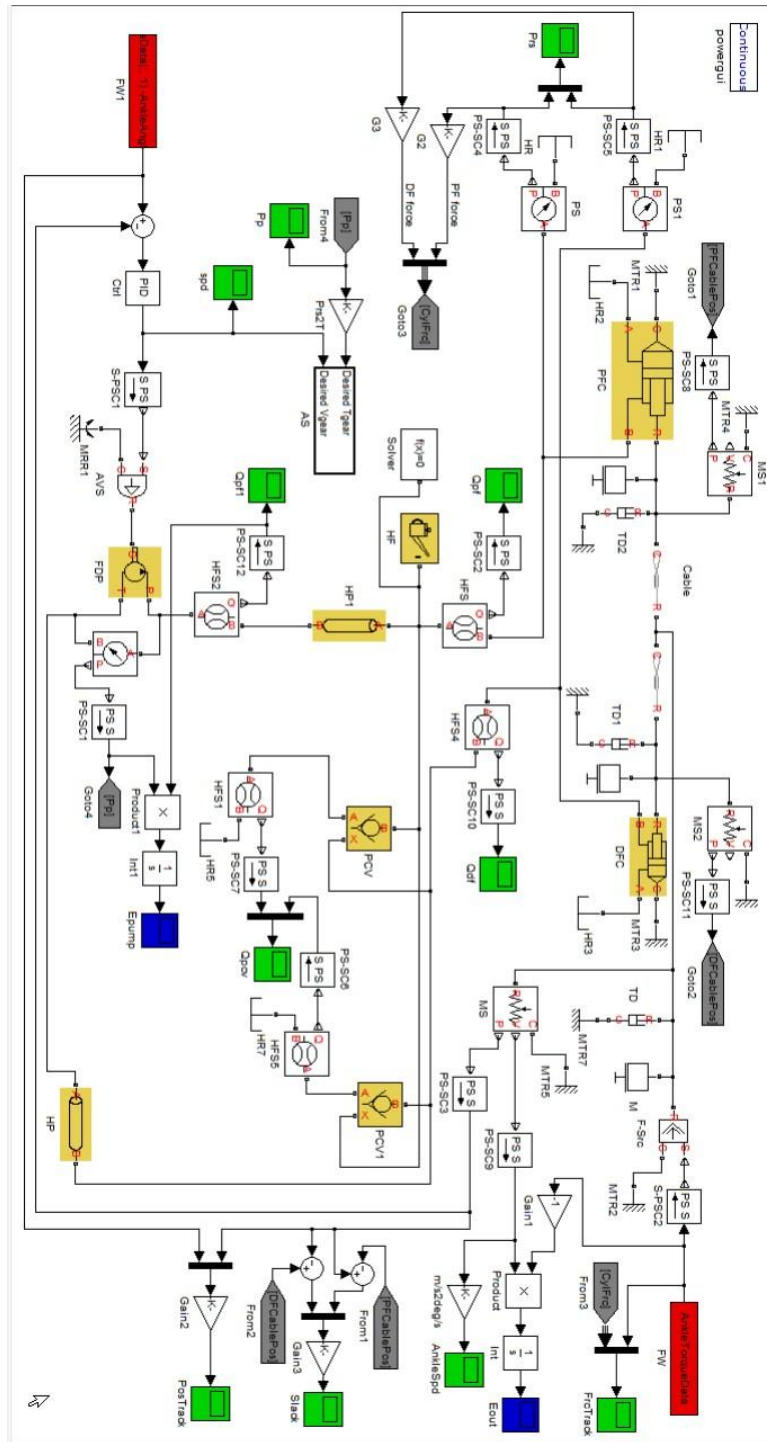


Figure 9.1: SimHydraulics model for the HAFO system.

```

component cable
    % Airplane cable : 1.0 : fixed
    % This block describes a stainless steel airplane cable that can only
    % be subject to tension.
    %
    % The positive direction is from R to C.
nodes
    R = foundation.mechanical.translational.translational; % R:left
    C = foundation.mechanical.translational.translational; % C:right
end
parameters
    k = {200*1e9*pi/4*(0.0254/4)^2/0.5, 'N/m' }; % Spring rate
end
variables
    x = { 0, 'm' }; % displacement
    f = { 0, 'N' }; % force, through variable
    v = { 0, 'm/s' }; % velocity, across variable
end
function setup
    if k < 0
        error( 'Cable stiffness must be greater than zero' );
    end
    through(f, R.f, C.f); % force through from node r to node c
    across(v, R.v, C.v); % velocity across from node r to node c
end
equation
    if x <= 0 % x = x_R - x_C
        f == k*x; % same governing equation as a spring for tension
    else
        f == 0; % zero force for compression
    end
    v == x.der;
end
end

```

Figure 9.2: SimScape script for the customized cable rod.